UILU-ENG-94-2013

CIVIL ENGINEERING STUDIES

Structural Research Series No. 593

ISSN: 0069-4274

ASSESSMENT AND DETECTION OF DAMAGE IN STRUCTURAL SYSTEMS

By
Soobong Shin
and
Keith D. Hjelmstad

A report to sponsors:
The Army Research Office
The National Science Foundation

Department of Civil Engineering
University of Illinois at Urbana-Champaign
Urbana, Illinois

October 1994

Assessment and Detection of Damage in Structural Systems

Soobong Shin

and

Keith D. Hjelmstad

Department of Civil Engineering
University of Illinois at Urbana–Champaign
Urbana, Illinois USA

A report to sponsors:
The Army Research Office
The National Science Foundation

October 1994

Soobong Shin
and
Keith D. Hjelmstad

Department of Civil Engineering
University of Illinois at Urbana–Champaign
205 N. Mathews Avenue
Urbana, Illinois 61801
U.S.A.

Assessment and Detection of Damage in Structural Systems

Printed in the United States of America.

9 8 7 6 5 4 3 2 1

50272-101

REPORT DOCUMENTATION PAGE	1. REPORT NO. UILU-ENG-94-2013	2.	3. Recipient's Accession No.

4. Title and Subtitle

Assessment and Detection of Damage in Structural Systems

5. Report Date: October 1994

6.

7. Author(s)

Soobong Shin and Keith D. Hjelmstad

8. Performing Organization Report No.: SRS 593

9. Performing Organization Name and Address

Department of Civil Engineering
University of Illinois at Urbana-Champaign
205 N. Mathews Avenue
Urbana, Illinois 61801, USA

10. Project/Task/Work Unit No.

11. Contract(C) or Grant(G) No.
(G) *CES 86-58019 (NSF)*
DAAL-03-87-K-006 (ARO)
DAAL-03-86-G-0186 (ARO)
DAAL-03-86-K-0188 (ARO)

12. Sponsoring Organization Name and Address

National Science Foundation, Washington D.C.

Army Research Office, Washington D.C.

13. Type of Report & Period Covered

14.

15. Supplementary Notes

16. Abstract (Limit: 200 words)

This report presents a new damage detection and assessment algorithm based on a system identification method. The algorithm can be used as a non-destructive diagnostic technique to aid in decisions of repair and rehabilitation of existing structures. The developed algorithm is able to detect and assess damage in a structure when the measured data are sparse and polluted with noise.

Damage is defined as the reduction in estimated parameters between two time separated inferences. Damage is localized by updating parameter groups hierarchically and assessed by perturbing measured data. Parameter groups are continuously subdivided until all the existing damaged parts in a structural system are completely localized. The measured data are perturbed to examine the sensitivity of each parameter with respect to the measured data, and to thereby provide a statistical basis for assessing damage. The bias of the mean estimate from the baseline value and this bias divided by the standard deviation of the Monte Carlo perturbation sample are calculated as damage indices. The upper limit values for both damage indices are determined from the simulation study for the undamaged baseline structure and are used to determine damage in the existing structure.

Case studies are performed to examine the developed algorithm. Simulated static responses are used to identify damaged planar bowstring truss structures. Real measured modal responses from a laboratory experiment are used to identify the cracked cantilever structure.

17. Document Analysis a. Descriptors

Damage assessment, damage detection, system identification, parameter estimation, parameter grouping, parameter group updating scheme, measured data perturbation scheme, Monte Carlo simulation

b. Identifiers/Open-Ended Terms

c. COSATI Field/Group

18. Availability Statement	19. Security Class (This Report): Unclassified	21. No. of Pages: 109
	20. Security Class (This Page): Unclassified	22. Price

(See ANSI-Z39.18)

OPTIONAL FORM 272 (4-77)
Department of Commerce

Acknowledgements

The research reported herein was supported by the U.S. Army Research Office, as part of a program at the University of Illinois Advanced Construction Technology Center (grant numbers *DAAL 03–87–K–006, DAAL 03–86–G–0186, DAAL 03–86–K–0188*), and the National Science Foundation (grant number *CES 86–58019*). Joseph P. Murtha is the director of the Advanced Construction Technology Center and S.–C. K. Liu is the cognizant program officer at the National Science Foundation. The support of these agencies is gratefully acknowledged. The results, opinions, and conclusions expressed in this report are solely those of the authors and do not necessarily represent those of the sponsors.

Table of Contents

List of Tables

List of Figures

Chapter One

Introduction

Civil structures experience severe loads or impacts from earthquake, blast, gust, or fire. Most structures must also carry various kinds of live loads that may lead to fatigue failure. A structure may survive a damaging event if designed properly, but its safety often cannot be guaranteed after such an experience. Damage is inevitable in civil structures over their lives. Undetected and unrepaired damage may lead to a structural failure requiring costly repair or worse costing human lives. To prevent a catastrophe during the life of a structure, regular inspections for damage in structures are necessary.

Many non-destructive testing methods have been developed to inspect structures for damage. Generally, these methods can be categorized as either local or global. Local methods include numerous techniques such as visual inspection, ultrasonic techniques, magnetic flux leakage techniques, radiographic techniques, penetrant techniques, eddy current techniques, *etc.* (Bray and Stanley 1989). These non-destructive testing methods are adequate for a detailed local inspection, but when it is necessary to find damage in a large structure they are time-consuming and expensive. In addition, these methods can be applied only for the members that are easily accessible. Global damage detection using a system identification method requires a mathematical model and measured responses of the structure. To detect damage in a structure by a system identification method, the changes in its characteristic properties are evaluated. System identification methods can be applied not only for local inspections but also for global damage assessments. A variety of system identification methods for evaluating damage in structural systems have been developed and are still actively studied in many areas. Even though different sources of ideas have been used to develop the methods, they have one thing in common. They define damage by comparing certain properties between two time separated inferences, which can be deduced from measured test data. The differences among methods lie mainly in what kinds of properties are compared to determine damage, and what kinds of schemes are used to localize and evaluate them.

1.1 System Identification Methods for Damage Assessment

System identification methods solve inverse problems to identify properties of a structure from measured data. Alcoe and Hjelmstad (1992) used the terms of *global modification methods* and *local*

modification methods to classify different system identification methods. Global modification methods identify a given system by estimating nodal components of the structural stiffness or mass matrix, while local modification methods identify a structural system by altering some subset of coefficients of the stiffness or mass matrix. Generally, global modification methods are capable of inexpensively producing an improved structural model, giving responses that better simulate test responses. However, because errors are minimized in a global norm, improvements are spread throughout the mass or stiffness matrix. Since global moditification methods allow changes anywhere in the stiffness and mass matrix, they often face a difficulty in the physical interpretation of the resulting system. To justify the physical meaning of the estimates, additional criteria, such as mass orthogonalization and load path preservation, are often required. Local modification methods are generally cast as optimization problems, where parameters of specific subsets of the stiffness and mass matrices are altered in some optimum manner to best recreate the measured data. In this way, more physically justifiable changes in the finite element model can be realized.

A damage detection algorithm based on a global modification method cannot provide the information of which members are actually damaged and how much they are damaged, because the changes in nodal properties are detected rather than the changes in the member properties. If a structural model is simple, the changes in member properties can be deduced from the nodal value changes. However, as a structure becomes complex like most civil structures, it will be harder to pin-point the damaged members by investigating damage associated with degrees of freedom in the stiffness or mass matrix. Therefore, most damage detection and assessment algorithms based on the global modification methods have developed additional tools for checking damage at the element level in addition to the evaluation of the changes in the nodal components of structural matrices.

Among the local modification methods, parameter estimation methods have been proposed to identify a structural system using a parameterization based on kernel matrices (Alcoe and Hjelmstad 1992; Banan and Hjelmstad 1993; Clark 1989; Hajela and Soeiro 1990a, 1990b; Hjelmstad, *et. al.* 1990; Sanayei and Nelson 1987; Sanayei and Scampoli 1991; Sanayei, *et. al.* 1992). These methods estimate the unknown parameters using either a constrained or unconstrained nonlinear optimization problem. Because parameter estimation methods can determine parameters for each member, damage can be detected and assessed directly at the element level.

To develop a damage assessment algorithm based on a system identification method, it is necessary to understand some fundamental issues related to system identification methods. Unawareness or misunderstanding of any of the issues would result in a poor algorithm. The main issues concern (*1*) the construction of the structural model and (*2*) the quality and quantity of measured data.

The construction of the structural model is the first important task that any identification method must face. Eykhoff (1974) defined a model as a representation of the essential aspects of a system that presents knowledge of that system in a usable form. Simplification and thus approximation are indispensable aspects of model construction. The level of simplicity that is appropriate depends on the situation. However, in most structural identification problems one can assume that the topology

and geometry of the structure are known. The unknowns comprise the constitutive properties of the structure. There exist two schools of thought in creating a structural model in the identification process. The first branch selects a model that can recreate the measured behavior of the structure as closely as possible. The detail of the model can be varied in accord with the required accuracy and the availability of measured information. Model refinement or model reduction is done to improve the fit to the measured data. The main focus of this approach is to produce a model whose response is close to the measured response. The relevance of the mathematical model as regards the measured data must be always considered. The second branch has a little different point of view in developing a model, and is well described by Sage (1972): "an essential problem in identifying a large scale system is the need to correctly represent the structure of a system rather than just to satisfy to accurately reproduce observed data". First, a system model has to be defined, that can describe the behavior of the structure well, with the given topological and geometrical information of the structure. Then, the physical properties are identified to reproduce the measured response as closely as possible. Parameter estimation methods generally follow the second philosophy with a pre-determined finite element model for the structure. After a model is established once, the refined structural finite element model and the types of structural parameters are fixed for future identification processes. Only the values of the parameters vary in accord with the measured data at each inference. If a finite element model for a candidate structure can be established before testing the structure, an engineer may be able to decide how many and which displacements should be measured to produce good estimation results. Simulation studies can be used to help make the decision. Between two different approaches of creating a mathematical model of a structure, however, it may be difficult to figure out which one is more feasible and useful for identifying structural systems. The decision of which philosophy is applied to create a structural model may depend on which damage detection and assessment algorithm is used.

Noise and sparsity of measured data are inevitable in testing civil structures, and are the biggest enemies in identifying structural systems correctly. The development of measuring skill and instruments may lower the noise level, but noise cannot be eliminated completely. An important fact about noise is that noise is random in nature. We can say that it is deterministic if repeated identical experiments provide the same results. If, however, when all conditions under control of the experimenter are maintained the same, the records continually differ from each other, the process is said to be random. In such a case a single record is not as meaningful as a statistical description of the totality of possible records (Crandall and Mark 1963). Therefore, without considering noise in measurements and without considering statistical aspects due to the randomness of noise, an identification algorithm cannot provide useful information about the structure.

In addition to noise, sparsity of measurements is a problem for identification of civil structures. Because most civil structures require a large number of degrees of freedom in their finite element models due to their size and complexity, only a small subset of all the degrees of freedom in the model can be practically measured. It is difficult and expensive in practice to measure static or modal displacements at many locations. There is a lower limit to the number of measurements, below which

the estimated parameters are completely unreliable. The reliability of the estimated parameters is a function of the ratio of measurements to unknown parameters (Banan and Hjelmstad 1993).

An additional issue for parameter estimation methods is about the selection of an estimator which can produce a robust parameter estimation algorithm. Different types of estimators have been proposed and studied in the literature (Banan and Hjelmstad 1993; Hajela and Soeiro 1990b; Natke 1982). A different definition of error function can lead to a different type of estimator. Equation error estimators and output error estimators are the two most widely used types. A disadvantage of the output error estimators is that the inverse of a structural model must be obtained. Due to the necessity of the inverse model, the error functions of the output error estimators are intrinsically more nonlinear than those of the equation error estimators. However, for sparsely measured data, the number of unknown variables for an output error estimator is smaller than that for an equation error estimator, and thus the optimization problem for output error estimators can be solved in a lower dimensional space (Banan and Hjelmstad 1993).

1.2 Definitions of Damage, Localization, Detection, and Assessment

Damage can be identified from a reduction in the physical properties of a structure between two time separated inferences. Those physical properties might include stiffness, damping, and mass parameters, or some scalar factors that represent global measures of damage. Generally, structural parameters or damage factors are computed for each member. Some researchers detect damage by investigating the changes of all the available parameters in the structure, while others determine damage by the reduction in some dominant parameters which rule the behavior of the structure. For example, Hajela and Soeiro (1990a) estimated the selective dominant variables by fixing inactive member variables at nominal values. The idea of selecting dominant parameters in detecting damage can be supported by the fact that not all the parameters are sensitive with respect to the applied loading and measurement conditions. Natke (1989) discussed the capability of system identification techniques to find the most sensitive parameters to be chosen for the inspection of early damage. Sensitivity of member parameters could be also checked by the variation of normalized member strain energy (Clark 1989; Hjelmstad, *et. al.* 1990). Hjelmstad, *et. al.* (1990) observed that the members less excited by the applied loads are harder to accurately identify than those more excited. Theoretically, it may be possible to reduce the number of insensitive member parameters in a structure by measuring more data from various load or mode cases or by applying an adequate load pattern or mode case that can excite those members that are hard to excite. However, practically, it is necessary to investigate which parameters are insensitive with respect to the current test condition.

Damage localization is a process of separating potentially damaged regions from the undamaged parts, and damage detection can be defined as the process of distinguishing which members are actually damaged. If the amount of measured data is sufficient, the damage state of individual member can be evaluated directly and a damage localization process may not be required. Many available damage assessment algorithms have not considered the localization process, because they have dealt with only

the cases with enough measured data. However, when the measured data are sparse, damage must be generally associated with substructures composed of many members rather than for individual members, and damage must be localized before damage detection and assessment steps are performed. Damage assessment is the step in a detailed evaluation of damage in a structure whereby the severity of damage is calculated for each member. Because uncertainty in detecting damage is a matter of fact rather than speculation, damage detection and assessment should be based on some statistical properties possibly deduced from the identification results. Damage detection and assessment may be carried out simultaneously.

1.3 Literature Review of Damage Assessment Algorithms

In this section, damage detection and assessment algorithms based on system identification techniques are reviewed. Even though a number of different ideas and schemes have been used in the available damage detection and assessment algorithms, most of them can be categorized by the following classifications: (*1*) direct methods, (*2*) sensitivity methods, (*3*) local methods, and (*4*) global methods.

Direct methods are the most classical and aged methods in the development of damage detection and assessment algorithms. Damage is detected by directly comparing the current measured data with the previously measured data, or by comparing measured data with an analytical response. The compared properties include the changes in natural frequencies (Cawley and Adams 1979; Springer, *et. al.* 1988; Vandier 1975) or some eigenparameters such as rotation and translation eigenproperties (Yuen 1985) and curvature mode shape (Pandey, *et. al.* 1991). Yao, *et. al.* (1992) investigated the strain mode shape change to determine the location of damage. These direct methods usually lack a quantitative measure of the severity of structural damage and provide only a global measure of the existence of damage in a structural system.

The most widely used method seems to be the second category of *sensitivity methods*. These methods perturb structural matrices to detect damage, and determine some physical parameters to assess damage. Usually they define physical parameters for each element, but not in all the sensitivity methods. Several types of parameters are used to determine damage, including error factors (Chou and Wu 1990), correction factors for mass, stiffness, and damping (Natke 1989), member mass, stiffness, and geometric parameters (Natke and Cempel 1991; Ricle and Kosmatka 1992; Stubbs, *et. al.* 1990b; Tavares, *et. al.* 1993; Linder, *et. al.* 1993). Chen and Garba (1988) evaluated element stiffness changes without using any physical parameter and computed the stiffness change for each element by solving a system of equations deduced from matrix perturbations. However, since most of these algorithms detect damage by nodal perturbation of structural matrices, they have difficulties in defining a structural model due to mass orthogonality and load path preservation problems. Since the structural model varies depending on the number of measured degrees of freedom, a model reduction or expansion scheme had to be implemented to complete the structural model.

Local methods have been developed using parameter estimation methods. These methods separate element parameters from the structural matrices. Hence, by estimating parameters for each member, they determine the location and the severity of damage. Sanayei and Onipede (1991) solved an overdetermined system of equations deduced from a constrained optimization problem for estimating cross sectional properties from static data. Hajela and Soeiro (1990a, 1990b) solved an unconstrained nonlinear optimization problem to estimate changes in element stiffness due to the variations in geometry and material properties. They estimated only the selected dominant variables by fixing inactive members as they were. Since these methods determine damage by estimating element properties, they detect and assess damage at each element in the structural system simultaneously.

In either of the sensitivity methods or the local methods, it may be difficult to justify how much change indicates damage when measured data are noise-polluted. For some insensitive members or degrees of freedom, their variations would be unpredictable. It may be therefore impossible to figure out if there exists any damage in the structure only by checking the changes of parameters or error factors without studying their sensitivity based on statistical evaluations.

Another category of available damage detection and assessment algorithms is by checking the changes in nodal properties of structural matrices identified by a system identification technique. These *global methods* use global modification methods in the system identification technique and usually determine global physical parameters or changes of nodal properties (Agbabian, *et. al.* 1991; Kaouk and Zimmerman 1993; Kim and Bartkowicz 1993; Zimmerman and Kaouk 1992). Compared with other categories of damage algorithms, these methods are not so refined to detect and assess damage. Especially when damage must be evaluated for each element, these methods are not attractive. These methods usually do not offer any means of relating the changes in nodal properties to the changes in member properties.

In addition to these reviewed algorithms, many *ad hoc* ideas for damage detection and assessment are available in the literature. However, the fundamental concepts are similar to those mentioned above.

1.4 Motivation

In testing a civil structure whose finite element model contains a large number of degrees of freedom, sparse and noisy measurements are inevitable. Even though many damage detection and assessment algorithms have been proposed, few of them seem to be successful in dealing with noisy and sparse measured data. Many algorithms have been developed without even considering these important aspects. Therefore, the motivation for developing a new damage assessment algorithm arose naturally from the questions of how to deal with sparseness in measured data and how to provide a reasonable evaluation of damage with noisy measurements. Both sparseness and noise are the properties associated with the condition of measured data. The sparseness is more related to the quantity of measured data, while noise indicates the quality of measured data.

1.4.1 About Severe Sparseness in Measured Data

The sparseness in measured data is critical when the number of measurement locations are few compared with the number of degrees of freedom in the finite element model of the structure. When measured data are so sparse that the resulting system of equations in the parameter estimation process becomes underdetermined, none of the available algorithms seems to be successful in providing a satisfactory solution. To overcome the sparseness, three schemes can be considered.

The first scheme consists of simplifying the structural model itself to reduce the number of degrees of freedom (Freed and Flanigan 1991; Hoff 1989; Kammer, *et. al.* 1989; Kammer and Flanigan 1991). This scheme is usually associated with static or dynamic condensation methods (Guyan 1965; Irons 1981; Paz 1984) which are useful in system identification methods with incompletely measured data. They studied the appropriateness of reduced analytical models compared with test data. Hoff (1989) reduced a large finite element model to a subspace of significant eigenfrequencies. The size of the subspace was chosen such that the measured frequencies match accurately with the results from the large analytical model. This approach might be good for certain purposes, but eventually this process makes it difficult to pin-point damaged portions in a structure correctly. Of course, the use of a reduced structural model might make the damage detection problem simpler and give a rough idea of the existence of damage in the structural system somehow, but it can not be useful for damage detection algorithms because most damage occurs in a few local portions of the structure.

The second scheme consists of expanding the measured displacement or eigenvector (Berman and Nagy 1983; Smith and Beattie 1990; Zak 1983; Zimmerman and Kaouk 1992). Basically, they expanded the measured data to the dimension of the analytical model, instead of reducing the dimension of the structural model. The scheme to expand measured data varies from one method to the next, but they have some common features; (*1*) the methods require a modification either in the mass matrix or the measured eigenvectors to satisfy the mass orthogonality condition, if modal data is used, and (*2*) they require a technique to compute the displacements or eigenvectors of the unmeasured degrees of freedom. The expanded responses definitely contain approximation errors in addition to the noise error in measurements. Most sensitivity methods in damage assessment algorithms as classified in section 1.3 use either of the model reduction or model expansion scheme. Kim and Bartkowicz (1993) developed a model adjustment technique by combining both schemes.

The third scheme to overcome the sparseness problem is the use of parameter grouping (Hjelmstad, *et. al.* 1990). Some similar ideas of subsystem modeling are introduced in the references (Lim 1990; Natke 1989; Natke and Cempel 1991). The main idea behind the parameter grouping is that the number of unknown parameters can be reduced by grouping similar parameters together without modifying the already well-defined structural finite element model itself. This scheme is tempting because most civil structures are constructed with a limited number of different types of members which have the same member properties. This scheme does not require any modifications in measured data as the eigenvector expansion scheme nor any modifications in the structural finite element model as the model reduction scheme. The only problem for the scheme is that the parameter grouping must

be known in advance. Otherwise we must have an algorithm capable of searching for the best grouping. For damage detection problems, the baseline group case can be assumed as known, because damage is detected by comparing certain properties between the baseline case and the current case. However, this parameter grouping scheme cannot be used directly for a damage localization algorithm, because most damage usually exists in a few members within certain parameter groups each of which may consist of a large number of structural members.

Among the three possible schemes to overcome the sparseness, the last scheme with parameter grouping seems to be the most attractive, because it does not require any modifications in either the measured data or in the finite element model. However, the parameter grouping scheme alone cannot localize damage. If the parameter groups containing damage can be subdivided to separate damaged members from undamaged ones by consecutive updates of the parameter groups, then we may finally reach at a parameter group case which can clearly identify all the damaged members. The basic concept of updating parameter groups is graphically illustrated in Fig. 1.1.

Which parameter group should be subdivided can be decided by comparing identification error values among possible subgrouping cases. Some termination criteria should also be developed to avoid excessive refinement. The number of degrees of freedom in the finite element model is unchanged when parameter groups are subdivided sequentially. The only variable in the proposed parameter group updating scheme is the number of parameter groups. Even if the application of the parameter group updating scheme for localizing damage in a structural system seems to be promising, no research has been published in the literature. Details of our proposed scheme are discussed in *Chapter Two*.

1.4.2 About Noise in Measured Data

Noise in measured data is inevitable and is random in nature. Therefore, a statistical description of the estimated parameters is desirable. Agbabian, *et. al.* (1991) introduced some interesting damage indices obtained from a time-domain identification procedure. They demonstrated the usefulness of

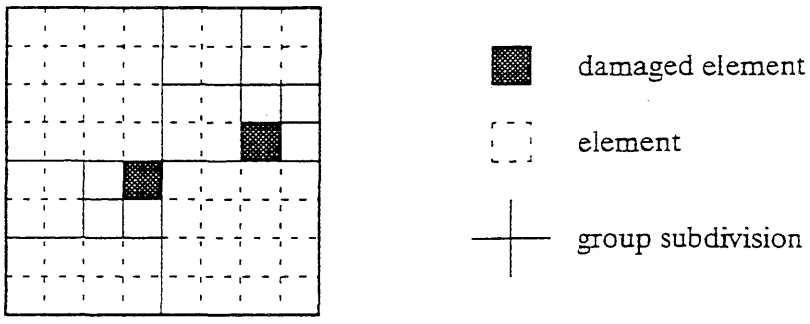

Fig. 1.1 Conceptual drawing of damage localization by updating parameter groups

some statistical properties in detecting damage with a simple mathematical model whose order is reduced to be compatible with the number of sensors used. Few other algorithms have used statistical properties in detecting and assessing damage in structural systems. Many available algorithms compute the sensitivity of the parameters rather than the statistical variability, and they use those sensitivities for detecting damage. Some researchers have eliminated the insensitive parameters from the damage detection process by fixing their values, simply because they might not be able to verify damage in those insensitive members by their algorithms when measured data are noise-polluted and sparse. It may be true that the members with the insensitive parameters are difficult to correctly identify, but it cannot be true that those members cannot be damaged or are always lightly damaged compared with the members with sensitive parameters. Therefore, it is necessary to develop an algorithm which can detect and assess damage of a member by considering its sensitivity with respect to the test conditions.

To compute some statistical properties of the parameters, it is necessary to measure or create the information needed. For time-domain test data, it may be possible to collect a number of data sets by selecting a number of time windows (Banan and Hjelmstad 1993). For static or modal response, data sets may be collected by repeating a test under nominally identical condition. However, since it will be difficult in practice to obtain a sufficient amount of data from field tests to compute the sensitivity of parameters, it is proposed herein to create artificial data sets by adding random noise to the measured data. By using a number of created data sets a significance of the computed statistical properties can be achieved. The idea is presented graphically in Fig. 1.2. From a number of perturbation iterations, mean and standard deviation for each member parameter can be obtained and used to determine damage. The perturbation iteration scheme can be applied not only directly to the existing structure but also to the baseline structure. Damage may be directly detected by the relative statistical evaluation of the existing structure. However, a more reliable verification of damage can be achieved by the statistical evaluation of the baseline structure in addition to that for the existing structure. Details of the measured data perturbation scheme are described in *Chapter Two*. The procedure of developing the statistical properties from the baseline structure and its use of detecting damage in the existing structure will be demonstrated through simulation studies in *Chapter Three*.

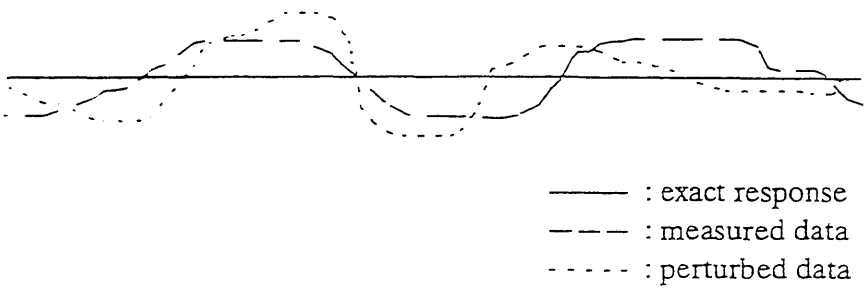

Fig. 1.2 Conceptual drawing of the application of perturbation to noisy measured data

1.5 Objective and Scope

The objective of the research is to develop a new damage assessment algorithm that can detect and assess damage even when measured data are sparse and noise-polluted. The method is a non-destructive diagnostic technique for structures that can be used in making decisions of repair and rehabilitation of the structures. To localize damage, a parameter group updating scheme is proposed. To examine the sensitivity of each parameter and to provide statistical basis for assessing damage in a structural system when measured data are polluted by noise, a data perturbation scheme is proposed. For the simulation studies, the Monte Carlo simulation method is applied to simulate measured data with uniformly generated random noise. The types of measured data considered in the current research are limited to static and modal response. For the purpose of illustration, simulated cases are selected with sparsely measured data so that the system of equations are underdetermined if a proper technique is not used. The amplitude of applied noise has been selected within practical ranges for the simulation studies.

Some assumptions have been used in developing the damage assessment algorithm, and those assumptions may affect the accuracy and behavior of the algorithm. Basic assumptions for the current damage assessment algorithm are: (*1*) a refined finite element model for the structure is defined, (*2*) the baseline undamaged properties of the structure are known, (*3*) the amplitude of noise in measurements is known, (*4*) for the modal response, mass is not subject to damage, (*5*) the stiffness of each member may not increase from the previous investigation or from the baseline value without any intervening repair, and (*6*) only linear structural systems are considered. The baseline structure is defined as the structure whose finite element model is the same as the existing structure, but whose member properties are known from a previous test.

The manuscript consists of five chapters and one appendix. *Chapter Two* provides the fundamental ideas involved in developing a new damage assessment algorithm. The parameter group updating scheme is explained in detail. *SME* (squared model error) is proposed to provide a termination criterion for the sequential subdivision of parameter groups, and the measured data perturbation scheme is developed to provide a statistical basis for detecting and assessing damage in structural systems. From the perturbation test, two damage indices for each member are computed and used to detect damage. In *Chapter Three*, simulation studies are carried out for static response. A simulated single component damage in a two-dimensional bowstring truss structure is studied. Through the simulation studies, the procedure of detecting and assessing damage is illustrated. Some additional simulation cases for static responses are summarized in *Chapter Four* to demonstrate the usefulness of the developed damage assessment algorithm for various damage cases. In *Chapter Five*, real test data are used to identify the actual location of a crack and its properties in a cantilever beam. The experiment was carried out by Rizos, *et. al.* (1990). Three natural frequencies and the corresponding modal displacements from a cracked beam were measured, and some of the material and sectional properties are provided. They measured modal displacements at limited locations. The real case study demonstrates the effectiveness of the algorithm and the usefulness of the statistical properties in detecting

the actual crack and assessing the member properties of the cracked cantilever beam. *Chapter Six* summarizes some conclusions obtained from the case studies, and discusses future work. *Appendix* illustrates the decomposition of the element stiffness matrix by constitutive parameter functions and kernel matrices.

Chapter Two

A Damage Assessment Algorithm

This chapter describes the development of a new damage assessment algorithm. The parameter estimation method of Banan and Hjelmstad (1993) is implemented in the damage assessment algorithm as the main tool for estimating structural parameters. Some existing and new ideas used in the algorithm are introduced and explained. As pointed out in *Chapter One*, the main motivation for developing a new damage assessment algorithm is the fact that few of the available damage detection and assessment algorithms seem to be successful in dealing with noisy and sparsely measured data.

Damage is defined herein as the reduction of a structural parameter from its baseline value. In determining damage by an identification process, the first task is to furnish a reasonable answer to the question: *does an estimated parameter reduction indicate a real damage or is it the result of noise in the measurements?* Because noise in measured data is inevitable in testing structural systems, the most reasonable way of explaining the uncertainty in the estimated parameters is by examining statistical aspects of the behavior of the parameters. The statistical descriptors can also be used to detect and assess damage in structural systems. After damage is detected and quantified by statistical evaluation, the next important task is to clarify *how much reduction can be considered as serious*. The decision on damage severity may not be answered directly by the reduction in parameters. The decision may be more dependent on the engineer's judgement based on his or her experience and through analytical studies. Engineers may have to verify the effects of the parameter reduction on the global behavior of the structure under various loading conditions. Therefore, the role of a damage assessment algorithm should be limited to providing the fundamental information that can qualify damage in a useful form that can help an engineer make a decision about the necessity of repairing or rehabilitating a structure.

Localization and assessment are the two main steps for determining damage in a structural system. As discussed in section 1.2, localization can be described as a process of isolating damaged parts in a structural system, and assessment is the process of evaluating damage with the estimation results from the localization process. The processes of damage localization and damage assessment are separately developed in the proposed damage assessment algorithm. If sufficient measured data are provided so that each group is composed of a single member, the damage localization process is not neces-

sary because each member parameter can be estimated individually and can be evaluated for damage. However, in general, the use of a parameter grouping scheme and thus the use of a damage localization scheme is required. Damage detection and assessment process can be carried out after a number of damage localization processes are completed.

To localize damage, a parameter group updating scheme is proposed. This scheme searches for an optimal group case that can produce the minimum error in estimating parameters within the allowable range of the number of groups. Starting from the known grouping with the baseline properties, the grouping is modified by subdividing suspicious parameter groups hierarchically. To provide a useful information of the estimated parameters when the measured data are polluted with noise, a number of sets of estimation results should be available from various sets of test data. To iterate the localization process with artificially created sets of test data, a data perturbation scheme is proposed. Each perturbation iteration is carried out by imposing additional random error to the measured data. Damage indices for each member parameter are calculated from a number of measured data perturbation iterations and can be used to detect and assess damage in structural systems. The process of determining damage by using the computed damage indices is illustrated through the simulation studies in *Chapter Three* and *Chapter Four* for static response. In *Chapter Five*, the usefulness of the developed algorithm is tested with real modal experimental data from a cracked cantilever beam.

2.1 Element Parameter Estimation Method

The damage assessment algorithm developed in this chapter requires a parameter estimation method to estimate group parameters at each localization step. The estimated group parameters are transformed into each member parameter, and the deduced member parameter is compared with the baseline value to determine damage for the member. The output error estimator proposed and tested by Banan and Hjelmstad (1993) is selected as the parameter estimation tool. When the measured data are complete with respect to the degrees of freedom in the finite element model, equation error estimators may be simpler to use, because they do not require the use of inverse models as output error estimators and the number of unknowns are the same for both equation error and output error estimators. However, when the measured data are sparse, the output error estimators require a lower dimensional space in estimating parameters due to the reduced number of unknowns. Banan and Hjelmstad (1993) observed that their output error estimator has an acceptable amount of bias for a wider range of noise amplitude than does the equation error estimator.

In this section, the output error estimators from the equilibrium equation for static response and the generalized eigen-equation for modal response are briefly summarized. The method of decomposing element parameters from the structural stiffness matrix, and the parameter grouping scheme to reduce the number of unknowns are also reviewed. Details of the parameter estimation method and other important aspects are referred to the references (Banan and Hjelmstad 1993; Clark 1989; Hjelmstad, *et. al.* 1990).

2.1.1 Static Response

The output error for the static response can be defined by:

$$e_i^s(x) = QK^{-1}(x)f_i - \hat{u}_i \qquad i = 1, ..., nlc \tag{2.1}$$

where $e_i^s(\hat{n}_d \times 1)$ is the output error vector from the static equilibrium equation for the ith load case, $K^{-1}(n_d \times n_d)$ is the inverse of the stiffness matrix, $x(n_p \times 1)$ is the vector of parameters, $f_i(n_d \times 1)$ is the equivalent nodal force vector for the ith load case, nlc is the number of applied load cases, n_d is the number of degrees of freedom, $\hat{n}_d$ is the number of measured degrees of freedom in the finite element model of a structure, n_p is the number of unknown parameters, and $Q(\hat{n}_d \times n_d)$ is a Boolean matrix that extracts the measured response $\hat{u}_i(\hat{n}_d \times 1)$ from the complete displacement vector $u_i(n_d \times 1)$ by the relationship of $\hat{u}_i = Qu_i$. The possibility of different measuring locations for each load case is ruled out for convenience in the current work. We also assume that the number of measured degrees of freedom $\hat{n}_d$ is the same for all the load cases.

Eq. (2.1) can be formulated from the governing static equilibrium equation of a structure subjected to nlc static load cases:

$$K(x)u_i = f_i \qquad i = 1, ..., nlc \tag{2.2}$$

In the current study, the force vectors are assumed to be error-free and linearly independent. Therefore, the only source of error in the output error estimator is from the measured displacements. Since the unmeasured components in displacement vectors are completely excluded from consideration, the only unknown variables in the output error estimator become the physical parameters $x(n_p \times 1)$.

To separate the physical parameters from the stiffness matrix, the kernel matrix concept has been proposed (Clark 1989; Hjelmstad, *et. al.* 1990). The decomposition of parameters can be mathematically expressed as:

$$K(x) = \sum_{m=1}^{n_e} \sum_{p=1}^{\Pi_m} z_p^m(x) G_p^m \tag{2.3}$$

where n_e is the number of structural members in the finite element model, Π_m is the number of different parameter types, $z_p^m(x)$ is the pth constitutive function of the parameters x in the mth member, and $G_p^m(n_d \times n_d)$ is the pth globalized kernel matrix in the mth member. Generally the constitutive functions involve only parameters associated with the mth member. When the stiffness matrix is linear with respect to the parameters, $z_p^m(x)$ simply is equal to x_p^m of the pth parameter type in the mth member. The topology of the structure is preserved by this decomposition. Only the constitutive parameters $x(n_p \times 1)$ alter depending on the test results.

The unknown parameters are obtained by minimizing an objective function formulated by the output error vector defined by Eq. (2.1). A constrained nonlinear optimization problem is solved for the optimal parameters by minimizing the objective function of the output error.

$$\begin{aligned} &\underset{x \in \mathbb{R}^{n_p}}{Minimize} && J(x) = \frac{1}{2}\sum_{i=1}^{nlc} a_i \parallel QK^{-1}(x)f_i - \hat{u}_i \parallel^2 \\ &s.t. && \underline{x} \le x \le \bar{x} \end{aligned} \tag{2.4}$$

where $\underline{x}(n_p \times 1)$ and $\bar{x}(n_p \times 1)$ are the lower and upper bound vectors, and a_i is the weight factor for the ith load case. The gradient vector and Hessian matrix can be obtained from Eq. (2.4) to solve for optimal values of the parameters. For the output error estimator of the static response, the identifiability criterion was determined by Banan and Hjelmstad (1993) as follows:

$$(nlc \times \hat{n}_d) \ge n_p \tag{2.5}$$

This relationship indicates how many load cases and nodal displacements should be applied and measured for the identification problem to provide a reasonable solution. If this equation is not satisfied, the parameter estimates are completely unreliable. As reviewed in section 1.4.1, several schemes can be considered to overcome the deficiency, especially when the measured data are sparse. Among them, the parameter grouping scheme is selected as the most attractive.

Without grouping parameters, the total number of parameters can be computed as the sum of different types of parameters in each element:

$$n_p = \sum_{m=1}^{n_e} \Pi_m \tag{2.6}$$

2.1.2 Modal Response

The generalized eigenvalue problem for modal analysis of a structure subjected to *nmd* measured mode cases can be expressed as:

$$K(x)\phi_i = \lambda_i M\phi_i \qquad i = 1, \ldots, nmd \tag{2.7}$$

where $K(n_d \times n_d)$ is the stiffness matrix, $M(n_d \times n_d)$ is the mass matrix, λ_i is the ith measured eigenvalue or the square of the measured natural frequency ω_i^2, and $\phi_i(n_d \times 1)$ is the modal displacement vector for the ith natural frequency. In the developed damage assessment algorithm, the mass components are assumed not to change or at least the variation of mass components from the baseline property is assumed to be known. Therefore, the only unknowns are again the stiffness parameters $x(n_p \times 1)$ for the modal case as for the static response.

By dividing the known and unknown information, Eq. (2.7) can be transformed to:

$$\left[K(x) - \lambda_i\left[\hat{O}\ \overline{M}\right]\right]\phi_i = \lambda_i\left[\hat{M}\ \overline{O}\right]\phi_i \tag{2.8}$$

where $\hat{M}(n_d \times \hat{n}_d)$ and $\overline{M}(n_d \times \overline{n}_d)$ are the submatrices of mass components corresponding to the measured and unmeasured degrees of freedom, and $\hat{O}(n_d \times \hat{n}_d)$ and $\overline{O}(n_d \times \overline{n}_d)$ are the zero matrices corresponding to the measured and unmeasured degrees of freedom, respectively. By defining a pseudo stiffness matrix $K_i^*(n_d \times n_d)$ and a pseudo force vector $f_i^*(n_d \times 1)$, the equation can be transformed into an equation similar to the static equilibrium equation as:

$$K_i^*(x)\phi_i = f_i^* \qquad i = 1, ..., nmd \tag{2.9}$$

where $K_i^*(x) = K(x) - \lambda_i[\hat{O}\ \overline{M}]$ and $f_i^* = \lambda_i[\hat{M}\ \overline{O}]\phi_i$. Even though the equation seems to be similar to the static case as Eq. (2.2), some differences can be observed. The first difference is that the pseudo stiffness matrix also varies depending on the measured eigenvalue and thus should be computed for each mode. The second observation is that the pseudo force vector $f_i^*(n_d \times 1)$ is not error-free because both of the natural frequencies and the modal displacements may contain measurement error. In addition, the pseudo force vectors are not necessarily linearly independent, because the linear independence of the complete modal displacement vectors does not guarantee the linear independence of the measured components of the modal displacement vectors. The possibility of linear independence of the pseudo force vector $f_i^*(n_d \times 1)$ may increase by measuring more degrees of freedom $\hat{n}_d$.

The output error for the modal response is defined from the pseudo equilibrium equation by:

$$e_i^m(x) = QK_i^{*-1}(x)f_i^* - \hat{\phi}_i \qquad i = 1, ..., nmd \tag{2.10}$$

where $e_i^m(\hat{n}_d \times 1)$ is the output error vector from the pseudo equilibrium for the ith mode case, $K_i^{*-1}(n_d \times n_d)$ is the inverse of the pseudo stiffness matrix, and $\hat{\phi}_i(\hat{n}_d \times 1)$ is the measured components of the modal displacement vector for the ith mode case. The definition of the Boolean matrix $Q(\hat{n}_d \times n_d)$ is similar to the static case by the relationship of $\hat{\phi}_i = Q\phi_i$. The separation of constitutive parameters from the stiffness matrix using the kernel matrix concept and the formulation of a constrained nonlinear optimization problem are similar to the static case. The identifiability criterion for the modal measured data is defined by:

$$(nmd \times \hat{n}_d) \geq n_p \tag{2.11}$$

2.1.3 Parameter Grouping Scheme

The number of parameters can be reduced by grouping similar parameters together without changing the finite element model itself. Through grouping parameters, the number of unknowns can

be reduced to a certain level where the parameter estimation problem can be solved reliably. The maximum allowable number of group parameters is limited by Eq. (2.5) or Eq. (2.11). This grouping scheme may be useful for civil structures because most of them are composed of a limited number of different types of member properties. One important point is that the parameter grouping should be based on prior knowledge of the structure to provide correct estimation results.

When the parameter grouping scheme is applied, the stiffness matrix defined by Eq. (2.3) can be reformulated as:

$$K(x) = \sum_{g=1}^{M_g} \sum_{p=1}^{\Pi_g} \sum_{m \in \Omega_g} z_p^m(x) G_p^m \tag{2.12}$$

where M_g is the number of groups, Π_g is the number of constitutive parameter types in the gth group, and $G_p^m(n_d \times n_d)$ is the pth kernel matrix in the mth member composing the gth group Ω_g. Thus, the number of total unknown parameters n_p can be computed by:

$$n_p = \sum_{g=1}^{M_g} \Pi_g \tag{2.13}$$

If all the members in a structure are simply modeled by one element type, Eq. (2.13) can be modified by $n_p = M_g \times \Pi_g$. As a structural model becomes complex, the reduction in the number of unknowns will be more apparent as far as the system is identifiable.

A similar idea of reducing the number of unknowns by decomposition is by the substructure approach (Lim 1990; Natke 1989). The substructure technique is popular in the analysis of very large finite element systems, where the technique can demonstrate economical advantages. By decomposing the stiffness matrix by submatrices and multipliers, the unknown parameters can be the multipliers for the submatrices. Natke (1989) used the multipliers as the error factors to determine damage. Some drawbacks of the substructure modeling are discussed in some references. Cook, *et. al.* (1989) indicated the loss of accuracy produced by substructuring in dynamic analysis due to the condensation process of interior degrees of freedom to the substructures. In static analysis no approximation is produced by substructuring. A substructure must be a connected region of the structure, and the subregion stiffness may comprise stiffnesses of varying characters. Because both of these problems may conflict with the prior knowledge of the structure, Hjelmstad, *et. al.* (1990) concluded that the parameter grouping scheme would make more physical sense and cures the two ills of the substructure model. One of the main advantages of substructuring is the computational efficiency especially when a structure contains many repetitions of the same form. However, for detecting damage in the structure, this merit cannot be achieved any more because damage in each substructure should be investigated individually.

2.2 Damage Localization

The localization process is the first important part of the developed damage assessment algorithm. A successful separation of damaged parts from the undamaged members is the key to estimate parameters close to their actual values when the parameter grouping scheme is used. To localize damage in a systematic manner, the parameter group updating scheme is proposed herein. The main idea of the scheme is to separate damage parts in the finite element model by subdividing parameter groups sequentially. At each subdivision a new set of parameter groups and their group parameters are established and estimated. The group parameter estimation is carried out by the parameter estimation method summarized in section 2.1. By subdividing a suspicious parameter group, parameters become more sensitive and more representative of the actual values. Because several damaged regions with different levels of severity may coexist in a structural system, the subdivision should be continuously carried out until all the damaged members are completely extracted. As a tool to terminate the continuous process of the subdivision at a certain point, the squared model error (*SME*) is proposed. *SME* controls the number of group parameters which may get too large otherwise.

2.2.1 Parameter Group Updating Scheme

The parameter grouping for the undamaged baseline properties is assumed to be known. When a structure is damaged, the parameters estimated with the known baseline grouping may not detect the damaged members correctly, simply because damage is usually hidden within certain parameter groups with contributions from many members. Group parameters containing damaged members may pollute the estimation results. Only by separating those damaged members from the undamaged ones does the estimation error reduce and yield parameters close to the actual values.

The scheme proposed herein is to subdivide a suspicious parameter group hierarchically starting from a known baseline grouping. The possibility of pinpointing the locations of damage in a structure by such a sequential grouping scheme was mentioned by Hjelmstad, *et. al.* (1990). They introduced a general idea of the procedure without numerical proofs. This idea is modified a little for the current algorithm.

In developing a parameter group updating scheme, two important features are considered. The first problem regards the question of *which subset should be divided?* In selecting the candidate subset that should be subdivided in the current grouping state, the simplest measure may be the error between the estimated value and the baseline value of a subset as used by Natke (1989) and Natke and Cempel (1991). In other words, a subset whose estimated parameter is the most distant from the baseline value can be selected as the candidate subset. However, when noise exists in the measured data, it cannot be concluded that a subset may contain damage simply because the deviation is the biggest. Due to noise in measured data some subgroups may behave as if they contain damage even though actually they do not. If insensitive but undamaged members exist within a group, the group parameters may show large deviations from the baseline values, and thus give the impression that damage really exists in that group. The sensitivity of a group parameter may increase if the group is subdivided as pointed out by Natke (1989). However, the seemingly reduced estimation error is not only due to the

fact that the hidden damage may affect the estimation results but also due to the fact that the increased number of parameters may reduce the estimation error because the model has more flexibility. The estimation error may decrease remarkably only when damage is clearly separated from undamaged parts. What, then, is the most reasonable measure to determine the candidate subset?

In the current algorithm, a candidate subset is sought by comparing minimized error function values each of which can be computed when a possible candidate subset is subdivided. Possible candidate subsets are with the deepest group level in a hierarchical order, and the candidate subset is the one with the smallest error function value among them when each is divided. By subdividing the candidate subset, the parameter group is updated with a new set of parameter grouping. The level of grouping is determined in a hierarchical manner and updated at each iteration of subdivision. In searching for a candidate subset, more than two subdivision cases can be compared concurrently. This way of searching for the candidate subset definitely requires extra computation compared with the direct selection by the deviation measure. However, this measure is a more reliable and robust way of searching for the right direction in localizing damage. Subsets need not always be divided in half. If measured information is adequate, a candidate subset can be divided completely by constructing each subgroup with a single member. Details of group updating are illustrated in section 2.2.4 with an example.

The second consideration in a sequential subdivision scheme is the *termination criterion* for the group parameter estimation process and the subdivision process. If the estimated group parameters are sure to indicate non-damage in the group, or if the value of a group parameter is not disturbed by consecutive subdivisions of the other parameter groups, the subset need not be subjected to further modification. The parameters of such subsets can be fixed at their baseline values or their current estimated values. Any subset can be excluded from further subdivision and from the parameter estimation process if its parameters change only within a pre-determined tolerance. An unintentional advantage of fixing parameter values is that the number of unknowns is reduced by excluding such parameters from further estimation. A deeper level of subdivision can then be investigated for the same quantity of measured data. Another important criterion for the subdivision is to decide when to stop the whole process. In providing such a termination criterion, a flexibility in the sequential subdivision should be guaranteed. In addition to the forward subdivision process, a hierarchical backward process should be also allowed. When no more subdivision can be achieved from the deepest level of subgrouping, the process should be able to retreat one step back to a parent level of subgrouping. After all the possible subdivision cases are investigated and when no more subdivision is possible, the process should stop.

A similar idea of a hierarchical halving scheme was also introduced by Natke (1989) and Natke and Cempel (1991). They used subsystem modeling and modification factors to evaluate damage. They suggested that significant deviations of the estimated modification factors from unit values would indicate damaged subsystems. A subsystem that contains the smallest modification factor is subjected to a hierarchical halving for localizing damaged regions. When no observable deviation in

the modification factors is noted, a continuous halving of the submodels is carried out to increase the sensitivity. The insensitivity may happen when a considered submodel is large in size but the effect of damage on the estimation is small. The updating is repeated with the new submodels by leaving the remaining submodels as they were. Natke (1989) compared those factors only for sensitive parameters to determine damage. A disadvantage is that this method may leave estimation errors in the remaining submodels permanently because the factors of the remaining submodels are obtained before a submodel containing damage is subdivided and thus the smeared estimation error remains. Another concern is that the number of subsystems seems to increase continuously without any stopping criterion. Some other drawbacks of the subsystem modeling are already pointed out in section 2.1.3.

Another interesting idea for isolating damaged members is to find the optimal grouping that provides the smallest estimation error. The best grouping may be obtained simply by enumerating all the possible grouping cases within the allowable limit of number of groups. However, to enumerate all the cases, the number of investigation cases will be extremely large for complex structural models. To diminish the computational burden, Dzemyda and Senkiene (1990) solved a combinatorial optimization problem to find a global optimal parameter grouping. They attempted to solve the problem with a simulated annealing strategy to find a global optimal point. A difference in their problems from damage localization problems is that no prior information regarding the number of groups and group size is provided. In addition, they didn't allow a flexibility in the number of groups and only tried different group cases with a fixed number of groups to obtain optimal group parameters. For damage localization problems, however, the optimal number of groups cannot be known until all the damaged members are separated. They dealt with the problem of extremal parameter grouping that is not actually related to the damage localization problems. However, more research may be interesting to verify the usefulness of their approach for a damage localization algorithm with the prior knowledge of the baseline properties.

2.2.2 A Termination Criterion: Squared Model Error (*SME*)

The subdivision of parameter groups implies the variation in the number of groups, and thus indicates a continual change in the parameterized model. The values of parameters change with different parameterizations. We must devise a tool to control the number of groups in the selection of the best model. A change of parameterization does not imply a change in the finite element model of the structure. When we face the parameterized model selection problem in addition to the objective error minimization problem, the objective function as defined by Eq. (2.4) alone does not provide a complete for the best model. An additional term, which penalizes the variation in the number of groups and thus the number of parameters, should be also considered to select an optimal grouping case. There are some useful definitions to compare errors from the difference in the number of parameters (Akaike 1972; Barron 1984). They developed procedures for selecting the best model by ranking different model structures. Barron (1984) proposed the predicted squared error (*PSE*) as the sum of the original squared error and an overfitting penalty term, and Akaike (1972) introduced the finial predic-

tion error (*FPE*) by directly multiplying a penalty term to the squared error. If their definitions are modified to be applicable for the current parameter model selection problem, the following definitions obtain:

$$\begin{aligned} PSE(x) &= \bar{J}(x) + 2\sigma_p^2 \frac{n_p}{N^*} \\ FPE(x) &= \frac{N^* + n_p}{N^* - n_p} \bar{J}(x) \qquad\qquad x \in \mathbb{R}^{n_p} \end{aligned} \tag{2.14}$$

where σ_p^2 is an estimate of the true error variance that does not depend on the particular parameter model being considered, $\bar{J}(x)$ is a normalized objective function that has the same order of error as the penalty term of $PSE(x)$, n_p is the number of unknown group parameters, and N^* is the upper limit number of unknown parameters. From the definitions, some interesting behaviors of the two squared errors can be observed. First, $PSE(x)$ estimates the two sources of error separately, while $FPE(x)$ combines them in a single term. Since the value of the penalty term is the same order as $\bar{J}(x)$, the influence of the penalty term on $PSE(x)$ linearly increases, but $FPE(x)$ increases rapidly as n_p approaches N^*. In both definitions, when n_p is small $\bar{J}(x)$ controls the error values, but when n_p becomes relatively a big number the penalty terms control the errors. In other words, $\bar{J}(x)$ tends to reject overly simple models, and the penalty terms tend to reject overly complex models.

For the current damage localization algorithm, a modified definition is proposed by considering the limited range of the number of group parameters. A nonlinear constrained optimization problem is formulated to minimize the squared model error (*SME*) rather than the objective function $J(x)$ itself.

$$\begin{aligned} &\underset{x \in \mathbb{R}^{n_p}}{Minimize} && SME(x) = 2\, J(x) + n_{lmt} \left(\frac{n_p}{n_{sum} - n_p}\right)^2 \bar{\sigma}^2 \\ &s.t. && \underline{x} \le x \le \bar{x} \end{aligned} \tag{2.15}$$

where $\bar{\sigma}^2$ is the prior estimate of the averaged random noise variance, n_p is the number of unknown group parameters as defined by Eq. (2.13), n_{lmt} is the upper limit number of unknown parameters as defined in the left-hand-side of the inequality equation of Eq. (2.5) or (2.11), and n_{sum} is the sum of the number of different types of parameters in each member of a structure as defined by n_p in Eq. (2.6). The prior estimate $\bar{\sigma}^2$ can be computed from the assumed noise distribution and the known noise amplitude for each perturbation iteration. If n_{min} denotes the minimum number of allowable group parameters determined by the baseline information, the range of the number of unknown group parameters n_p can be defined by:

$$n_{min} \le n_p \le \text{MIN}\left[n_{lmt}\,, n_{sum}\right] \tag{2.16}$$

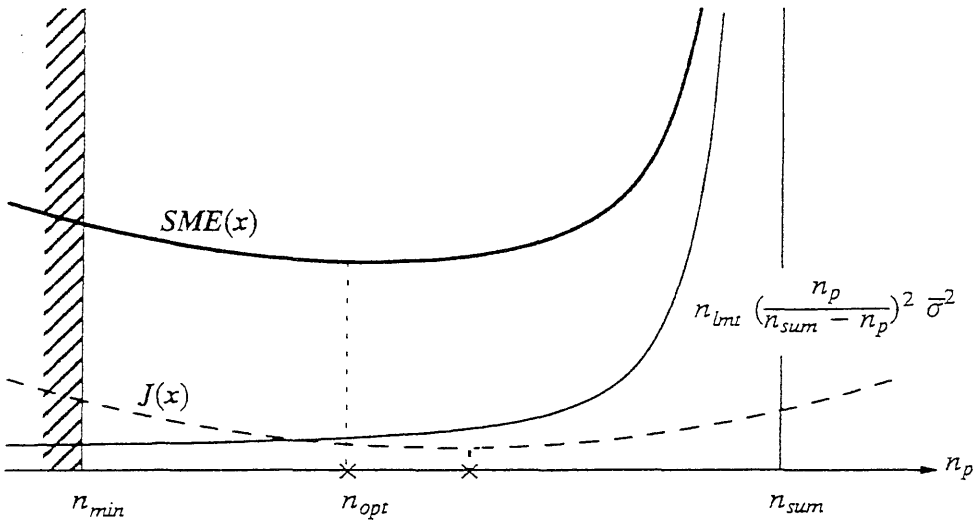

Fig. 2.1 Conceptual drawing of the relationship between the error terms in Eq. (2.15)

The two terms in the right-hand-side of Eq. (2.15) are designed to have the same order of error magnitude. The objective function may or may not have the minimum point within the allowable range of the number of unknown parameters. However, *SME* would have a minimum within the range or at either bound, because the penalty term is designed to increase rapidly as the number of unknowns n_p approaches n_{sum} as shown in Fig. 2.1. In the figure the value of n_{lmt} may locate at either side of n_{sum} depending on the amount of measured data, which decides the upper bound of the number of unknowns. However, the number n_{sum} is a fixed value after a finite element model for the structure is once decided. That is the main reason why n_{sum} is used as a reference in the penalty term. Like the behaviors of *PSE* and *FPE*, when n_p is small *SME* is controlled by $J(x)$, but as n_p increases *SME* is governed by the penalty term. Therefore, the algorithm will stop at a certain point n_{opt} where two competing terms make $SME(x)$ minimal. The minimization problem of Eq. (2.15) prevents the optimization problem from pursuing a complicated model, especially when the given measured data are polluted by noise. In other words, *SME* prefers making a model as simple as possible.

2.2.3 Damage Localization: Algorithm

The existence of the prior knowledge of the baseline property provides the initial grouping and its initial parameters for the parameter group updating algorithm. With the given baseline property, the proposed parameter group updating algorithm can be summarized in Table 2.1. In the algorithm, step 3 describes a local termination criterion to remove a parameter from further modification if the parameter varies within a given tolerance from the previously estimated value. Step 4 is to search for a candidate subset by comparing minimized *SME* values of all the possible candidate subsets and to stop the whole localization process if no more alternative subdivision is available. After the candidate subset is determined and subdivided, the grouping is updated and its parameters are newly estimated. As the parameter grouping is updated, the group level for each updated group is also modified to keep the hierarchical order of grouping. A brief overview of the algorithm is shown schematically for the *i*th static load case in Fig. 2.2.

Table 2.1 Damage Localization Algorithm

1. *a*. Set up the initial grouping $\Omega^{(o)}$ and its parameters $x^{(o)}$ based on the baseline information Ω^*, x^*.
   b. Set $k = 1$.
2. Estimate parameters $x^{(1)}$ by minimizing $SME(x^{(1)})$.
3. *a*. Set *smemin* = $SME(x^{(k)})$.
   b. If $|x_p^{(k)} - x_p^{(k-1)}| \leq$ tolerance, remove the pth parameter from further estimation.
   c. If all the parameters are fixed, **STOP**.
   d. Otherwise, update $\Omega^{(k)}$ and $x^{(k)}$.
4. *a*. Set *smeold* = *smemin*.
   b. Determine the deepest level of grouping.
   c. If all the groups have been investigated, **STOP**.
   d. Otherwise, determine the candidate subset.

```
do i = 1, nset
   · subdivide the ith possible candidate subset
   · estimate x_i^(k) by minimizing SME(x_i^(k))
   · if ( SME(x_i^(k)) < smemin ) then
       smemin = SME(x_i^(k))
       icandidate = i
     endif
continue
if ( smemin < smeold ) then
   · update Ω^(k) and x^(k) by subdividing the subset icandidate
   · update group level
else
   · return to the parent grouping
endif
```

   e. Set $k = k + 1$.
   f. Go to 3.

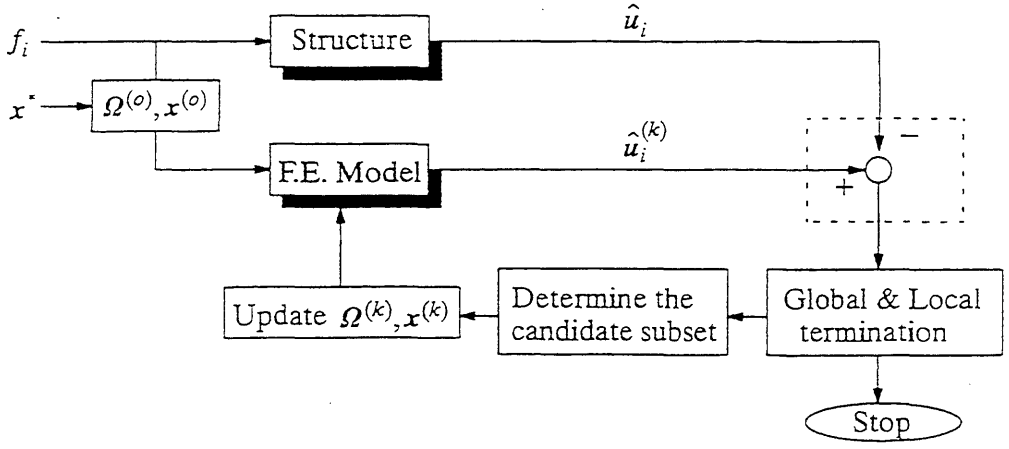

Fig. 2.2 Schematic representation of damage localization algorithm using the parameter group updating scheme for the ith static load case

2.2.4 Damage Localization: Illustration

To illustrate the damage localization process, a simple example is presented graphically in Fig. 2.3. For the example, a damage case is simulated with a structure that has 12 elements, each of which has one parameter. We assume that two different static load cases are applied and displacements are measured at three different locations. Therefore, we find that $n_{sum} = 12$ from Eq. (2.6) and $n_{lmt} = 6$ from Eq. (2.5). The undamaged baseline structure had a uniform stiffness property, the initial grouping for the localization process is with a single group, and the number of unknowns can vary within the range of $1 \leq n_p \leq 6$ from Eq. (2.16).

Fig. 2.3 shows how the damage localization proceeds by determining a candidate subset at each grouping step. Step 1 is the initial grouping with the baseline property. The group level starts from 0 as denoted inside the box representing a group. Since the number of elements is larger than $n_{lmt} = 6$, the initial group cannot be divided completely into 12 subgroups, and instead it is divided in half as in step 2. The newly created grouping has a smaller *SME* value than that from the initial grouping. The level of each group is updated by increasing the value of the previous group level by 1 as shown inside the boxes in step 2. In step 3, two different subdivision cases are compared with their minimized *SME* values and the candidate subset is determined as the one with a smaller *SME* value, because parameter group updating continues in the direction that *SME* value reduces. The subdivided groups are updated group level $lv = 2$. In step 4, we can observe that two subgrouping cases are investigated by dividing the groups which had the deepest group level ($lv = 2$) at the previous grouping step 3. The group with a lower group level ($lv = 1$) is not considered in determining the candidate subset at this stage. When a parameter varies within a given tolerance from a previously estimated value, the parameter is removed from further modification and its group level is fixed by $lv = -2$ as shown in step 5. When no more subgrouping can be achieved in the half branch of elements (*1*)–(*6*), the localization process continues on the remaining half branch from step 7 as shown. When *SME* value does not reduce and no alternative grouping is available as shown in the process between step 8 and step 9, the process must return back to the previous grouping step 8 and stop.

Even though the number of groups increases more than 6, parameter groups can be subdivided sequentially as far as the number of unknown parameters is within the allowable range as shown from step 6 to step 9 in Fig. 2.3. The number of unknown parameters can be reduced by satisfying the local termination criterion. A final number of parameters usually does not reach at the upper limit number and stops at a number in-between the allowable range. Group updating is continuously performed until all the subdivision cases are investigated and *SME* does not reduce.

The group level is updated in a hierarchical manner at each grouping, and indicates which subgroups can be investigated to determine a candidate subset. When a group is subdivided, the newly created subgroup has a group level increased by 1 from its parent group level. Only the groups that have the highest group level can be investigated to determine the candidate subset by comparing *SME* values. When a subdivided group contains only a single element, the group level is defined by -1 as

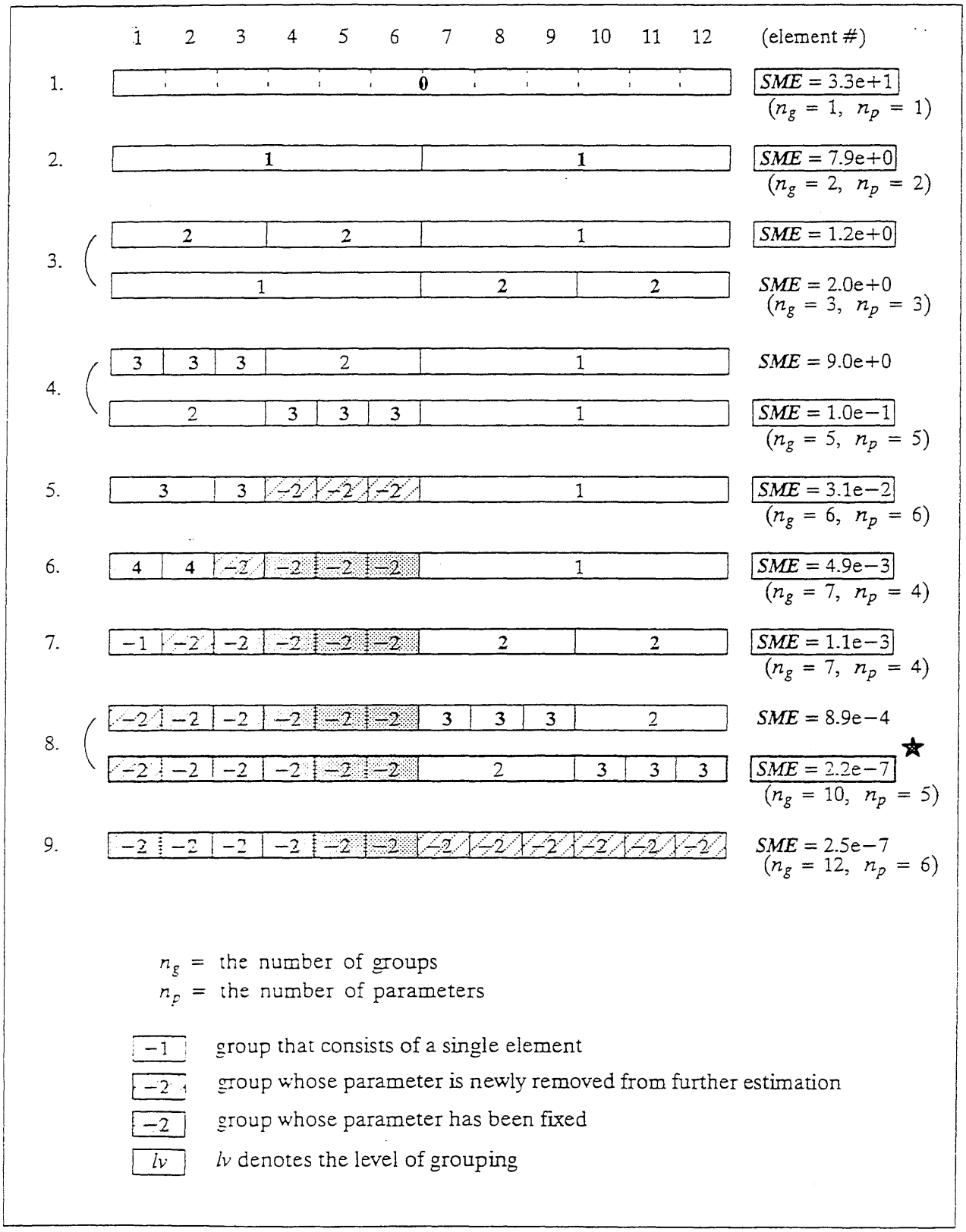

Fig. 2.3 Schematic illustration of the damage localization process by a parameter group updating scheme

shown in step 7. The parameter in such a group is left for further modification until the parameter satisfies the local termination criterion. When a parameter is removed completely from further estimation and fixed by a determined value, the level of such a group is defined by -2.

2.3 Damage Detection and Assessment

Damage detection and assessment are the steps to determine which members in a structure are actually damaged and how much they are damaged. Damage detection is considered as a separate step from the damage localization process in the developed algorithm. Damage detection and assessment can be performed after all the localization processes are completed. If the measured data are virtually error-free, a single cycle of damage localization process with the measured data is enough to determine damage. However, since noise in measurements is unavoidable, the damage localization process would produce a different set of estimated parameters if the test condition changes. Therefore, damage detection and assessment should be based on statistical evaluations of the structural parameters. To provide a statistical basis for evaluating damage in a structural system, a number of sets of measured data should be provided from real field tests. From a number of sets of estimated parameters some statistical properties such as mean and standard deviation for each member parameter can be obtained. However, because it is difficult to obtain many sets of measured data from field tests in practice, the measured data perturbation scheme is proposed herein to create artificial sets of measured data. In this section, the main ideas involved in the proposed measured data perturbation scheme are explained. Two damage indices which can be obtained for each member parameter from the measured data perturbation iterations are introduced and their usefulness in detecting damage in structural systems is discussed.

2.3.1 Measured Data Perturbation Scheme

The measured data perturbation scheme is proposed as a tool to produce statistical information for each member parameter with the given loading and measurement conditions. Each artificial set of perturbed data is created by adding a uniformly distributed random noise vector to the measured data as conceptually shown in Fig. 1.2. The mathematical description of the measured data perturbation process can be expressed as:

$$\hat{\boldsymbol{u}}_{ij}^{pt} = \hat{\boldsymbol{u}}_i + \zeta_{ij} \tag{2.17}$$

where $\hat{\boldsymbol{u}}_i$ is a vector of measured data, $\hat{\boldsymbol{u}}_{ij}^{pt}$ is the jth perturbed vector, and ζ_{ij} is a generated random noise vector to create the jth perturbed vector for the ith load or mode case. The actual measured data already contain the measurement errors with a known amplitude of noise. The amplitude of the additional noise perturbing the measured data is selected as the same as that of the actual measured data. The use of the same amplitude of noise seems to increase the magnitude of noise in the perturbed data so that it may be more difficult to estimate parameters correctly. However, by generating a random

number between plus and minus one, the actual distribution of noise in the perturbed data may fluctuate around the exact solution by the same manner as the measured data.

Even though the measured vector $\hat{u}_i$ does not change during the perturbation iterations for the ith load or mode case, a different random error vector perturbing the measured data will lead to a slightly different final group case and thus a different set of estimated parameter values by the developed parameter group updating algorithm. Through a number of perturbation iterations, some statistical properties for each member parameter can be computed. The mean value represents the best optimal unbiased estimator for the parameter under the given environment. The standard deviation indicates the sensitivity of a member parameter with respect to the applied loads and measured data. Insensitive members may show larger values of standard deviations. One assumption in creating artificially perturbed data by the current definition is that only the measured degrees of freedom are exposed to the perturbation iterations. In other words, the sizes and the locations of measured components of the random error vector ζ_{ij} and the perturbed vectors $\hat{u}_{ij}^{pt}$ are the same as those of the measured data $\hat{u}_i$. The schematic representation of the perturbation iterations is described in Fig. 2.4 for the ith static load case.

2.3.2 Damage Indices

After a set of mean and standard deviation values for each member is obtained from a number of the measured data perturbation iterations, it will be the next task to judge if a member is really damaged or not. Since the baseline values are assumed known, damage may be detected by comparing the mean of the estimated member parameters with the baseline value. However, if a member parameter is insensitive with respect to the given test conditions, its mean value would be distant from the

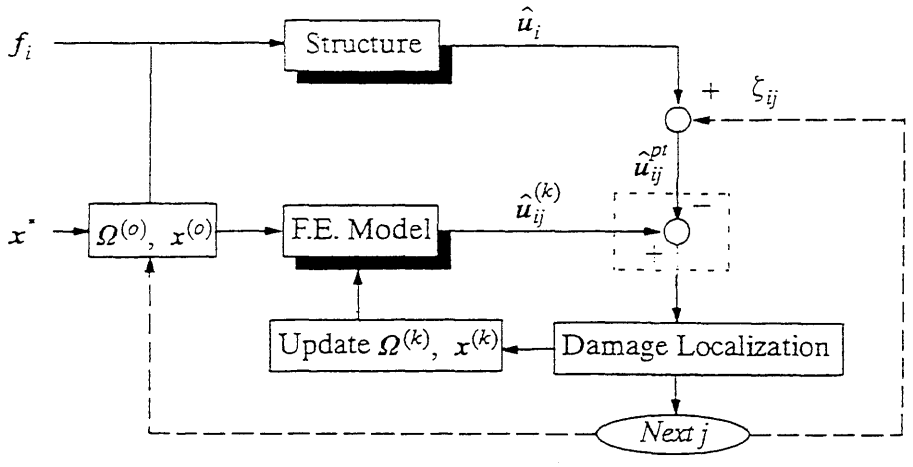

Fig. 2.4 Schematic representation of perturbation iterations combined with the parameter group updating scheme for the ith static load case

baseline value even if the member is not damaged, and in addition, the standard deviation for the member parameter is relatively larger than the standard deviations of other sensitive member parameters. Therefore, by considering the standard deviation in addition to the mean value, damage may be detected more reliably.

Two aspects must be considered when the standard deviation as the measure of sensitivity is used for detecting damage in a structural system. First, the sensitivity of parameters is not an inherent characteristic of the members, but rather dependent on the test conditions. Theoretically, any member in a structural system can be well excited by a special pattern of load or mode case. Second, even insensitive members for the given loading and measuring conditions can be damaged. Insensitivity is not determined by the state of damage in the member but by the test conditions which excite it. Therefore, existing damage in a member should be detected regardless of the sensitivity of member parameters.

Two damage indices for each member parameter are introduced to assist the damage detection and assessment. They are computed by the mean and standard deviation values from the perturbation iterations. The mathematical definitions for the two damage indices are given by:

$$bias\_cx_p^m = \frac{|\bar{x}_p^m - x_p^{m^*}|}{x_p^{m^*}}$$
$$bias\_sd_p^m = \frac{|\bar{x}_p^m - x_p^{m^*}|}{\sigma_p^m} \qquad (2.18)$$

where $bias\_cx_p^m$ is the bias of the mean with respect to the baseline value, $bias\_sd_p^m$ is the bias of the mean from the baseline property with respect to the standard deviation of the pth parameter type of the mth member, $\bar{x}_p^m$ is the mean, $x_p^{m^*}$ is the baseline value, and σ_p^m is the standard deviation of the pth parameter type of the mth member. The two indices are defined for each member parameter.

The first index $bias\_cx_p^m$, indicates how close the averaged member parameter $\bar{x}_p^m$ is to the baseline value $x_p^{m^*}$. Therefore, if the imposed random noise is not significant and if a member is sensitive enough to give a nice estimation results regardless of noise, it may be a good measure for detecting damage in a structure. However, when the noise level is not so low or when a member is insensitive, it may be difficult to detect damage only based on the first index. Since an insensitive member usually possesses a high variation in its estimated member parameters from the perturbation iterations, we can reduce the risk of identifying an actually undamaged member as a damaged one by considering the variation in estimations. The second index *bias_sd* is devised for this purpose. Therefore, the first index can be used to evaluate the sensitivity of each member parameter and the second index can be used to detect damage. However, there is a numerical trap in calculating *bias_sd*. It is possible for $bias\_sd_p^m$ to become a large value when σ_p^m is relatively too small compared with the bias of $|\bar{x}_p^m - x_p^{m^*}|$ due to an excellent estimation. From the definitions of the two indices, therefore, the two damage indices must be used together to detect damage in structural systems, since the use of a single index may lead to a misinterpretation.

After we obtain the two damage indices for each member parameter, the remaining job is to decide how much of the *bias_cx* and *bias_sd* can be allowed for the member to be considered as undamaged. If a single member in a structure is highly damaged, the member may be easily detected as damaged from the two damage indices, because the values of two damage indices of the member may be clearly larger than the others. However, if a member is lightly damaged or if multiple members are damaged at the same time by various damage severities, it is necessary to determine how large damage indices can be considered to indicate damage. To detect damage with the computed damage indices, we may need to define upper limit values for the indices. If the upper limit values can be defined, any member both of whose damage indices are larger than the limit values can be considered being damaged. In other words, if either of the computed damage indices is less than the defined upper limit value, the member can be determined as undamaged. Since the evaluation of damage depends on the choice of the upper limit values *cxlmt* and *sdlmt*, it is desirable to establish a standard methodology to determine them, where *cxlmt* is defined as the upper limit value for *bias_cx* and *sdlmt* is the upper limit for *bias_sd*. If a reasonable choice of the two limits cannot be determined, the limit values will be subjective to the engineer's choice.

From the assumptions for the developed damage assessment algorithm, the finite element model and its baseline properties are known in advance. Therefore, the sensitivity of each member parameter can be checked from the baseline structure with the same test conditions applied to the existing structure. The simulation study of the baseline structure can verify the sensitivity of each member parameter from the first index and can show a rough range of the second index where the member can be considered undamaged. The study of the baseline structure will produce the information useful for evaluating the statistical properties obtained from the existing structure. The two limit values of *cxlmt* and *sdlmt* can be also obtained from the study of the baseline structure. From the simulation study in *Chapter Three*, the methodology to determine *cxlmt* and *sdlmt* from the baseline structure is introduced and examined by the results from the existing structure.

Chapter Three

Simulation Study – Static Response

This chapter describes the procedure of detecting and assessing damage in structural systems from static response by using the damage assessment algorithm developed in *Chapter Two*. The capability of the algorithm is demonstrated through a simulation study. The main concern will be how accurately damage can be pin-pointed and how closely each damaged member property can be estimated. In accord with the assumptions of the algorithm, a refined finite element model with known baseline properties is given. In addition, field test conditions are also known before or after testing a candidate structural system. The test conditions include the applied load cases, the measured degrees of freedom of the finite element model, and the amplitude of noise in measurements.

The damage detection and assessment procedure proposed herein starts from evaluating the baseline structure. The baseline structure means the structure whose finite element model is the same as the candidate structure but whose actual structural parameters are the known baseline values. The information obtained by investigating the baseline structure with the same field test conditions will be used to determine damage in the candidate structure. Therefore, the success of damage detection and assessment for the candidate structural system may depend on how much useful information can be extracted from the study for the baseline structure. Most damage detection and assessment algorithms compare estimated parameters directly with the baseline values without considering the behaviors of the parameters. In doing so, they miss many important observations that can be used to detect damage. If a structural system is sure to contain a single damaged member, it would be unnecessary to obtain statistical information from the baseline structure. The damaged member can be detected directly by selecting a member whose statistical properties from the candidate structure indicate the most possibility of damage. However, if there are multiple damaged members with different levels of damage, it would be difficult to detect all the damaged members. The purpose of the simulation study for the baseline structure is to demonstrate how to use statistical information for detecting all the damage in a candidate structure.

Separately from studying the baseline structure with known test conditions, the damage assessment algorithm is applied to the candidate structure. The information obtained from the baseline structure will be used to judge the statistical properties of the estimated parameters obtained from

the possibly damaged candidate structure. One disadvantage of the proposed procedure is the computation time to prepare the additional statistical information from the baseline structure. However, this disadvantage will diminish if we inspect a structural system regularly with the same test conditions. For the regular inspections, we may need to develop the baseline information only once.

3.1 Numerical Simulation Study

To demonstrate the capabilities of the developed algorithm and the proposed procedure in detecting and assessing damage without real experimental data, numerical simulation studies are proposed. Simulation is defined as the process of replicating the real world based on a set of assumptions and conceived models of reality (Ang and Tang 1975). Numerical simulation is a useful tool to investigate a new algorithm before it is utilized in the real world. Numerical simulation may be used to obtain simulated data, either in lieu of or in addition to actual real-world data.

Monte Carlo simulation is employed for the current study due to the nonlinearity of the error function of the output error estimator with respect to noise in measurements. Because random variables are present in the algorithm, Monte Carlo simulation is required. In each Monte Carlo trial, a set of measured displacements is simulated by applying a random error vector to the actual displacements obtained from the finite element model of the structure. Within each Monte Carlo trial for creating a simulated measured displacement vector, a number of measured displacement perturbation iterations with different sets of random errors are carried out to produce some statistical properties of the member parameters. Fig. 3.1 shows a process of one trial of Monte Carlo simulation study. The same finite element model is used for constructing the simulated actual displacement vector $\hat{u}_i^o$ and for computing displacements at each updated grouping case $\hat{u}_{ij}^{(k)}$ within a measured data perturbation iteration. The use of the same finite element model is acceptable for simulation purposes since

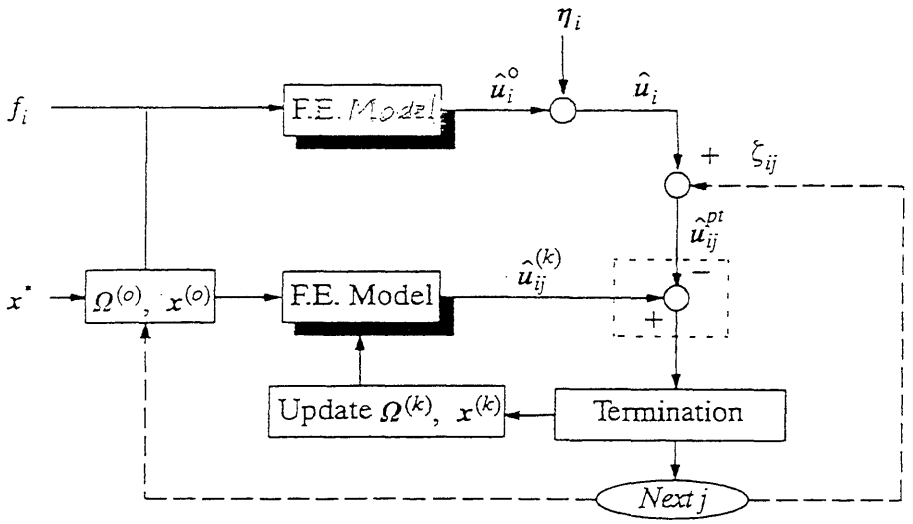

Fig. 3.1 : Schematic representation of one trial of Monte Carlo simulation with a number of measured data perturbation iterations

structural geometry and topology are well defined. The geometry and topology of the structure are assumed not to change after damage, as changes are represented only by changes in the structural parameters.

Simulated measured displacements are mandatory for studying the behavior of the parameters of the baseline structure, but simulation cannot be applied to the existing candidate structure in real cases. The application of Monte Carlo iterations to simulate measured displacements for the candidate structure in the current simulation study is, therefore, only for verifying the usefulness of the proposed procedure and for assessing the behavior of the developed algorithm.

Two error types can be considered to create the random noise for Monte Carlo simulation and for the measured displacement perturbation iterations. The first type is an absolute error of known amplitude ε multiplying a uniform random variable between plus and minus one. The error is added to the calculated displacement to simulate measured displacement. Thus, a simulated displacement vector is expressed by:

$$\hat{u}_i = \hat{u}_i^o + \varepsilon \, R\{-1, 1\} \tag{3.1}$$

Absolute errors represent actual experimental errors well when all instruments have the same sensitivity and are used to measure response of the same type and order of magnitude. If some of the measurements are small, the absolute errors tend to overwhelm the actual responses. The smaller deformations may be unfairly penalized, because in practice, when the deformations are suspected to be small, the sensors would be set to a greater sensitivity. Also, if the same error amplitude is applied to measurements of different character (such as displacements and rotations) the smaller response can be completely dominated by the errors (Hjelmstad, *et. al.* 1990).

The proportional error type is introduced to take this effect into account. The known amplitude of proportional errors is a fraction of the calculated displacement $\hat{\varepsilon}$ multiplying a uniform random variable. A simulated displacement vector with proportional measurement errors are given by:

$$\hat{u}_i = \hat{u}_i^o\left[1 + \hat{\varepsilon} \, R\{-1, 1\}\right] \tag{3.2}$$

True measurement errors lie somewhere between the bounds of absolute and proportional errors. These two extreme models of noise should provide effective bounds of a physical system subjected to measurement errors.

The variations of identification errors with respect to both error types have been studied for the currently implemented parameter estimation method by Banan and Hjelmstad (1993). Generally, both error types produce similar trends in the variations of identification errors. For the current simulation studies, only the proportional error type has been applied, but the results with absolute errors are not expected to be much different.

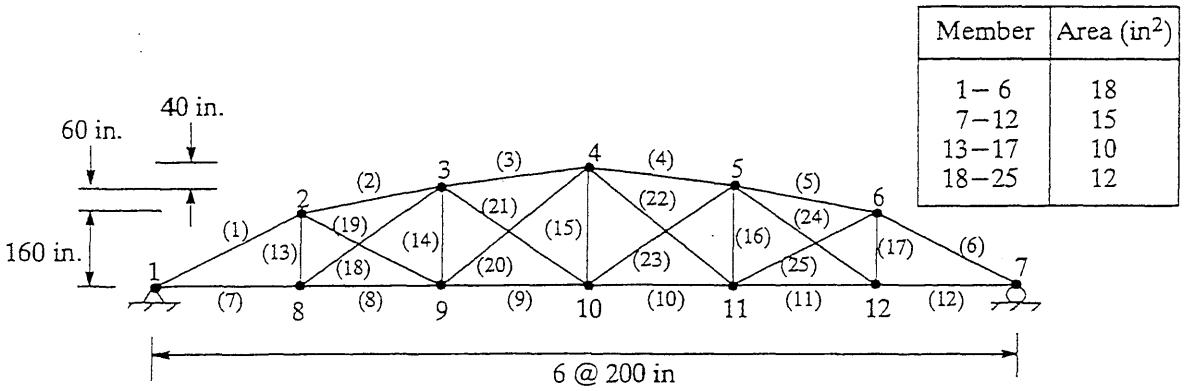

Member	Area (in^2)
1 – 6	18
7 – 12	15
13 – 17	10
18 – 25	12

Fig. 3.2 : Geometry and baseline properties for bowstring truss

3.2 A Case Study

To verify the usefulness of the proposed procedure with the developed damage assessment algorithm, a variety of cases should be tested. However, since it can be reasonably assumed that the results from the algorithm will improve with increased quantity and improved quality of measured data, some critical cases are pursued in the current study. It is our main interest to see the capability of the algorithm for the cases where the data are insufficient if the grouping scheme is not utilized. A damage case with a single but highly damaged member is first considered for the case study in this chapter. Some other cases that deviate from the standard case will be studied in the next chapter. For the simulation purpose, damage is imposed as reduced sectional areas. The sectional area can be a reasonable choice to represent the stiffness parameter for the truss structures.

3.2.1 Example Structure

The structure under consideration for the simulation study is a planar bowstring truss structure with known geometry and topology as shown in Fig. 3.2. This structure consists of twenty-five elements with twenty-one degrees of freedom. The baseline properties with four different cross sectional areas are given inside the figure. From the baseline structure, the number of the initial groups for the damage assessment algorithm is taken to be four and the corresponding initial parameters are to be the given baseline cross sectional areas. The behavior of the structure is considered as linear for the current research.

The simulated damage is with the reduced sectional area in member (*10*) at the bottom of the bowstring truss structure. The sectional area is reduced from 15.0 in^2 to 1.0 in^2, that is, by 93%.

3.2.2 Test Conditions

The employed load cases and the measured degrees of freedom for the case study are shown in Fig. 3.3 and Fig. 3.4, respectively. The number of load cases is selected as three and the measured degrees of freedom for the case study are selected at the seven degrees of freedom from the bottom nodes of the truss model. It means that the identifiability criterion of Eq. (2.5) is not satisfied without

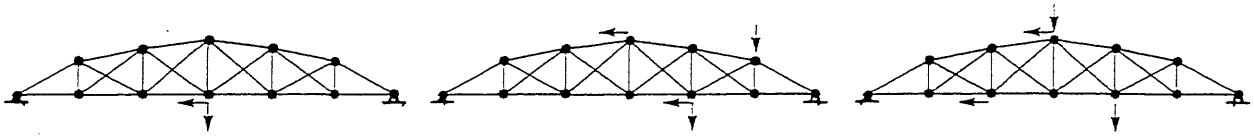

Fig. 3.3 : Three independent load cases for the case study

using the grouping scheme, because the number of measured information is twenty-one now, which is smaller than the total number of member parameters of twenty-five. Magnitude of the applied loads are adjusted for the maximum displacements of each load case to be less than a pre-determined value. The known amplitude of noise in measurements is assumed to be 10% proportional error for the current case study.

3.2.3 Consistency Check-up for Steady Results

Before starting to evaluate the baseline structure and the candidate structure, we need to verify first how many iterations are required to obtain steady results with respect to the measured displacement perturbation iterations and Monte Carlo trials to simulate measured data. With both of the determined numbers of iterations, some statistical properties are computed and thus damage is detected and assessed. To obtain consistencies, the number of trials with different random noise should be sufficiently large. However, since a greater number of trials requires more computational effort, a compromise between the sufficient consistency and the computational effort must be sought.

Consistency with respect to the measured displacement perturbation iterations

The number of measured data perturbation iterations that will be large enough to provide steady estimation results should be determined first. The consistency can be checked from the baseline structure with the known information of the field test conditions, and then can be applied to identify the existing candidate structure. The consistency with the selected number of measured data perturbation iterations can be verified by the same test on the existing candidate structure.

Fig. 3.5 shows the variations of some statistical properties with the number of perturbation trials for the baseline structure. The loading and measuring conditions are the same as the standard simulation case as specified in the section 3.2.2. The reason why the statistical values rather than identification errors are compared is simply because those statistical properties are used to detect and assess

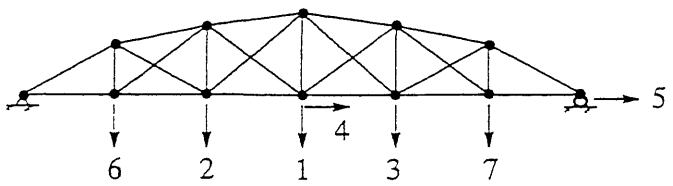

Fig. 3.4 : The measured displacements for the case study

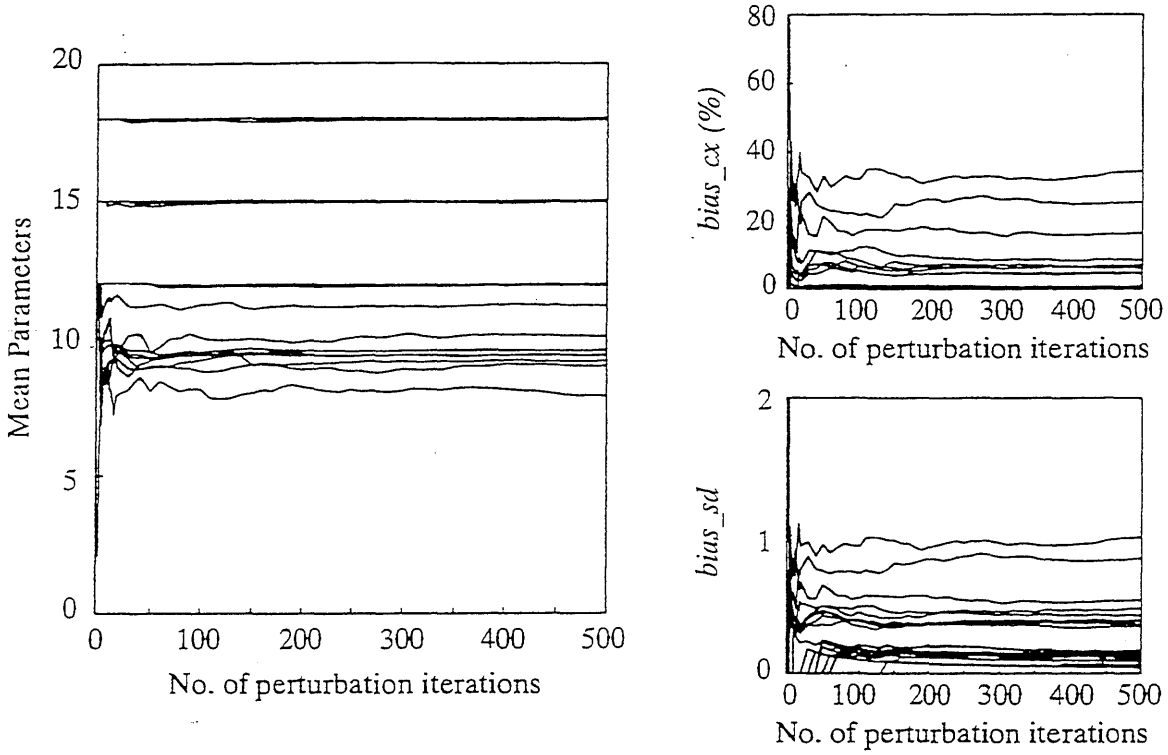

Fig. 3.5 : Variations of mean parameters and biases with respect to the number of perturbation iterations for the baseline structure

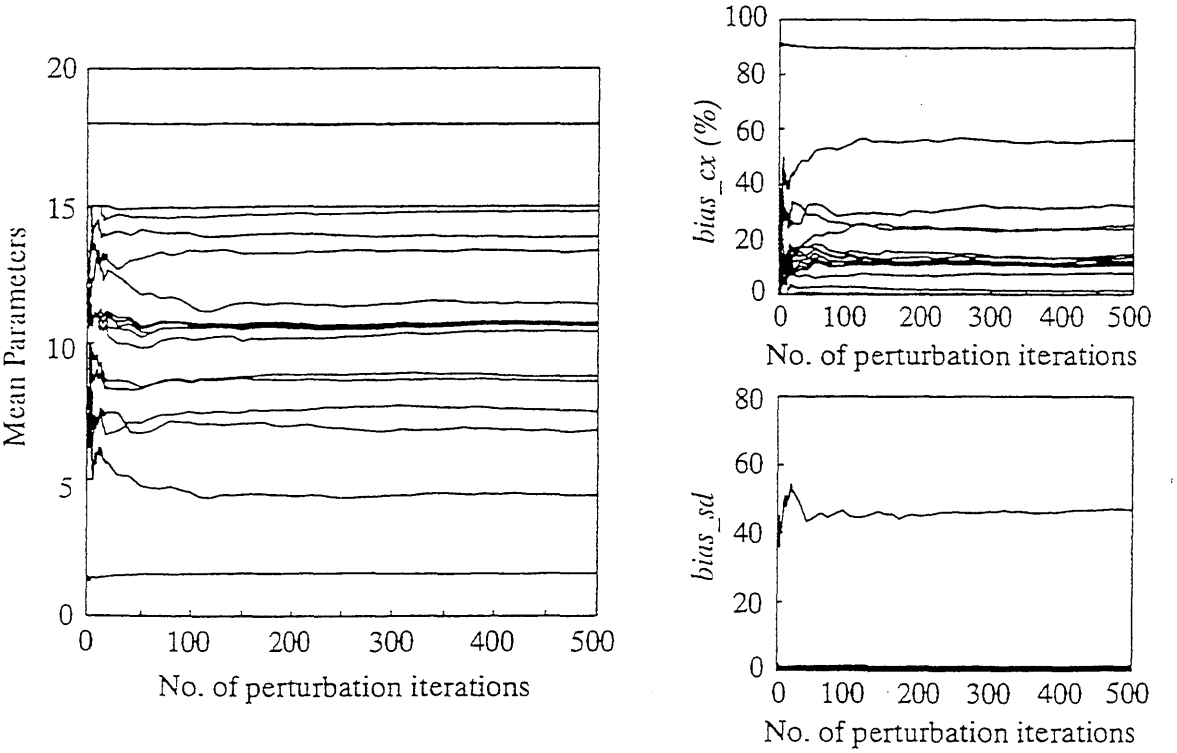

Fig. 3.6 : Variations of mean parameters and biases with respect to the number of perturbation iterations for the damaged structure

damage in the existing candidate structural system later. The figure seems to demonstrate that a relatively large number of perturbation iterations may be required to obtain consistent results. The similar trend of consistency is observed for the damaged case structure in Fig. 3.6. From the two figures, it can be concluded that the number of measured displacement perturbation iterations determined from the baseline structure can be applied for the existing candidate structure. Likewise, the number of iterations determined from the damaged structure after its responses are measured can be used for evaluating the baseline structure. From the figures, more than 100 iterations seem to be necessary to have consistent estimations. However, even 50 iterations seem to be sufficient to reveal which members have parameter values distant from the baseline values.

Consistency with respect to Monte Carlo trials

Several measures of identification error are computed to check the consistency with respect to the number of Monte Carlo trials for simulating the measured displacements. They are the average mean identification error (*AMIE*), the average standard deviation (*ASD*), the average root mean square error (*ARMS*), and the average quadratic bias (*ARQB*). *AMIE* represents the global mean of the identification error and *ASD* represents the average scattering of the output around the estimated value. *ARMS* and *ARQB* both represent the distance between the baseline values and the estimated parameters. The errors are defined by the total number of member parameters rather than by the number of group parameters, because the number of the final groups at each simulation trial may vary depending on the distribution of noise in measured data but the number of member parameters does not vary regardless of the amplitude of noise. The mathematical expressions for the errors are defined by:

$$
\begin{aligned}
AMIE(T) &= \frac{1}{T\, n_{sum} \,\| x^* \|} \sum_{t=1}^{T} \sum_{m=1}^{n_e} \sum_{p=1}^{\Pi_m} |x_p^{m^t} - x_p^{m^*}| \\
ASD(T) &= \frac{1}{n_{sum} \,\| x^* \|} \sqrt{\frac{1}{T-1} \sum_{t=1}^{T} \sum_{m=1}^{n_e} \sum_{p=1}^{\Pi_m} (x_p^{m^t} - \bar{x}_p^m)^2} \\
ARMS(T) &= \frac{1}{T\, n_{sum} \,\| x^* \|} \sum_{t=1}^{T} |x^t - x^*| \\
ARQB(T) &= \frac{\| x - x^* \|}{n_{sum} \,\| x^* \|}
\end{aligned}
\tag{3.3}
$$

where T is the number of trials, n_{sum} is the number of total member parameters, Π_m is the number parameter types in the mth member, $x_p^{m^t}$ and $x_p^{m^*}$ are the estimated value and the baseline value of the pth parameter in the mth member, respectively. The mean value of the pth parameter in the mth member $\bar{x}_p^m$ and norm of the baseline values $\| x^* \|$ are defined by:

$$\bar{x}_p^m = \frac{1}{T}\sum_{t=1}^{T} x_p^{mt} \qquad \| x^* \| = \sqrt{\sum_{m=1}^{n_e}\sum_{p=1}^{\Pi_m} x_p^{m*2}} \qquad \cdots (3.4)$$

The consistencies of the identification errors are investigated for the baseline structure in Fig. 3.7. For the current simulation, they are checked again for the damaged structure in Fig. 3.8. From both figures, we can observe that all the identification errors are almost constant in the whole range of trials. Even if a little fluctuation of identification errors are observed in the early stage of trials,

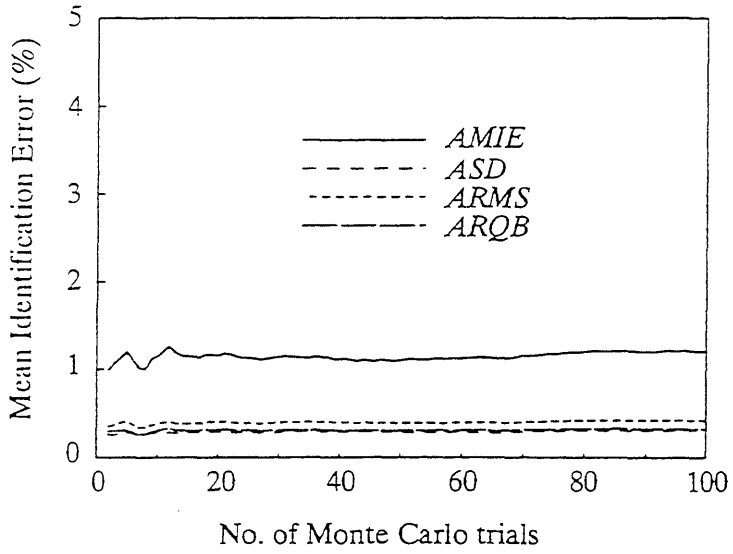

Fig. 3.7 : Variation of mean identification errors with respect to the number of Monte Carlo trials for the baseline structure

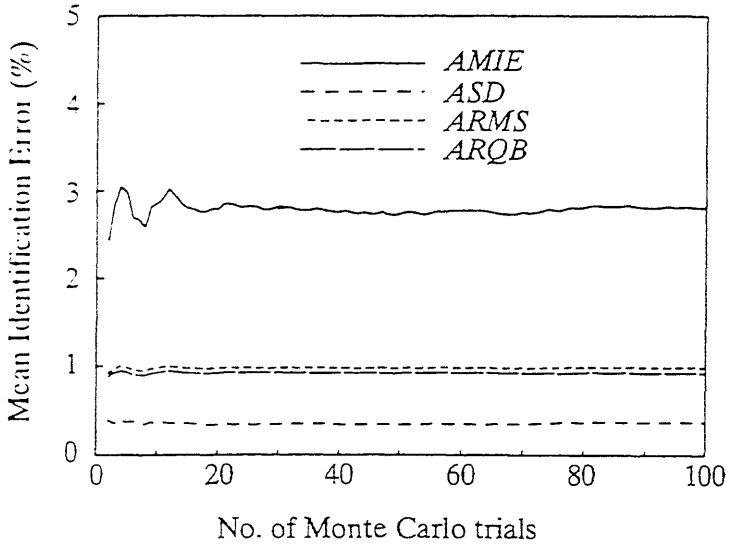

Fig. 3.8 : Variation of mean identification errors with respect to the number of Monte Carlo trials for the damaged structure

the magnitude of fluctuating error is fairly small. Comparing these figures with the figures for the perturbation iterations in Fig. 3.5 and Fig. 3.6, the required number of Monte Carlo trials for steady results is clearly smaller than that for perturbation iterations. An interesting observation is that the identification errors from the damaged structure are bigger than those from the baseline structure due to damage in the structure. Even for a virtual case with error-free measurements, the identification errors with the current definitions will not reduce to zero for the damaged structure, because the identification errors are defined by comparing the estimated parameters with the baseline values rather than by comparing them with the actual values. From the figures, 50 iterations of Monte Carlo simulation are believed to be large enough to provide steady results.

3.2.4 Evaluation of the Baseline Structure

After determining the numbers of iterations for steady results, some statistical properties can be obtained from the baseline structure. Without the statistical properties from the baseline structure, damage for the candidate structure can be evaluated, but it may be difficult to discern which members are actually damaged when the measured displacements are polluted by noise. As explained before, the usefulness of evaluating the baseline structure can be seen most clearly for the cases in which multiple members are damaged or for the cases in which a single member is lightly damaged. The current simulation is for the case that a single member (*10*) is highly damaged. Therefore, the evaluation of the baseline structure is expected not to be useful in detecting and assessing damage in the simulated damaged structure. Without the help of the study of the baseline structure, damage can be detected directly from the statistical evaluation for the damaged structure. However, the current case study is valuable to illustrate the complete procedure of damage detection and assessment.

From the measured displacement perturbation iterations at each Monte Carlo iteration, mean and standard deviation values for each member parameter can be obtained. From these statistical values, two damage indices, *bias_cx* and *bias_sd* as defined by Eq. (2.18), can be computed. Fig. 3.9 shows the averaged mean and standard deviations for the baseline structure after a number of Monte Carlo trials are carried out. The damage indices for each member parameter computed from the averaged mean and standard deviation are also shown in the same figure. From the mean stiffness parameter figure, we can observe that the vertical and diagonal members (*13*)−(*25*) are more difficult to be correctly estimated and have relatively larger standard deviation values than the top and bottom members (*1*)−(*12*). The *bias_cx* values of the vertical and diagonal members are much larger than those of the top and bottom members, but the *bias_sd* values are almost at the same level, even though a little higher values can be observed for the vertical members (*13*)−(*17*). From these observations, it can be concluded that *bias_cx* values shows the sensitivity of each member stiffness parameter with respect to the applied load cases and the measured degrees of freedom, and *bias_sd* value shows the range of the index where the members can be considered undamaged. One thing that should be remembered is that the damage indices drawn in the figure are the averaged values, and thus they have also variations at each Monte Carlo trial.

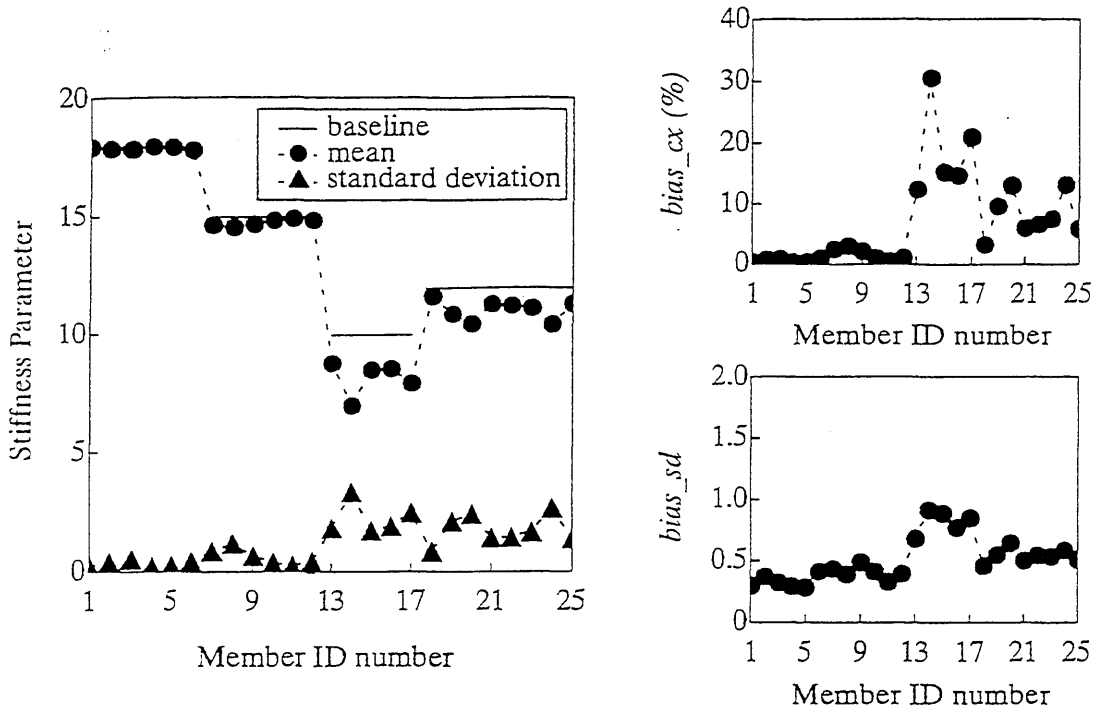

Fig. 3.9 : Average mean and standard deviation values, and damage indices of the baseline structure

The main purpose of evaluating the baseline structure is to provide some useful information that can help an engineer evaluate damage for each member in the candidate structure. As a useful tool, global upper limit values *cxlmt* and *sdlmt* for the two kinds of damage indices are sought herein rather than defining the limit values for each member parameter, where *cxlmt* is the upper limit value for the damage index *bias_cx* and *sdlmt* is the upper limit value for *bias_sd*. The selected global upper limit values will be used to judge which members are actually damaged in the candidate structure. If both of the computed damage indices of a member are larger than the determined global upper limits, the member can be considered damaged. A systematic way of determining the upper limit values is discussed and tested by the case study in this chapter.

To determine the global upper limit values for the two types of damage indices, the damage probability for each member is computed at each combination of the limit values. The damage probability for a member is defined as the probability that the member is regarded as damaged by the limit values from a number of Monte Carlo trials. By selecting a different combination of the limit values, the damage probability for each member also changes. The variation of the damage probabilities with respect to either limit value is shown for the current damage case in Fig. 3.10. Each figure is drawn with respect to the variation of one damage index threshold by fixing the other limit value. Each solid line is the variation of damage probability for each member. From the figure, it can be observed that most of the damage probability curves drop close to zero before a certain value of *bias_sd* or *bias_cx* threshold is reached. When the *sdlmt* value is fixed, the damage probabilities go steadily up to a relatively large

value of *bias_cx* threshold. If we consider the known amplitude of noise of the case study (10%) and the physically meaningful range of the *cxlmt*, even 20% *bias_cx* threshold seems to be a large value for *cxlmt*. The situation is clearly demonstrated by Fig. 3.11 where the maximum damage probability value at each combination of *cxlmt* and *sdlmt* is connected. From the figure, we can observe that the value of *sdlmt* where the damage probability envelope curve becomes flat is about the same point regardless of the variation of *cxlmt* values. Therefore, it may be reasonable to conclude that the damage probabilities are more dominated by the determination of *sdlmt* value rather *cxlmt* value. However, when *bias_sd* is a large value due to too small a standard deviation even if its estimated parameter is close to the baseline value, *cxlmt* rather than *sdlmt* can be used to determine damage. Another observation is that the *sdlmt* value where damage probability curves become flat in Fig. 3.10 is almost as twice the maximum value of the averaged damage index *bias_sd* in Fig. 3.9.

From Fig. 3.10, a proper choice of *sdlmt* seems to be around where the *bias_sd* threshold is 2.0. If a smaller value of *sdlmt* is selected, the probability that actually undamaged members are detected as damaged increases. If a larger value of *sdlmt* is selected, the probability that actually damaged members are detected as damaged may decrease even if the probability that actually undamaged members are determined as undamaged will be high. Therefore, an optimal point must be sought where the probability does not incline to either side. For the current approach, *sdlmt* is defined as a *bias_sd* threshold value whose maximum damage probability is less than 5% and where all the damage probability curves start to be flat. This definition allows a little flexibility in selecting *sdlmt*, but the results of damage detection and assessment would not be affected considerably. From Fig. 3.10, *sdlmt*=2.0 can be selected as a reasonable choice, where the damage probability is 3%. Compared with the selection of *sdlmt* value, the selection of *cxlmt* seems to be arbitrary. Within a meaningful range of *bias_cx* threshold, the damage probabilities are almost constant as shown in Fig. 3.10. Therefore, the selection of *cxlmt* seems not so important as *sdlmt* in detecting damage. However, since the

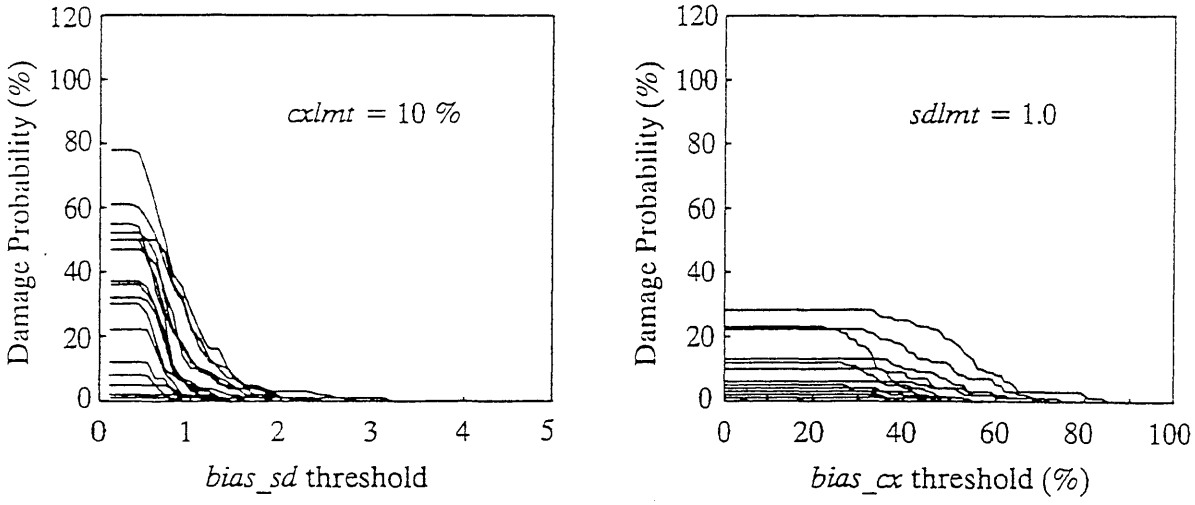

Fig. 3.10 : Variation of damage probability with respect to *bias_cx* and *bias_sd* thresholds for the baseline structure

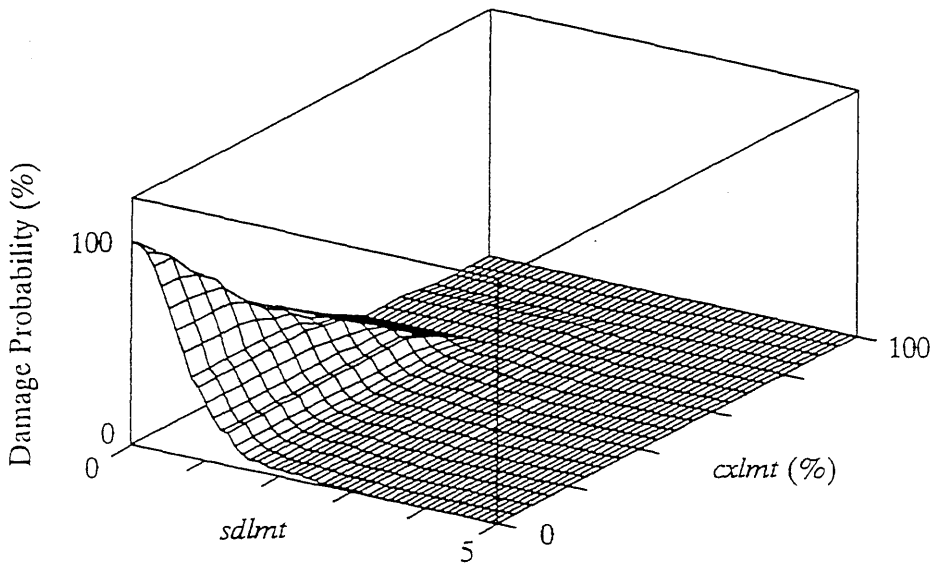

Fig. 3.11 : Damage probability envelope for the baseline structure

damage probability of a member changes depending on the amplitude of noise in measured displacements, *cxlmt* is defined as the same as the amplitude of average noise percent herein. This definition seems to work because *cxlmt* is used as the damage measure only when a *bias_sd* value is very large due to too small a standard deviation compared with the bias between mean and the baseline value. For the current case study, therefore, *cxlmt* is selected as 10%. From the definitions of both upper limit values, *sdlmt* value is used first to detect damage in the candidate structure and *cxlmt* value is used only when *sdlmt* cannot evaluate damage due to a large value of *bias_sd*. The proposed procedure of selecting the values of *cxlmt* and *sdlmt* is verified for the simulated damaged structure in the following section, and is tested with more case studies in *Chapter Four*.

3.2.5 Damage Detection and Assessment of the Case Structure

From the evaluation of the baseline structure, we could determine the limit values for the two damage indices as *cxlmt*=10% and *sdlmt*=2.0. The obtained limit values are used directly to detect damage in the damaged structure. Only the members detected as damaged by the two limit values are allowed to change their parameters by the estimated values. If any member is determined as undamaged, its member parameter stays with the baseline value without modifying it, even if the estimated parameter seems to be far distant from the baseline. The deviation is considered simply due to its insensitivity with respect to the test conditions.

In real cases, Monte Carlo trials cannot be applied to simulate the measured displacement vectors, and only the measured data perturbation iterations can be applied to provide mean member parameters and their sensitivities. However, for the purpose of simulation, the average member parameters and standard deviations are computed from a number of Monte Carlo trials herein. Damage

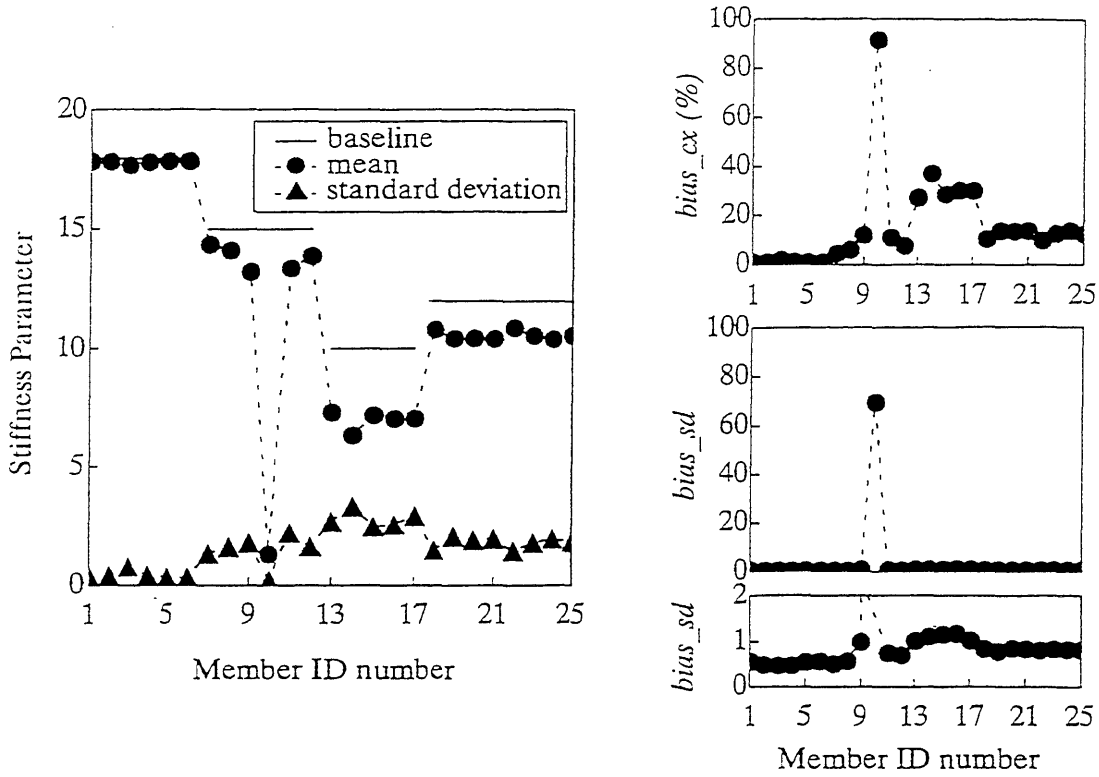

Fig. 3.12 : Average mean and standard deviation values, and damage indices of the damaged structure

indices are also computed from the averaged mean and standard deviations as shown in Fig. 3.12. However, if the results in Fig. 3.12 are assumed to be obtained from real data, member (*10*) can be easily verified as damaged when its *bias_cx* and *bias_sd* values are evaluated by the two limit values *cxlmt* and *sdlmt* determined from the baseline structure. Other seemingly damaged members, such as the vertical members (*13*)−(*17*), can be determined as undamaged when their *bias_sd* values are compared with the selected *sdlmt* even though their *bias_cx* values are higher than the selected *cxlmt*.

Even though the averaged *bias_sd* damage indices for all the members except member (*10*) are lower than the selected *sdlmt* value, the computed damage indices at some Monte Carlo trials may have higher values than the averaged ones and then can be detected as damaged with the pre-determined *sdlmt* value. Such possibility can be observed from Fig. 3.13, where the probability of being detected as damaged from a number of Monte Carlo trials is plotted for each member parameter with the pre-determined limit values. From the figure, we can observe that member (*10*) is always detected as damaged but there is also a small chance for some actually undamaged members to be detected as damaged by the selected limit values. This phenomenon could be expected when *sdlmt* value was selected as 2.0 by leaving extra tails of damage probabilities for large values of *bias_sd* threshold in Fig. 3.10. A little probability of incorrectness has been allowed by the current definition of *sdlmt*. Even if some of the actually undamaged members are detected as damaged, their computed *bias_sd* values

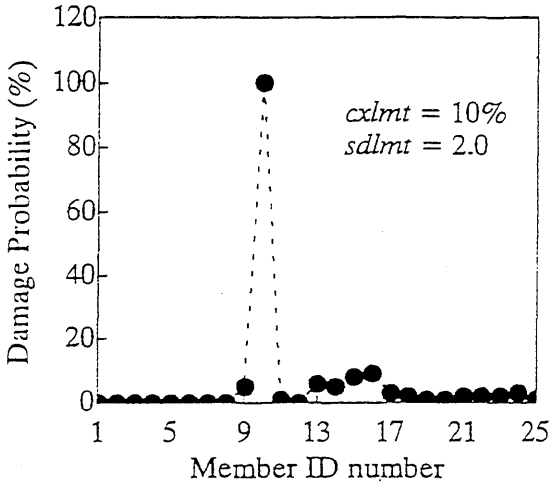

Fig. 3.13 : Damage probability of the members with the selected *cxlmt* and *sdlmt*

are sure to be much smaller than that of the damaged member (*10*) and are close to the selected *sdlmt* value. Anyway, it is difficult to determine damage for those members whose computed *bias_sd* values are a little higher than the selected *sdlmt*. The decision seems to be a subjective matter since the selected limit values cannot be perfect measures to draw a borderline between damaged and undamaged state. One observation from the current case study that can be useful for the decision is that most of the incorrectly detected members are from the vertical and diagonal members that have been proved as insensitive from the evaluation of the baseline structure. In addition, the members adjacent to the actually damaged member (*10*) also show some possibilities. Therefore, from the figures, all the damaged members can be detected and possibilities of some doubtful members can be also evaluated by considering their sensitivities.

In addition to pin-pointing the actually damaged member, the estimated value of the actually damaged member (*10*) is also obtained close to the actual parameter value as shown in Fig. 3.12. The use of limit values for the two damage indices will be more valuable when larger errors exist. In any circumstance, however, member (*10*) will be the first candidate damaged member to be inspected.

3.2.6 Verification of the Use of the Selected *cxlmt* and *sdlmt*

In this section, the limit values for the two damage indices, *cxlmt* and *sdlmt*, selected from the baseline structure are to be checked if they are still appropriate for the damaged structure. With the selected limit value of *cxlmt*=10%, the damage probability curves for the damaged case structure are drawn in Fig. 3.14 with respect to *bias_sd* threshold. From the figure, we can observe that the behavior of damage probability curves with the variations of *bias_sd* is surprisingly similar to the baseline case as shown in Fig. 3.10 except for the actually damaged member (*10*). From the figure when *cxlmt*=10%, if we draw a vertical line at *sdlmt*=2.0, we may observe the same damage probability for each member as shown in Fig. 3.13. Some actually undamaged members have small probability of being detected as damaged if the two limit values selected from the baseline structure are applied, but their probabilities are very small.

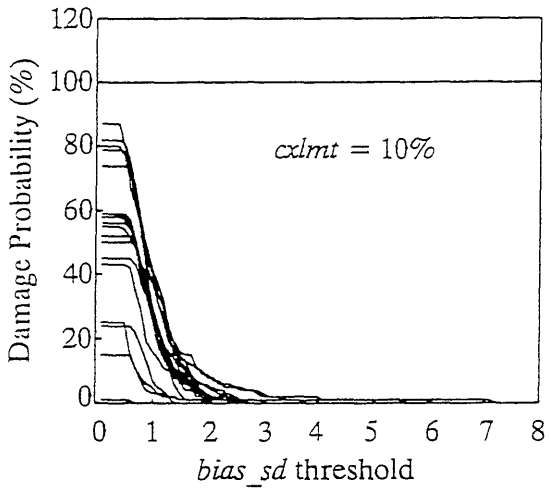

Fig. 3.14 : Damage probability of the members in the damaged structure

Unfortunately, Fig. 3.13 and Fig. 3.14 cannot be obtained for the real test cases, because the figures are obtained from a number of Monte Carlo trials to simulate the measured displacement vectors. The figures are obtained herein only for the simulation, but they clearly validate the usefulness of the two limit values obtained from the baseline structure.

3.3 Summary

The damage detection and assessment procedure is proposed and tested with a simulation case study for the bowstring truss structure. For the case study, a single member is simulated to be highly damaged. Through the simulated case study, the procedure of selecting the limit values for the damage indices from the baseline structure is described, and its usefulness for assessing the damaged structure has been demonstrated. The probabilistic aspects of the accuracy in pin-pointing the actually damaged members are investigated. The accuracy of the estimated parameters is also demonstrated.

Damage is detected by comparing the selected upper limit values with the computed damage indices for each member parameter. When both of the computed damage indices are larger than the selected limit values, the member is considered damaged. The damage index *bias_cx* shows the sensitivity of the parameter with respect to the applied test conditions, and the other damage index *bias_sd* reveals the possibility of damage. The upper limit value *sdlmt* for the damage index *bias_sd* is the main indicator for detecting damage, and another limit value *cxlmt* is used to determine damage when *sdlmt* cannot play its role due to a large value of *bias_sd*. Even though small possibility of misinterpreting some actually undamaged members as damaged was observed in the simulation case study by strictly observing the selected upper limit values, the possibility could be corrected by investigating the sensitivities of those member parameters.

More examples with variations from the standard case are studied in *Chapter Four*. The variations will include some real possibilities we might face; such as (*1*) several members are damaged at the

same time with different damage severities, (*2*) a member is lightly damaged, and (*3*) one of the damaged members is from the insensitive vertical or diagonal members. Through the case studies, the usefulness of the proposed damage detection and assessment procedure will be further investigated.

One disadvantage of the present algorithm may be the computation time compared with other algorithms, because a lot of iterations are involved to evaluate the candidate structure and the baseline structure. Especially, for evaluating statistical properties of the baseline structure, more iterations are required due to the required Monte Carlo trials. However, the most possibly damaged member may be detected directly from the evaluation of the candidate structure without the help of the statistical properties from the baseline structure, and thus an early recommendation can be delivered to the engineer. Details can be obtained after completing the evaluation of the baseline structure. If the test conditions do not change in regular inspections for the candidate structure, the statistical properties of the baseline structure need be computed only once in the beginning.

Chapter Four

Additional Simulation Studies for Static Response

In *Chapter Three*, the procedure of detecting and assessing damage in a bowstring truss structure was described in detail. A procedure of selecting the two limit values for the damage indices was proposed and verified by a simulation study. The considered damage case was with a single damaged member as summarized by damage case [*1*] in Table 4.1. In this chapter some additional simulation cases for the same bowstring truss structure are studied to test the developed algorithm more thoroughly. The additional cases are designed to have some variations from the standard case and are summarized in Table 4.1. In this chapter, the damage case [*1*] studied in *Chapter Three* is referred to as the standard case. In each damage case, the baseline structure is tested with the same test conditions for the damage case and statistical results are used to determine damage in the corresponding damaged structure. Through the simulation studies, the usefulness of the proposed procedure for detecting and assessing damage by the upper limit values is further investigated. In the table, *nlc* and *nms* indicate the number of load cases and the number of measured degrees of freedom in the structural model, respectively.

Table 4.1 : Summary of case studies

case	damage	*nlc*	*nms*	noise amplitude	variation from the standard case
[*1*]	$A_{(10)} = 1.0\ in^2$	3	7	10%proportional	• standard case from *Chapter Three*
[*1−1*]	$A_{(10)} = 1.0\ in^2$	1	7	10%proportional	• reduced number of load cases
[*1−2*]	$A_{(10)} = 1.0\ in^2$	3	3	10%proportional	• reduced number of measurements
[*2−1*]	$A_{(10)} = 12.0\ in^2$	3	7	5%proportional	• light damage in member (*10*) • lower amplitude of noise
[*2−2*]	$A_{(10)} = 12.0\ in^2$	3	7	1%proportional	• light damage in member (*10*) • 1% proportional noise
[*3*]	$A_{(3)} = 6.0\ in^2$ $A_{(9)} = 9.0\ in^2$ $A_{(10)} = 1.0\ in^2$	3	7	5%proportional	• three damaged members • different levels of damage • lower amplitude of noise
[*4*]	$A_{(10)} = 5.0\ in^2$ $A_{(15)} = 3.0\ in^2$	3	7	5% proportional	• two damaged members • one from the vertical members • the same level of damage • lower amplitude of noise

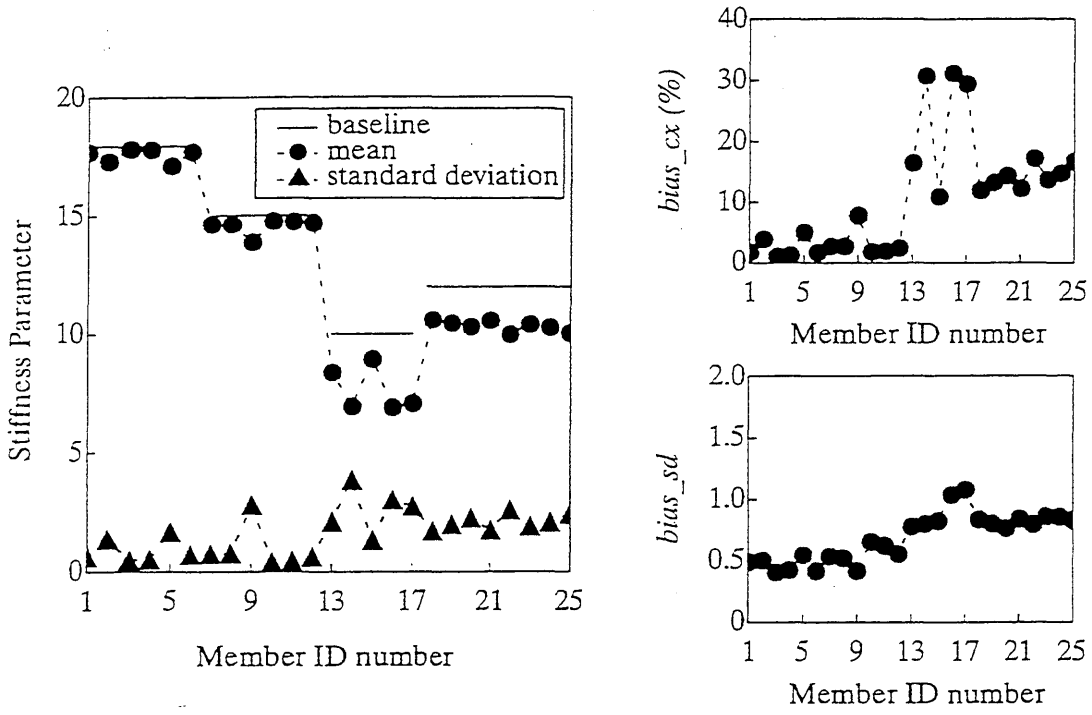

Fig. 4.1 : Mean parameters and damage indices for each member in the baseline structure with the same test conditions as damage case [*1*−*1*]

4.1 Damage Case [*1*−*1*]

The number of load cases is reduced from three to one in this case study. The location and the level of damage are the same as the standard case where the sectional area of the single member (*10*) is reduced by 93% from 15.0 in^2 to 1.0 in^2. Due to the reduced number of load cases, the maximum allowable number of parameters is limited by seven as defined by Eq. (2.5) and the minimum number is four by the number of different sectional areas in the baseline structure as shown in Fig. 3.2. Since the maximum allowable number of parameters is limited by a small number of seven, it will be impossible to identify all the damage if multiple members are damaged at the same time.

Fig. 4.1 shows the mean and standard deviation of each member stiffness parameter obtained by applying the same test conditions as damage case [*1*−*1*] for the baseline structure. Those values are the averaged of a selected number of Monte Carlo trials. Compared with the results in Fig. 3.9 for the baseline structure of the standard case, the damage indices for each member generally increase, and the damage indices for the vertical and diagonal members (*13*)−(*25*) show their insensibility more clearly. However, the maximum damage index values seem not to change much in both of the damage indices.

Fig. 4.2 shows the variation of damage probability with respect to the *bias_sd* threshold. Compared with Fig. 3.10 for the baseline structure of the standard case, the upper limit *sdlmt* value can be selected with a larger value. The increase of the *sdlmt* value can be verified again from the dam-

aged structure later in Fig. 4.4. The general behavior of the damage probability curves is similar to the standard case. The *cxlmt* value can be selected by the known noise amplitude of 10% proportional error. A proper *sdlmt* is selected as 3.0 where the damage probability is 3% from Fig. 4.2.

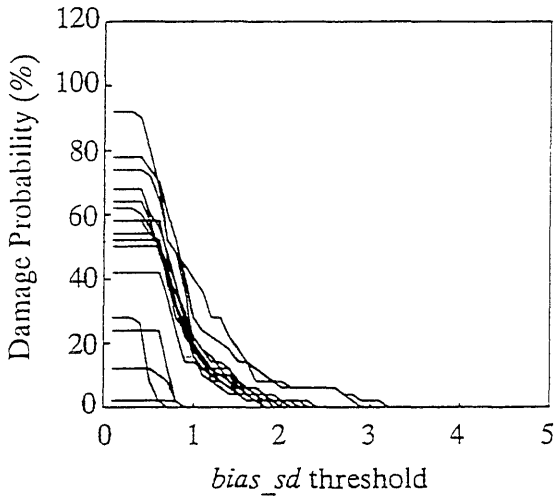

Fig. 4.2 : Variation of damage probability for the baseline structure in damage case [*1*−*1*] with respect to *bias_sd* threshold when *cxlmt*=10%

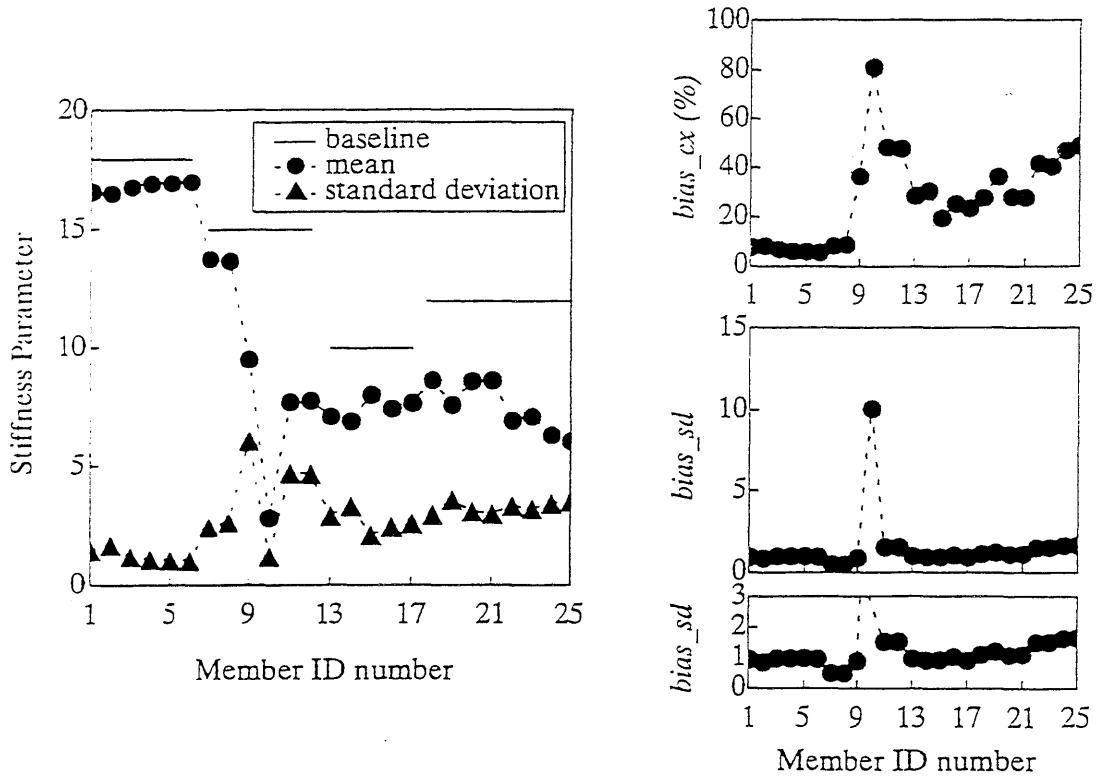

Fig. 4.3 : Mean parameters and damage indices for each member in damage case [*1*−*1*]

Fig. 4.3 collects the mean and standard deviation for each member of the damaged structure of damage case [*1*−*1*]. For the purpose of simulation, the values are averaged from a selected number of Monte Carlo trials even though the Monte Carlo simulation trials cannot be carried out for real data. The damage indices are computed from the averaged mean and standard deviations. By applying the selected two limit values of *cxlmt*=10% and *sdlmt*=3.0 to the computed damage indices, member (*10*) can be easily detected as the single damaged member. However, as discussed in *Chapter Three*, since the damage indices are computed from the averaged mean and standard deviation values, the effectiveness of the selected limit values should be investigated for each Monte Carlo simulation. The right-hand-side figure in Fig. 4.4 is drawn for this purpose and demonstrates the usefulness of the limit values. Even though some other members also have small probabilities of being detected as damaged, member (*10*) is always detected as damaged and the probabilities for the other members are relatively small. For real test data, even when some members are detected as damaged incorrectly by the limit values determined from the baseline structure, member (*10*) would easily be considered the most possibly damaged one from the figures of the damage indices such as Fig. 4.3. Its *bias_sd* value is much higher than those of the other members.

The selection of *sdlmt*=3.0 can be verified through the Monte Carlo simulation study for the damaged structure in the left-hand-side figure of Fig. 4.4. Even though some member parameters have tails after *sdlmt*=3.0, the general trend of dropping of the damage probability curves occurs around the same point of *sdlmt* selected from the baseline case of the same damage case. The remaining tails explain why some actually undamaged members can be detected as damaged in the right-hand-side figure. All the detected members that are not actually damaged are either from the insensitive vertical and diagonal members (*13*)−(*25*) or from the members connected to the actually damage member (*10*). This supports the fact that those members are difficult to correctly estimate due to their insensitivity with respect to the current test conditions.

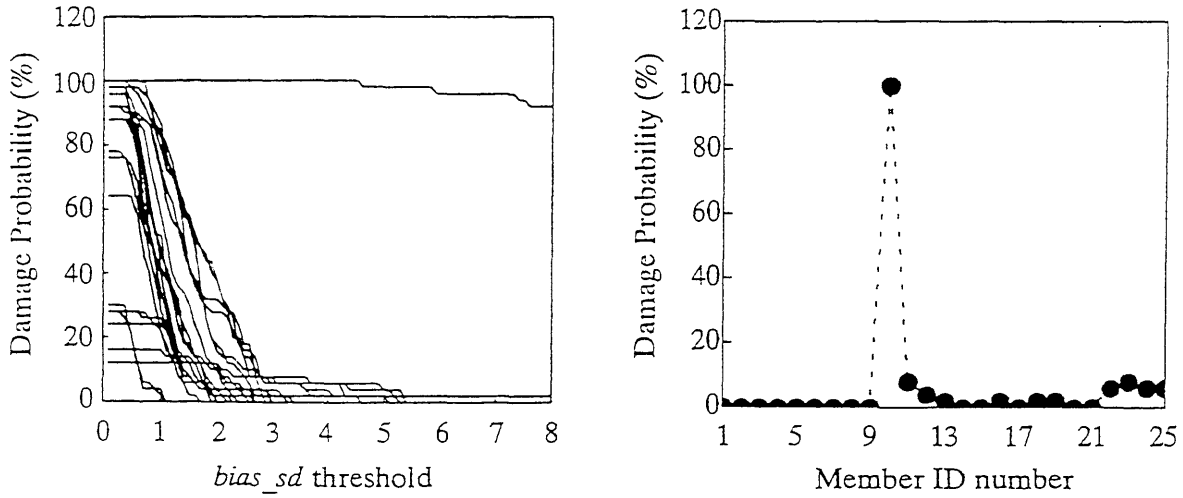

Fig. 4.4 : Variation of damage probability with respect to *bias_sd* for damage case [*1*−*1*], and damage probability of each member when *cxlmt*=10% and *sdlmt*=3.0 are selected

4.2 Damage Case [*1−2*]

Instead of reducing the number load cases, the number measured degrees of freedom is reduced from seven to three in this case study. The selected three degrees of freedom are as shown in Fig. 3.4. The intention is similar to damage case [*1−1*] by pushing the amount of measured information to the minimum. The location and the severity of damage are the same as the standard case. Due to the reduced number of measured displacements, the maximum allowable number of parameters is nine and the minimum number is four for this case study.

Statistical properties from the baseline structure with the same test conditions as the damaged structure [*1−2*] are drawn in Fig. 4.5, and the variations of damage probability with respect to *bias_sd* threshold are shown in Fig. 4.6. The distribution and magnitude of damage indices in the members are close to those of the standard case, and *sdlmt*, the limit value for *bias_sd*, can also be selected at the slightly higher point of 2.5 from Fig. 4.6, where the damage probability is 3% for the least sensitive member. The *bias_cx* values for the baseline structure are generally smaller than those from the case where the number of measured displacements was reduced in damage case [*1−1*]. However, this observation does not mean that the case with the reduction in the measured degrees of freedom can provide better results than the case with the reduction in the number of load cases. If the measured degrees of freedom are different with the same number of measured displacements, the estimated results would be different. If multiple damaged members exist at the same time, the detection of those members will not be so easy in this case, because the number of parameters are restricted by the limited amount of measured information.

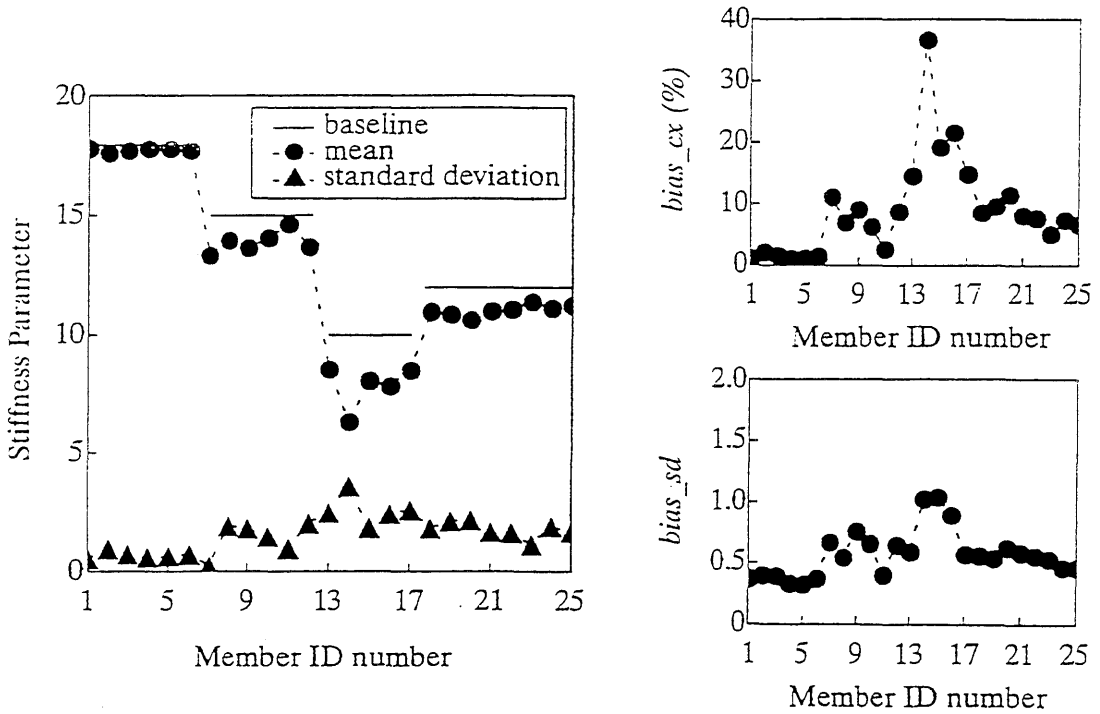

Fig. 4.5 : Mean parameters and damage indices for each member in the baseline structure with the same test conditions as damage case [*1−2*]

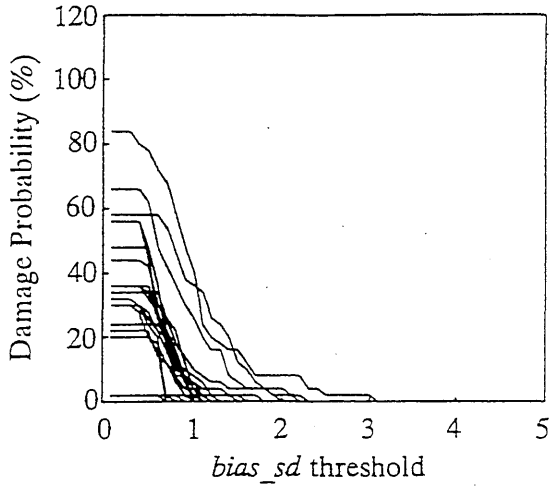

Fig. 4.6 : Variation of damage probability for the baseline structure in damage case [*1−2*] with respect to *bias_sd* threshold when *cxlmt*=10%

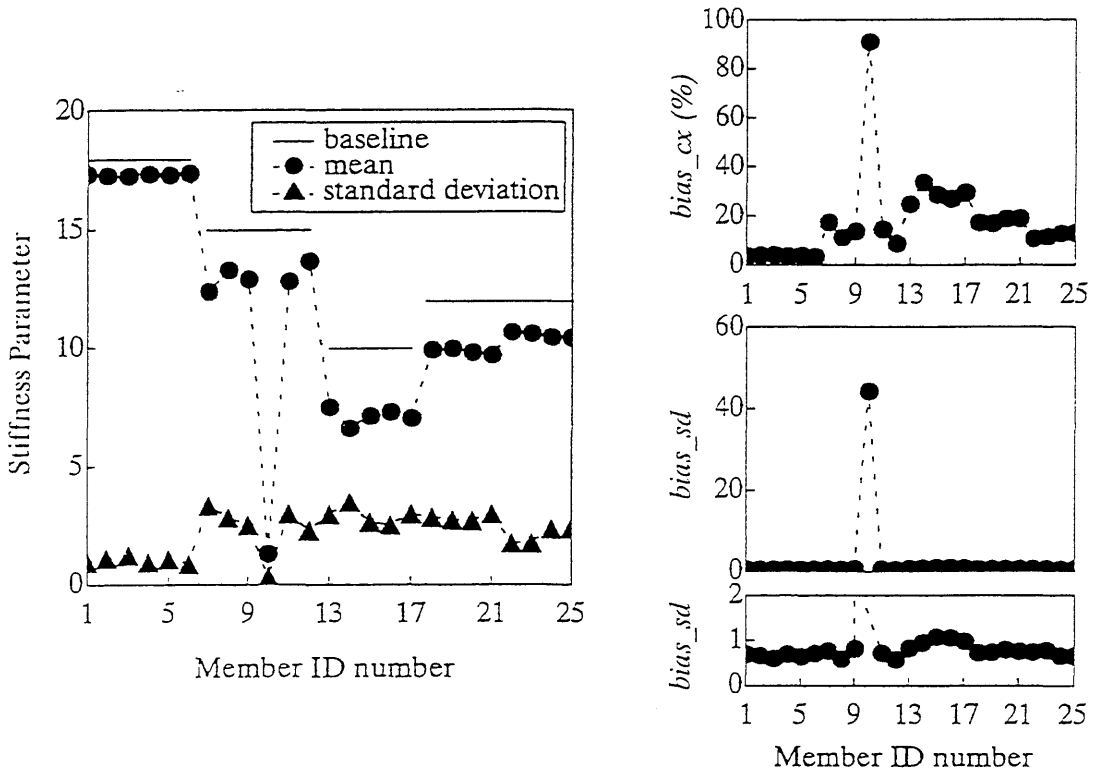

Fig. 4.7 : Mean parameters and damage indices for each member in damage case [*1−2*]

With the determined limit values of *cxlmt*=10% and *sdlmt*=2.5 from the evaluation of the baseline structure, the damage state of each member is investigated, and member (*10*) can be easily detected as damaged from Fig. 4.7. Since Monte Carlo trials are also carried out for the damaged structure for the simulation, the selected two limit values can be verified by computing the probability that the actually undamaged members are detected as damaged in the right-hand-side figure of Fig. 4.8.

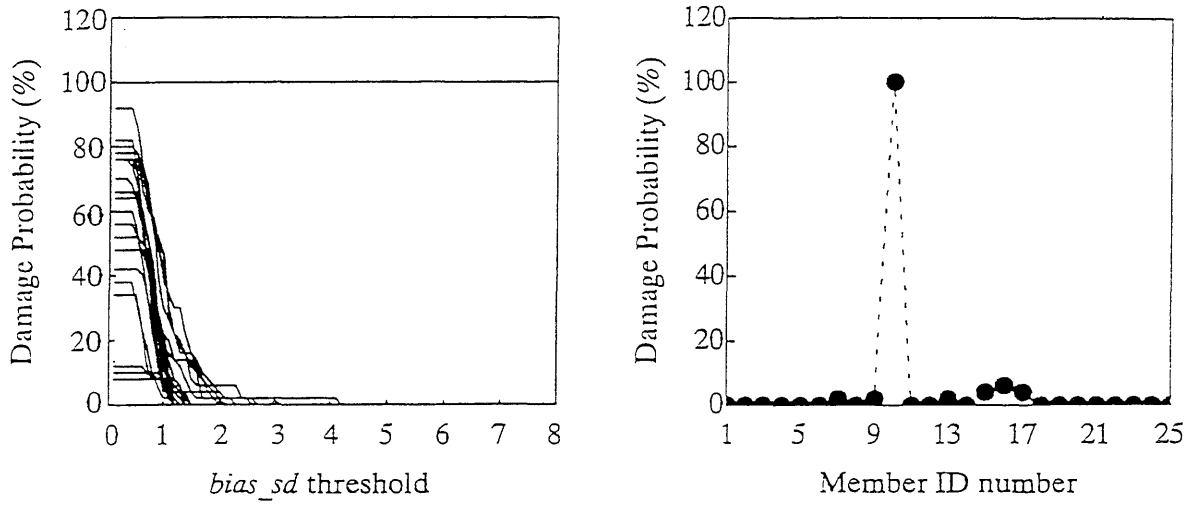

Fig. 4.8 : Variation of damage probability with respect to *bias_sd* for damage case [*1−2*], and damage probability of each member when *cxlmt*=10% and *sdlmt*=2.0 are selected

Even though there is some possibility that some of the vertical members can be detected as damaged by the selected upper limits for the damage indices, the possibility can be easily neglected by the engineer when he or she compares the figures for the damage indices from the damaged structure with the selected limit values. The computed *bias_sd* values for those members may be a little higher than but close enough to the selected *sdlmt*. The determination of damage should be based not only on the selected two limit values but also on the sensitivity of the member. From the right-hand-side figure of Fig. 4.8 for damage case [*1−2*], it can easily be verified that the damage probability curves drop around the same value of *sdlmt* from the baseline case when the same test condition of damage case [*1−2*] is applied.

4.3 Damage Case [*2−1*]

The variation of this damage case from the standard case is that a single member is lightly damaged by 20% rather than is highly damaged by 93% as the standard case. The same member (*10*) is damaged, but its sectional area is simulated to be reduced to 12.0 in^2 from 15.0 in^2. Another variation from the standard case is that the amplitude of noise in measurements is assumed to be 5% proportional error rather than 10% error. Since the level of damage is just 20%, even 5% measurement error may be high enough to pollute the damage assessment results.

The statistical properties from the study of the baseline structure are summarized in Fig. 4.9 with the same test conditions as damage case [*2−1*]. The mean and standard deviation values are averaged from a number of Monte Carlo trials, and thus the damage indices for each member are also computed from the averaged mean and standard deviation. From Fig. 4.9 comparing with Fig. 3.9 of the standard case, we can observe that the distributions of damage indices are similar to those from the standard case. The vertical and diagonal members are easily observed as insensitive with respect to the current test conditions.

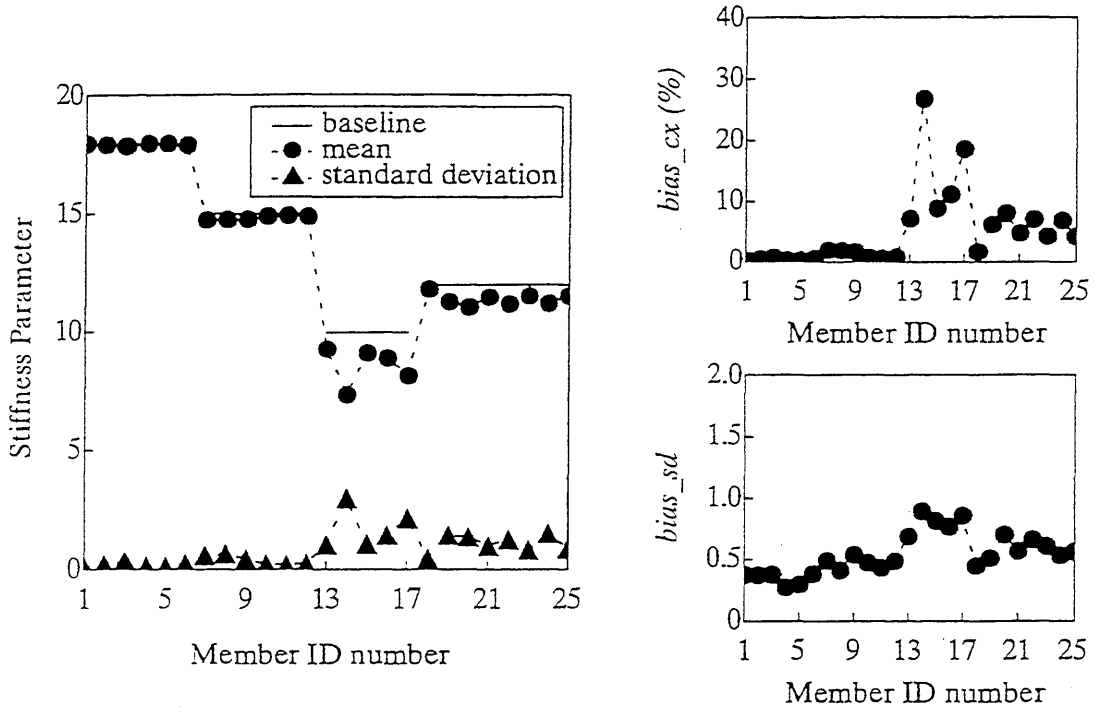

Fig. 4.9 : Mean parameters and damage indices for each member in the baseline structure with the same test conditions as damage case [2−1]

The limit value for the *bias_sd* damage index is determined from the damage probability curves as shown in Fig. 4.10 when *cxlmt* is defined as 5%. All the curves drop rapidly and can reveal a clear limit point *sdlmt* from the figure. For the current case, the value of *sdlmt* selected at 1.8 as the upper limit values for the *bias_sd* damage indices where the damage probability is 3%, and *cxlmt* is fixed at 5% as the same value as the known amplitude of proportional noise. The reduced value of *sdlmt* compared with the standard case is believed due to the decreased amplitude of noise in measurements.

Damage is determined for each member by comparing the computed damage indices with the selected limit values of *cxlmt*=5% and *sdlmt*=1.8 from the baseline case. If the averaged damage indices in Fig. 4.11 are compared with the selected limit values, unfortunately none of the members seem to be detected as damaged by the selected limit values, even though member (*10*) shows the highest possibility of damage due to its largest *bias_sd* damage index. To investigate the phenomenon in each Monte Carlo simulation trial, the damage probability for each member with the selected limit values for the damage indices are drawn in Fig. 4.12. The right-hand-side figure in Fig. 4.12 clearly reveals why member (*10*) cannot be successfully detected as damaged. When the selected value of *sdlmt*=1.8 is applied, the probability that member (*10*) can be detected as damaged is just 6%. The results may indicate that the proposed algorithm may not detect the actually damaged members when those members are lightly damaged but the amplitude of noise in measurements is relatively high. The left-hand-side figure in Fig. 4.12 also supports the same conclusion. In the figure, the damage probability curve

for member (*10*) is the top line. As *sdlmt* is selected with a larger value, the probability that member (*10*) is detected as damaged clearly diminishes even though it is still higher than the others. Member (*10*) cannot be detected as damaged with a larger *sdlmt*. Conversely, as *sdlmt* is selected with a smaller value, the probability that member (*10*) is detected as damaged increases but simultaneously the probability that the other actually undamaged members are detected as damaged also increases rapidly.

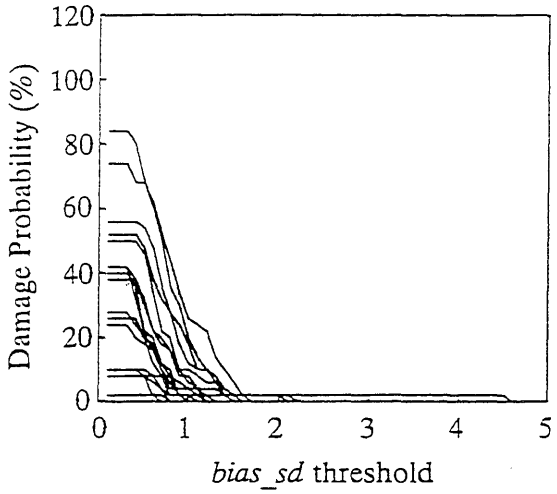

Fig. 4.10 : Variation of damage probability for the baseline structure in damage case [*2−1*] with respect to *bias_sd* threshold when *cxlmt*=5%

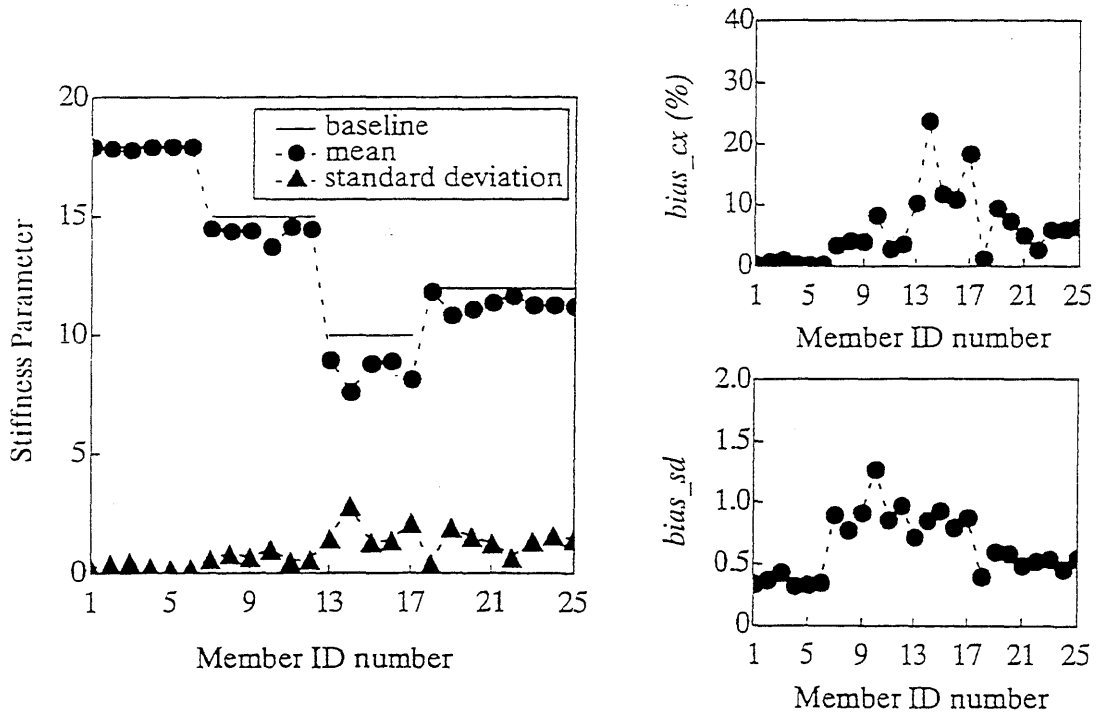

Fig. 4.11 : Mean parameters and damage indices for each member in damage case [*2−1*]

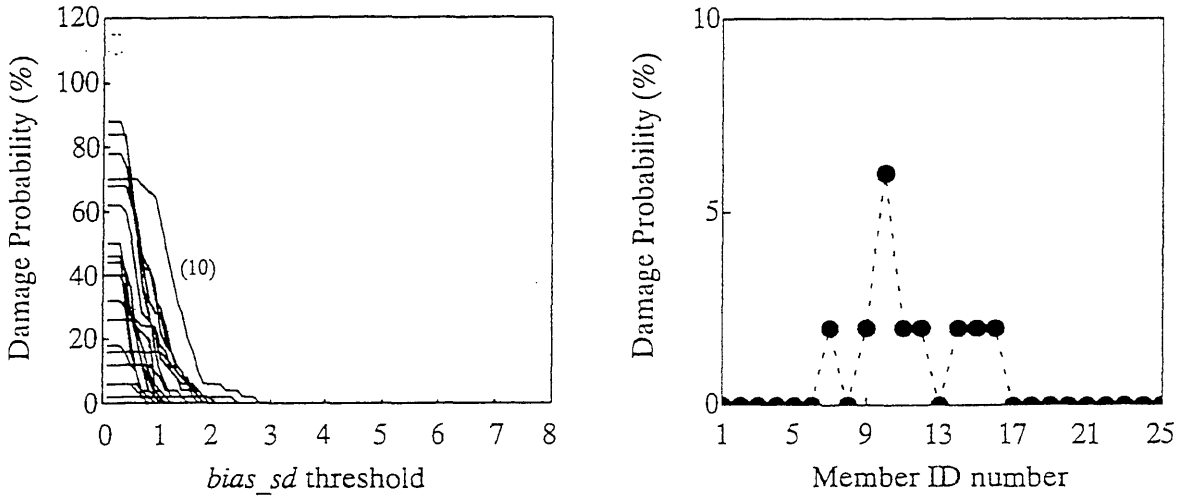

Fig. 4.12 : Variation of damage probability with respect to *bias_sd* for damage case [2−1], and damage probability of each member when *cxlmt*=5% and *sdlmt*=1.8 are selected

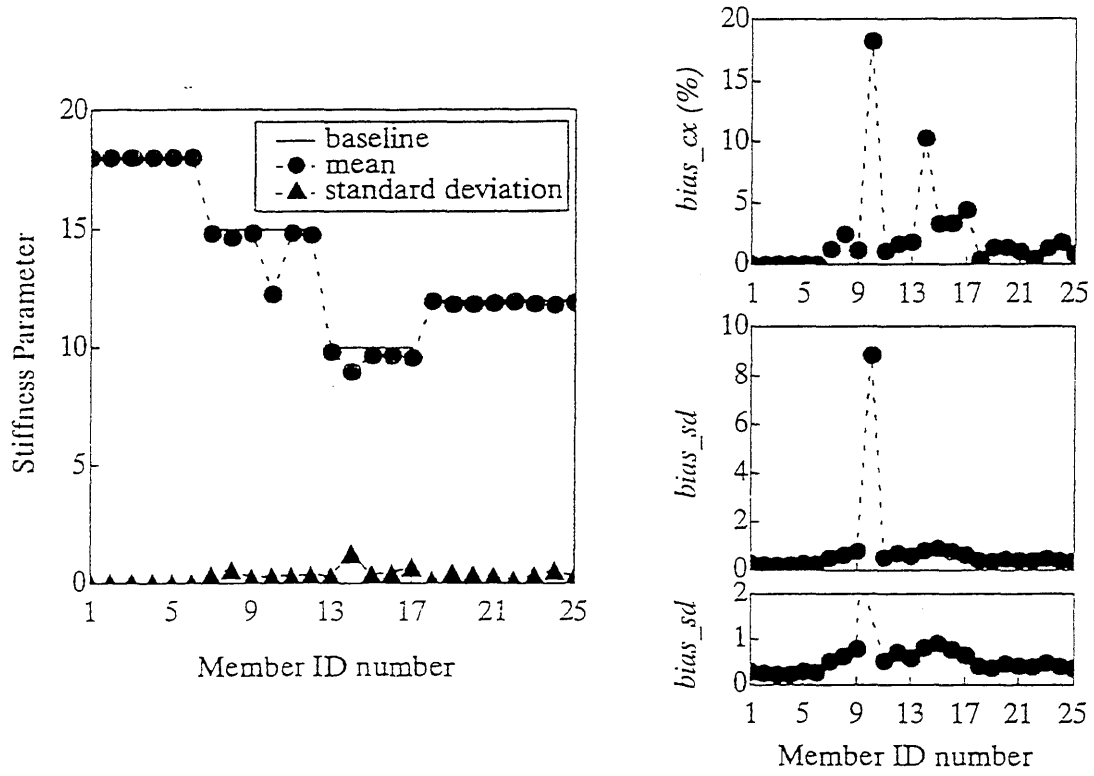

Fig. 4.13 : Mean parameters and damage indices for each member in damage case [2−2]

4.4 Damage Case [2−2]

From damage case [2−1], we could observe the difficulty in detecting the damaged member when it is lightly damaged with a reasonable but relatively high amplitude of noise compared with the severity of damage of the member. The current damage case [2−2] is studied by reducing the amplitude of noise in measurements from 5% to 1% proportional error without changing any other conditions.

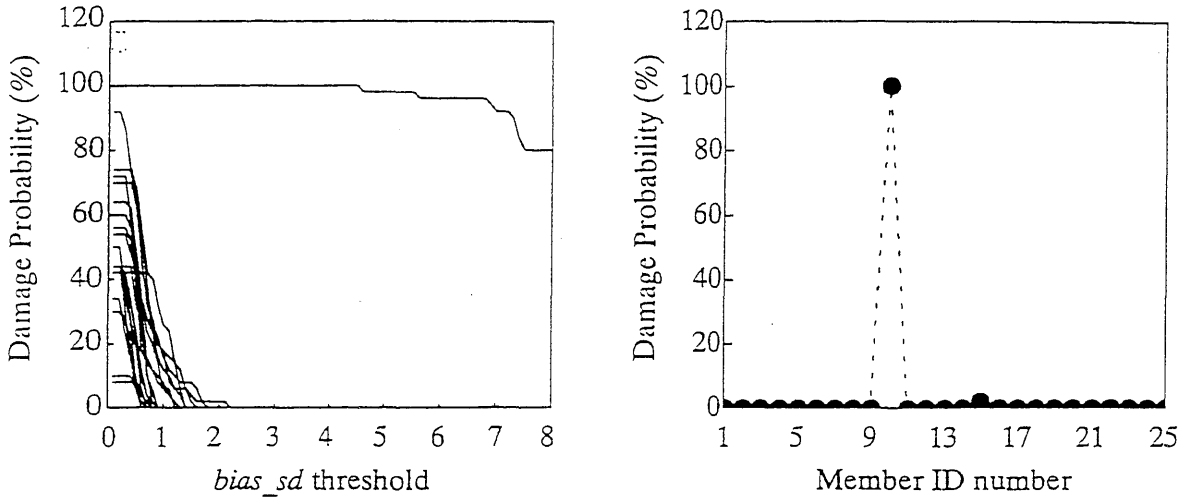

Fig. 4.14 : Variation of damage probability with respect to *sdlmt* for damage case [*2−2*], and damage probability of each member when *cxlmt*=1% and *sdlmt*=1.8 are selected

The results for the damage case averaged from a number of Monte Carlo simulation trials are shown in Fig. 4.13. If the two limit values are assumed by *cxlmt*=1% and *sdlmt*=1.8 as used for damage case [*2−1*], member (*10*) is clearly detected as damaged. The behavior of damage probability with respect to *bias_sd* threshold for the damaged structure of the case [*2−2*] also verifies the clear separation of member (*10*) as damaged by using the selected limit values in Fig. 4.14. The estimated parameter value of member (*10*) is also very close to the actual damaged value. Therefore, it can be concluded that even a lightly damaged member can be clearly detected and assessed if the measurements are accurate. However, if the amplitude of noise is not so low compared with the severity of damage, it will be hard to detect and assess damage. The noise in the measurements must be still the biggest enemy in correctly detecting and assessing damage by the developed algorithm.

4.5 Damage Case [*3*]

In this section, the capability of the developed algorithm is tested by a case where multiple members are damaged with different severities. Three members, member (*3*), (*9*), and (*10*) in the bowstring truss structure as shown in Fig. 3.2 are simulated to be damaged.

All the damaged members are selected from the top and bottom members whose parameters have been verified as relatively sensitive with respect to the current load cases and the measured degrees of freedom. Damage is simulated as 67% reduction in the sectional area of member (*3*), 40% reduction in member (*9*), and 93% reduction in member (*10*). The amplitude of noise in measurements is assumed to be known as 5% proportional error for this damage case. Since the amplitude of noise is 5%, the evaluation results of Fig. 4.9 and Fig. 4.10 for the baseline structure for the damage case [*2−1*] can be used directly. From the study for the baseline structure, two limit values for the damage indices were selected by *cxlmt*=5% and *sdlmt*=1.8.

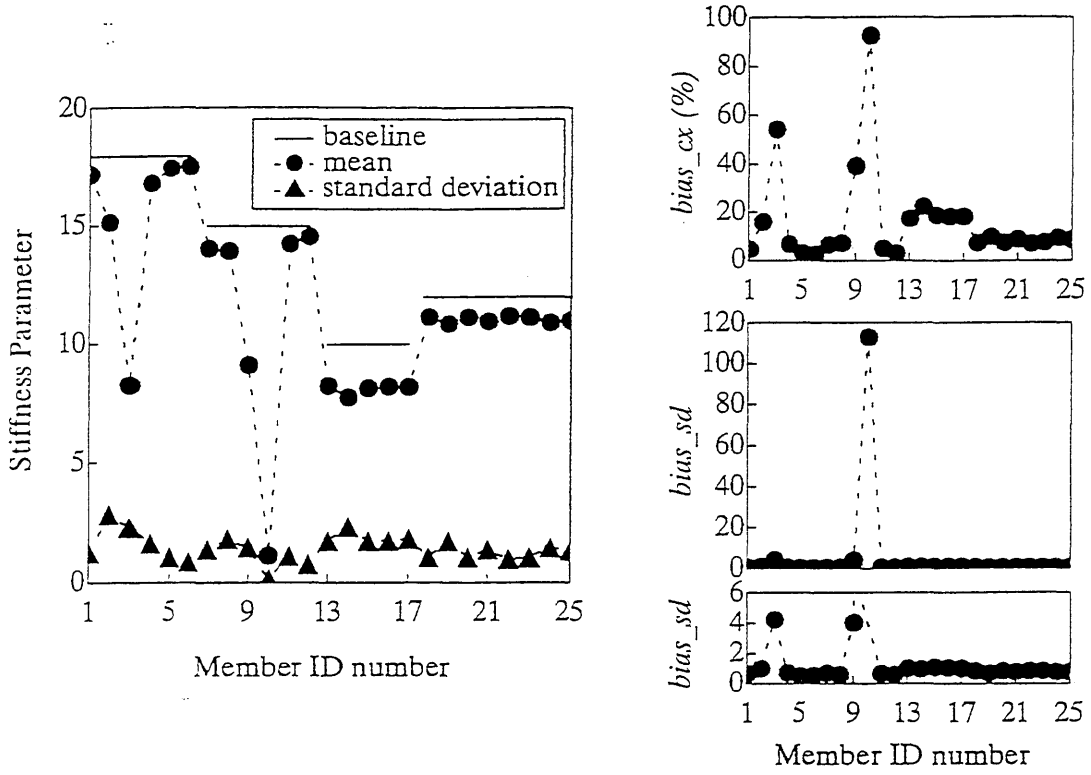

Fig. 4.15 : Mean parameters and damage indices for each member in damage case [3]

The member parameters and their damage indices averaged from Monte Carlo trials are drawn in Fig. 4.15. By applying the selected limit values, the three members can be easily detected as damaged from the damage index figures. The *bias_sd* value for member (*10*) is much higher than those of the other two damaged members, but the other two damaged members also have still relatively higher *bias_sd* values than the remaining members. Without the help of the limit values for the damage indices, it might be possible for an engineer to ignore the possibility of damage in members (*3*) and (*9*) or to consider the possibility of damage in the vertical members (*13*)–(*17*). The reason why member (*10*) has much larger *bias_sd* value may be because member (*10*) is more seriously damaged than the other two and its parameter is sensitive enough to provide a sound estimation result.

When the damage probabilities from simulated Monte Carlo iterations are drawn with respect to the *bias_sd* threshold for each member of the damaged case structure in Fig. 4.16, the simulation study demonstrates the clear separation of the damaged members from the other undamaged ones. An observation is that the probability that the actually undamaged members are detected as damaged is a little higher than the single member damaged cases. Another important feature which is demonstrated by the left-hand-side figure of Fig. 4.16 is that the figure can provide the answer for the question why the value of *bias_sd* threshold at the sudden-drop location should be used for *sdlmt*. When multiple members are damaged at the same time, a larger *sdlmt* value decreases the probability that actually damaged members are detected as damaged, even though the probability that actually undamaged members are detected as damaged decreases.

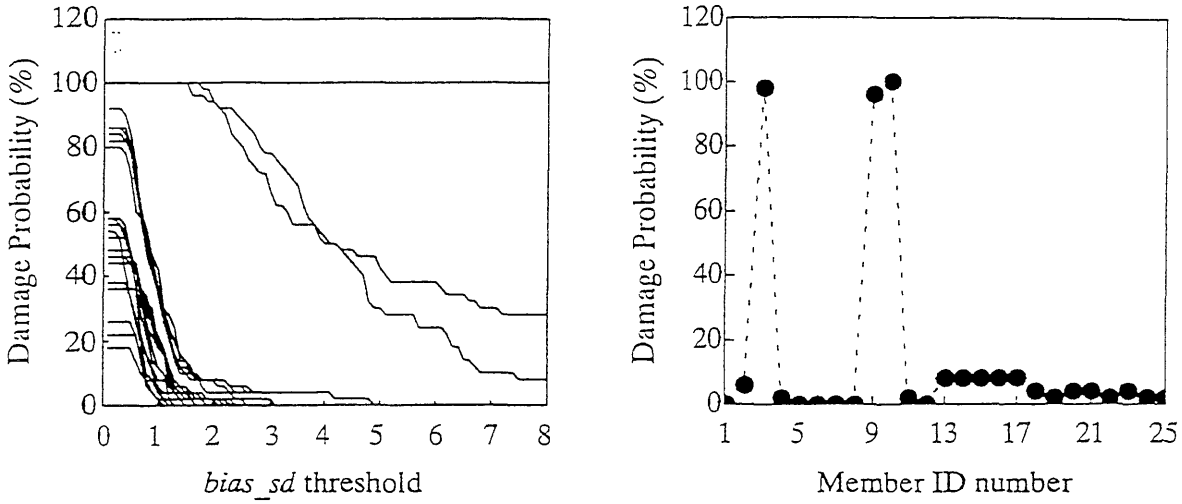

Fig. 4.16 : Variation of damage probability with respect to *bias_sd* for damage case [3], and damage probability of each member when *cxlmt*=5% and *sdlmt*=1.8 are selected

4.6 Damage Case [4]

This damage case also has multiple damaged members. Two members are simulated as damaged rather than three members. In addition, one of the damaged members is selected from the vertical member whose parameters have been observed as insensitive with respect to the current test conditions. The sectional area of member (*10*) is reduced to 5.0 in^2 from 15.0 in^2, and that of member (*15*) to 3.0 in^2 from 12.0 in^2. Both members are simulated to be damaged by 67%. Since the amplitude of noise is assumed to be 5%, the evaluation results for the baseline structure can be obtained from Fig. 4.9 and Fig. 4.10 for damage case [2−1]. The selected limit values from the baseline case therefore are *cxlmt*=5% and *sdlmt*=1.8.

By applying the selected limit values for the damage indices, the two damaged members can be detected as damaged from Fig. 4.17. The *bias_sd* value for member (*10*) is much larger than that of member (*15*), even though their damages are at the same level. That may be because member (*10*) is more sensitive than member (*15*) for the current test conditions. Even though the *bias_sd* value for member (*15*) is smaller than that for member (*10*), it is still large enough to be detected as damaged compared with the selected limit values.

The damage probability figures in Fig. 4.18 obtained from Monte Carlo trials for the simulation demonstrate the usefulness of the selected limit values for the damage indices, even though some actually undamaged vertical members (*13*)−(*17*) have relatively high possibility of being detected as damaged. From the figure, we can observe that the damaged member (*15*) from the insensitive vertical members have some possibility of being considered as undamaged when the two selected limit values are used. The aspect can be easily observed from the left-hand-side figure in Fig. 4.18. The damage probability curve for member (*15*) with respect to *bias_sd* threshold decreases gradually after a certain *bias_sd* threshold value. From the simulation study for this damage case [4], it can be concluded that

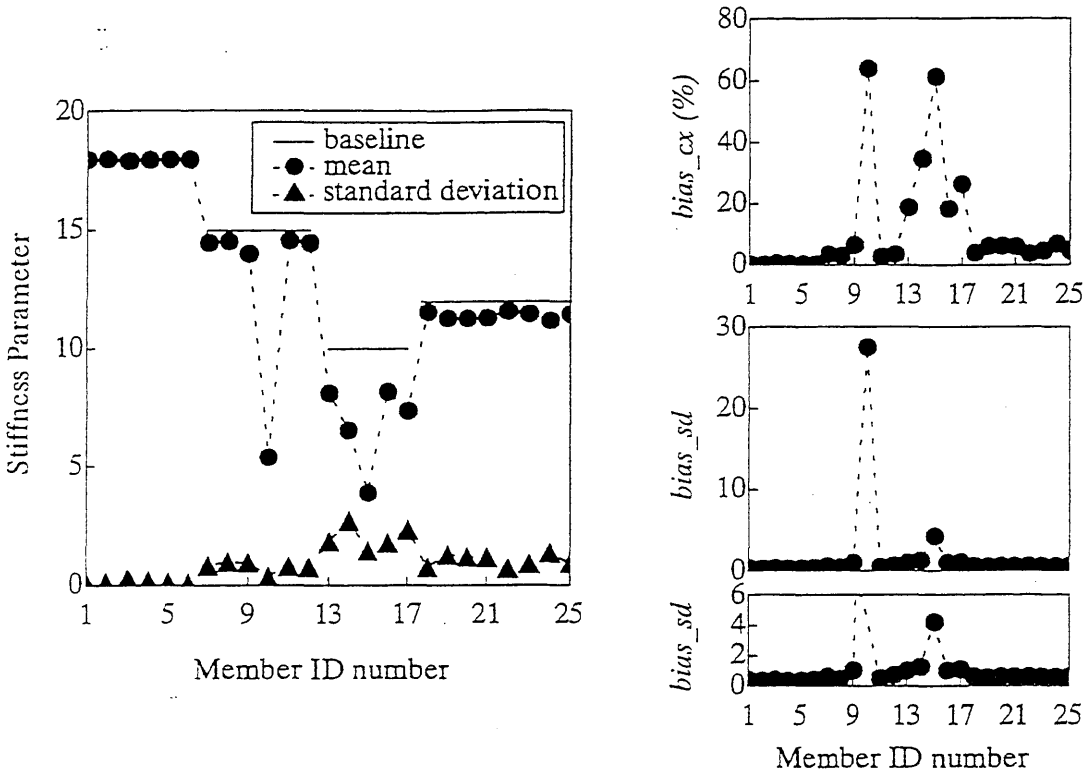

Fig. 4.17 : Mean parameters and damage indices for each member in damage case [4]

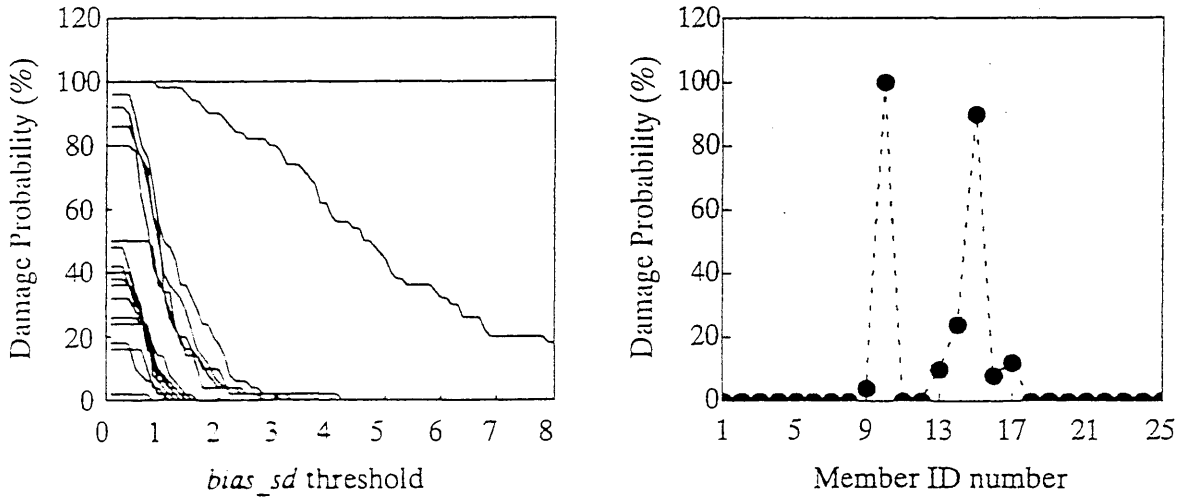

Fig. 4.18 : Variation of damage probability with respect to *bias_sd* for damage case [4], and damage probability of each member when *cxlmt*=5% and *sdlmt*=1.8 are selected

any insensitive but damaged members can be also detected successfully by the developed algorithm, but their applicability may be limited by the test conditions and the severity of damage. Generally, it may be true that damage in an insensitive member will be more difficult to detect and assess than damage in a sensitive member. However, when the amplitude of noise is small enough, any insensitive but damaged member can be detected by the developed algorithm.

4.7 Summary

Some damage cases have been studied with variations from the standard damage case described in *Chapter Three*. The cases are selected to test the developed algorithm and the proposed procedure of selecting the limit values for the damage indices at some critical conditions. Cases with the lowest amount of measured data have been tested in damage cases [*1−1*] and [*1−2*], and the cases with a lightly damaged member were tested in damage cases [*2−1*] and [*2−2*]. Also, the cases with multiple damaged members with different or same levels of damage were tested by damage cases [*3*] and [*4*]. From the simulation results, it has been observed that generally the developed algorithm can detect and assess damage successfully. However, there always exists the possibility that actually undamaged members will be detected as damaged or that the actually damaged members will not be detected as damaged depending on the test conditions and the sensitivity of the damaged members. A sure fact is that the results will be improved if the noise in the measurements decreases.

When some members are detected as damaged by a slight difference from the selected limit values, the engineer may judge its real possibility of damage from the figures for the damage indices. If the member is believed to be insensitive with respect to the current test conditions, the engineer must be suspect of its possibility of damage and may need to gather more information on the member. By comparing the behaviors of damage indices of the similarly insensitive members, the real possibility of damage in a member can be judged by the engineer. In any event, the most possibly damaged member can be detected and thus can be recommended to be inspected if it is believed to be considerably damaged.

The selected *sdlmt* values in the case studies range between 1.8 and 3.0 according to the test conditions. As the known amplitude of noise in measurements increases and as the amount of measured information decreases, a higher value of *sdlmt* is selected. From the case studies, the usefulness of *sdlmt* for detecting damage in a structural system has been verified. It has been observed that the selection of *cxlmt* is not so important as *sdlmt* value for detecting damage, but it can be used for the cases where *sdlmt* cannot be effectively used to determine damage due to a large value of *bias_sd* damage index.

Chapter Five

Real Case Study – Modal Response

Modal tests are often more practical than static tests in the field. Modal response can be measured more easily and effectively than the static responses because it is possible to measure modal accelerations rather than displacements. Experimental methods for measuring modal response of structural systems are well established (Ewins 1984). However, the applications of modal tests for civil structures seem to be relatively limited so far mainly because of their size, complexity, and inaccessibility. Some recent modal tests for bridge structures are available in the literature (Abel-Ghaffar, *et. al.* 1993; Douglas and Reid 1982; Gardner-Morse and Huston 1993; Jones and Thompson 1993; Mazurek and DeWolf 1990; Lintermann 1986; Raghavendrachar and Aktan 1992; Salene and Baldwin 1990; Yen and Baber 1993). A study of the Oakland city hall building with measured modal properties from a forced vibration was performed by Banan and Hjelmstad (1993).

In this chapter the developed damage assessment algorithm is used to locate a crack and to assess the member properties of the cracked cantilever structure as shown in Fig. 5.1. The modal responses were obtained from an experiment by Rizos, *et. al.* (1990). The geometry of the cantilever structure and all of the necessary baseline properties, except the density of the material, were given in the literature. They measured flexural vibrations of a cantilever beam with a rectangular cross-section having a transverse surface crack extending uniformly along the width of the beam. Experimental methods and the results of the experiment are summarized first. Then, the crack detection is carried out by our damage assessment algorithm with two different types of beam models: (*1*) Bernoulli-Euler beam

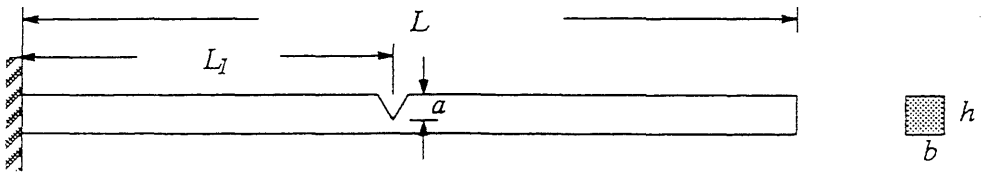

$L = 300\ mm$ $\quad a = 10\ mm$
$L_1 = 140\ mm$ $\quad b = h = 20\ mm$

Fig. 5.1 : Cracked cantilever beam specimen

elements and (2) Timoshenko beam elements. Since the finite element model is considered known in the damage assessment algorithm, the beam model is not refined after it is once established, but the parameter groups can be subdivided sequentially. Therefore, a fairly refined structural beam model is selected to insure a satisfactory discretization. In this chapter, for each beam type, various structural models with different numbers of beam elements are used to identify the cantilever structural system, and their results are compared.

5.1 Summary of the Experiment

The modal response of the cracked cantilever beam specimen shown in Fig. 5.1 were obtained from an experiment by Rizos, *et. al.* (1990). They measured natural frequencies and modal displacements of the cantilever beam with a transverse surface crack extending uniformly along the width of the beam. A 300 *mm* cantilever beam of cross-section $20 \times 20\ mm^2$ was clamped to a vibrating table. The modulus of elasticity of the material was $E = 2.06 \times 10^5\ MPa$, but the material density was not specified in the paper. Harmonic excitation was applied and only one mode at a time was investigated. The crack was initiated with a thin saw cut and propagated to the desired depth by fatigue loading. The crack depth was measured directly and verified with an ultrasonic detector for uniformity and actual depth of the crack. Even though they tested various cases with different crack locations and different crack depths, they provided the results of one case in the paper with the crack depth $a = 10\ mm$ and the crack location L_2 clamped end $L_1 = 140\ mm$ as shown in Fig. 5.1.

The vibration amplitude was measured at nine locations: 30 *mm*, 60 *mm*, 90 *mm*, 120 *mm*, 150 *mm*, 180 *mm*, 210 *mm*, 270 *mm*, and 300 *mm* from the clamped end. The amplitude at the uniform distance of 240 *mm* from the clamped end is missing. The measured modal displacements were normalized with respect to the maximum vibration amplitude. Mode shapes were measured by using two calibrated accelerometers mounted on the beam. One accelerometer was kept at the clamped end of the beam to give the reference input and the other accelerometer was moved along the beam to measure the mode amplitude. The mass of the accelerometer was negligibly small compared with

Table 5.1 : Normalized measured modal displacements of the cracked cantilever beam

† x/L	*1st* Mode ϕ_1	*2nd* Mode ϕ_2	*3rd* Mode ϕ_3
0.1	0.027	0.069	0.033
0.2	0.063	0.149	0.103
0.3	0.109	0.276	0.221
0.4	0.156	0.444	0.288
0.5	0.236	0.516	0.011
0.6	0.354	0.400	−0.387
0.7	0.487	0.200	−0.498
0.9	0.778	−0.455	−0.203
1.0	0.940	−0.899	0.435

† x = the distance from the clamped end

the mass of beam. The measured natural frequencies of the cracked beam were 171 *Hz*, 987 *Hz*, and 3034 *Hz* for the first, second, and third mode, respectively. The measured modal displacements at nine locations for each mode are extracted directly from the mode shape figures in the paper and summarized in Table 5.1. The digitized measured modal displacements therefore may contain the error in extracting the measured modal displacement from the published paper in addition to the measurement error. The amplitude of noise must be approximated before detecting the crack by the developed damage assessment algorithm.

5.2 Structural Models

Two different types of structural models for the cantilever structure are considered in the case studies: (*1*) the structure modeled by Bernoulli-Euler beam elements and (*2*) the structure modeled by Timoshenko beam elements. The only constitutive parameter associated with Bernoulli-Euler beam elements is the flexural stiffness EI of the beam, and the parameters for the Timoshenko beams are the flexural stiffness EI and the shear stiffness GA, where E and G are the elastic modulus and shear modulus, respectively, I is the inertia of moment, and A is the sectional area of the cantilever beam. The modulus of elasticity E is given by 2.06×10^5 *MPa* and the shear modulus is assumed as $G=0.4\,E$ for the case studies herein. The rotary inertia was neglected for all of the case studies.

A structural model for the cantilever beam is not exactly discrete as it was for the truss structure investigated previously. Depending on the engineer's judgement and the required accuracy, therefore, the model can vary with the number of beam elements. Models with different numbers of elements would produce different results, even if the same measured data are used for identifying a structure. Generally, a model with more beam elements would result in better estimation of the stiffness properties. For the developed damage assessment algorithm, a structural model should be as accurate as possible. Therefore, a finite element model with a reasonably fine mesh must be selected at first to reduce the error in the structural model discretization. Since the actual crack locations are unknown, a model with an equal size of beam elements should be considered for the developed damage assessment algorithm. In this chapter, some structural models with different numbers of beam elements are studied and their results are compared. The identified modal properties, the location of the detected crack, and the properties of the cracked element are evaluated and compared with the actual values.

For real experiments, a structural model should be verified first through a simulation study with the baseline structure. Then, the determined model can be used for detecting damage in the existing structure. The baseline information can be obtained from measurements on the undamaged structure, if measured response from the baseline structure is available. Since no measured data from the uncracked cantilever structure are available for the current problem, the missing information of the material density and the amplitude of noise should be assumed or deduced from the measured data from the cracked cantilever structure. Fortunately, since the exact crack location and uniform crack depth are given from the experiment in the paper, the missing information may be deduced.

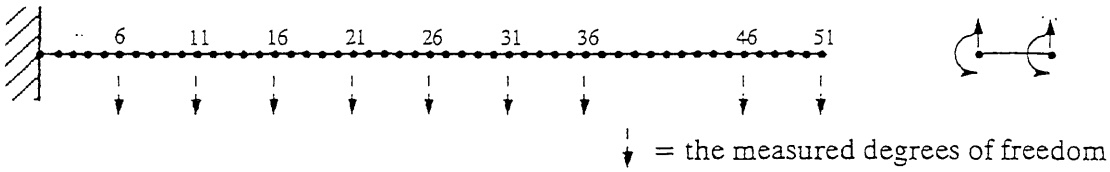

Fig. 5.2 : Structural model with 50 beam elements

5.2.1 Determination of the Mass Density

The geometry of the cantilever structure and the modulus of elasticity of the material are given by Rizos, *et. al.* (1990). However, the material density is not provided in the paper. From the value of the modulus of elasticity $E=2.06\times10^5$ *MPa*, the material seems to be *steel* with a usual density value of 7.8×10^3 kg/m^3 (Ashby and Jones 1980). To validate the density value, a structural model with 50 beam elements was created as shown in Fig. 5.2, and natural frequencies were computed and compared with the measured ones. Element (*i*) connects node *i* and *i+1*. Node *1* is completely fixed in all the degrees of freedom. Both Bernoulli-Euler beam and Timoshenko beam were used to validate the density value. The flexural stiffness of the baseline cantilever structure was input as $EI=2746.67\ MN\cdot mm^2$, and the flexural stiffness of the cracked element (*24*) in the structural model is input as $EI=343.33\ MN\cdot mm^2$ computed by the reduction of the sectional depth. For the Timoshenko beam, the shear stiffness was assumed to be $GA=32.96\ MN$ for the uncracked elements and by $GA=16.48\ MN$ for the cracked element. A lumped mass was considered to construct the structural model and the rotational masses were taken as zero for both models. By selecting a 50 beam-element-model, the actual cracked section is located in element (*24*). The computed three lowest natural frequencies from the model with the density of steel are summarized in Table 5.2 and show a little higher values than the actually measured ones. The reason may be because the material type may be different from steel, the end conditions may not be perfectly fixed, or the beam models may not be adequate to represent the behavior of the cracked cantilever structure. To determine a suitable mass, we searched for the density that minimizes the gap between the identified natural frequencies and the measured ones. By minimizing the average error, the mass density was determined as 8.587×10^3 kg/m^3 for the Bernoulli beam and as 8.303×10^3 kg/m^3 for the Timoshenko beam model. The computed natural frequencies with the selected density values are very close to the actual values in all the

Table 5.2 : Measured and computed natural frequencies corresponding to density

Density ϱ (kg/m^3)		Frequency (*Hz*)		
		1st	*2nd*	*3rd*
ϱ = unknown	(measured)	171	987	3034
$\varrho = 7.800\times10^3$	(Bernoulli beam)	178	1033	3218
$\varrho = 7.800\times10^3$	(Timoshenko beam)	177	1020	3110
$\varrho = 8.587\times10^3$	(Bernoulli beam)	169	985	3067
$\varrho = 8.303\times10^3$	(Timoshenko beam)	172	989	3014

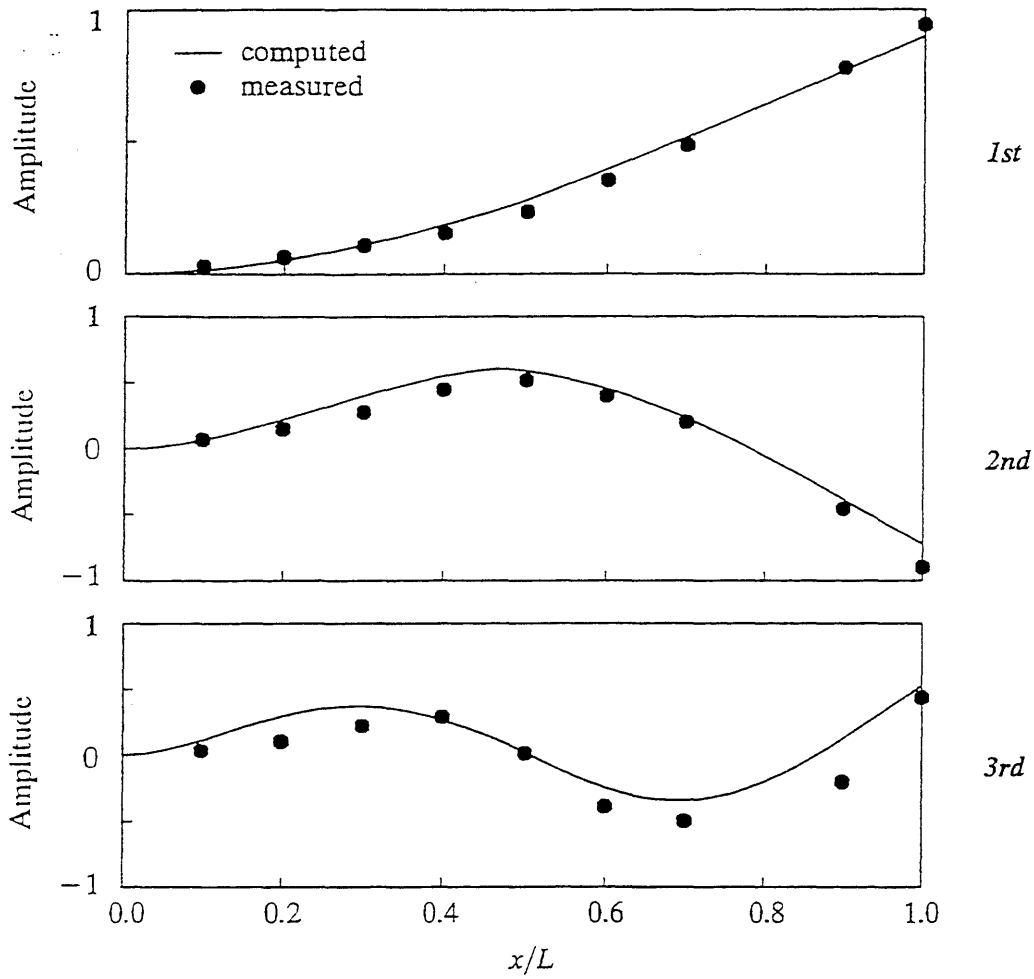

Fig. 5.3 : The computed lowest three mode shapes of the Bernoulli-Euler beam model with 50 elements when the flexural stiffness of element (*24*) is reduced ($\varrho = 8.587 \times 10^3\ kg/m^3$)

three modes with less than 1% error. Even though the obtained density seems to be a little high judged from its modulus of elasticity, the obtained densities are used in the case studies for detecting cracks in the cantilever structural system.

With the determined material density and the created Bernoulli-Euler beam model for the structure shown in Fig. 5.2, the modal displacements of the three lowest modes were computed and plotted as solid lines and are compared with the measured data in Fig. 5.3. The computed modal displacements are normalized for each mode by the norm of the computed displacement components at the measured degrees of freedom and by the norm of the nine measured displacements. The mode shapes of the Timoshenko beam model show trends similar to those of the Bernoulli beam model, even though the figures are not drawn here. It is observed from Fig. 5.3 that the computed first and second modes are close to the measured data but the computed third mode shape shows a relatively large discrepancy from the measured mode even though the modal frequencies are close to each other. We can explain this phenomenon by different points of view. The first explanation may be that the consid-

ered linear elastic beam models may not be adequate to describe the behavior of the cracked cantilever beam. In the proposed beam models, the property of the cracked region is represented simply by the reduced stiffness properties of the element containing the crack, and the size of the cracked element is the same as the rest. Since the crack was created by propagating an initial thin crack to a certain depth by fatigue loadings, and since the third mode was measured after the tests for the first and second modes, the cracked region might be more damaged. Another viewpoint is that the measurement error involved in the third mode may be larger than those in the other modes. Regardless of its origin, the discrepancy can be considered as a kind of measurement error in detecting cracked zones by the developed damage assessment algorithm.

5.2.2 Determination of the Amplitude of Noise

The amplitude of noise in the measured data from the experiment is another missing but necessary piece of information. To determine the approximate noise amplitude in the measured data, the errors in the natural frequencies and the modal displacements are evaluated. The total error in the modal displacements is the sum of the error in the actual measured data and the error in digitizing the plotted data from the paper. Since the material density was selected as the value which minimizes the gap between the measured natural frequencies and the computed frequencies, the error in the natural frequencies are negligibly small compared with the discrepancies in the modal displacements. To compute the error between the identified mode shape and the measured modal displacements, two error indicators are computed as defined by:

$$MDC_i = \frac{\| (\hat{\varphi}_i)_a - (\hat{\varphi}_i)_d \|}{\| (\hat{\varphi}_i)_d \|} \qquad i=1,2,3 \qquad (5.1)$$

$$MAC_i = \frac{[\ (\hat{\varphi}_i)_d \cdot (\hat{\varphi}_i)_a\ ]^2}{\| (\hat{\varphi}_i)_d \|^2\ \| (\hat{\varphi}_i)_a \|^2}$$

where MDC_i and MAC_i are the modal displacement closeness and the modal assurance criterion of the measured components of the modal displacements for the ith mode, $\hat{\varphi}_i$ is the ith modal displacement vector only at the measurement locations. The subscripts a and d denote the identified analytical solution and the measured displacements of the cracked cantilever beam, respectively. By definition, as the identified mode shape is closer to the measured shape, the value MDC approaches zero and the value of MAC approaches unity. However, eventually both indicators contain the same trend of error behavior in the identified modal displacements.

The errors for each mode are computed as the differences between the measured data and the computed response with the 50 Bernoulli beam-element model. Table 5.3 summarizes the computed errors for each mode. From the table, one can observe that the error in the natural frequencies are very small in all the modes, but the error in the modal displacements increases as a higher mode is compared. For the case studies in this chapter, therefore, 10% proportional error is assumed as a reasonable choice for the average amplitude of measurement noise.

Table 5.3 : Errors in natural frequencies and the modal displacements between the measured data and the computed response from the Bernoulli beam-element model

Errors		Mode		
		1st	*2nd*	*3rd*
in natural frequency (%)		1.0	0.3	1.1
in modal displacements	*MDC*	0.064	0.206	0.535
	MAC	0.996	0.958	0.734

5.3 Bernoulli-Euler Beam Model

For the Bernoulli-Euler beam model, the flexural stiffnesses of the beam elements are the only constitutive parameters that need to be estimated. By evaluating the reduction in the flexural stiffness in each element, we can detect damage. Since the number of measured modal displacements for each mode $\hat{n}_d$ is equal to 9 and the number of measured modes *nmd* is equal to 3 from the experiment, the limit number of unknown parameters n_{lmt} is 27 as defined by the identifiability criterion of Eq. (2.11). Since the member properties of the uncracked baseline cantilever structure can be assumed to be uniform over the whole length of the structure, the number of parameter group starts from one and can be subdivided up to 27 groups.

The cantilever structure is modeled by a certain number of beam elements with an equal size because the actual locations of cracks are unknown. Because a structural model is given and is not updated for the developed algorithm, a reasonably refined finite element model should be selected to start with. After the model is selected, only the parameter groups are subdivided hierarchically without modifying the selected finite element model for the structural system. The level of refinement in a structural model depends on the engineer's judgement. If an engineer selects a model that is not detailed enough to detect local damage, erroneous results may be obtained. For the current study, a model with 50 Bernoulli-Euler beam elements is considered as a reasonably refined model, and some simpler models with 10, 20, and 30 Bernoulli-Euler beam elements are studied to compare the identification results. For the comparison, we will first check that the estimated modal responses match well with the measured data. Then, we will examine how accurately the cracked section can be located and how closely the member properties of the cracked section can be estimated by the damage assessment algorithm.

5.3.1 A Model with 50 Bernoulli-Euler Beam Elements

The model with 50 Bernoulli beam elements is the most refined case among the currently proposed case studies. Since each Bernoulli beam element has one parameter, the flexural stiffness, the number of total member parameters n_{sum} can be as great as 50. Since the limit number of parameters n_{lmt} is 27, the parameter grouping scheme must be applied. Since the material properties of the undamaged cantilever beam can be assumed as uniform over the whole length of the beam, the initial number of parameter groups can be taken as one for localizing damaged elements by the developed algorithm.

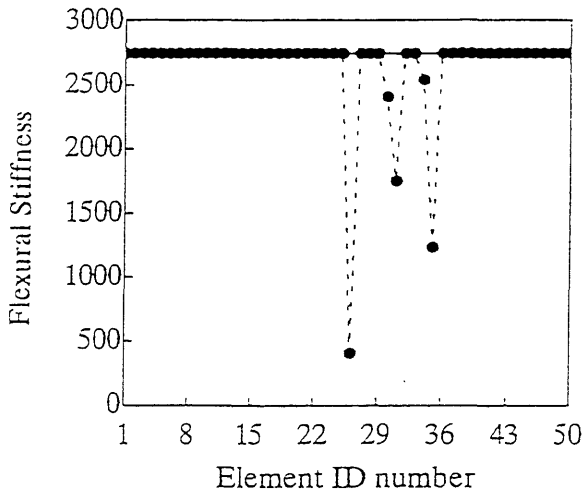

Fig. 5.4 : Estimated element flexural stiffness when the measured data are assumed to be exact

Before applying the measured data perturbation scheme to obtain statistical properties as proposed in *Chapter Two*, the candidate cantilever structure was identified assuming that the given measured data are exact. The purpose of this case study is to demonstrate how inaccurate most available damage assessment algorithms which do not consider the effects of noise in measurements on the estimation can be, even if the algorithms could overcome the sparsity of data by some special scheme. By neglecting the statistical aspects of the noise in the measurements, sensitivities of the parameters cannot be investigated and thus the obtained results may not provide enough information for detecting damage in the structure. The estimated flexural stiffness for each element is plotted in Fig. 5.4, assuming that the measure data are noise-free. Judging only from the figure, we might surmise that there are several cracks in the beam with different damage severities. Among them, element (*26*) is the most severely damaged one. The location of element (*26*) is very close to the actually cracked element (*24*). Its estimated flexural stiffness is also close to the actual value if damage can be represented simply by the reduction of the flexural stiffness. However, it is still difficult to justify that element (*26*) is the only cracked one in the cantilever structure from these results. Elements (*31*) and (*35*) are also likely to be cracked with less damage in the flexural stiffnesses.

To consider the statistical aspects of noise in the measured data, the measured modal displacement perturbation scheme was applied. By perturbation iterations, the sensitivities of the stiffness parameters with respect to the measured modes and measured degrees of freedom were investigated. The statistical properties obtained from the perturbation iterations may distinguish the damaged elements from undamaged ones more clearly. Before investigating the statistical aspects of the estimated parameters, we need to determine how many perturbation iterations are required to obtain statistical significance of the estimated flexural stiffnesses and the computed biases. Fig. 5.5 shows that at least 50 perturbation iterations are required for the estimation results to be steady, which is consistent with the result from the static case studies in *Chapter Three*.

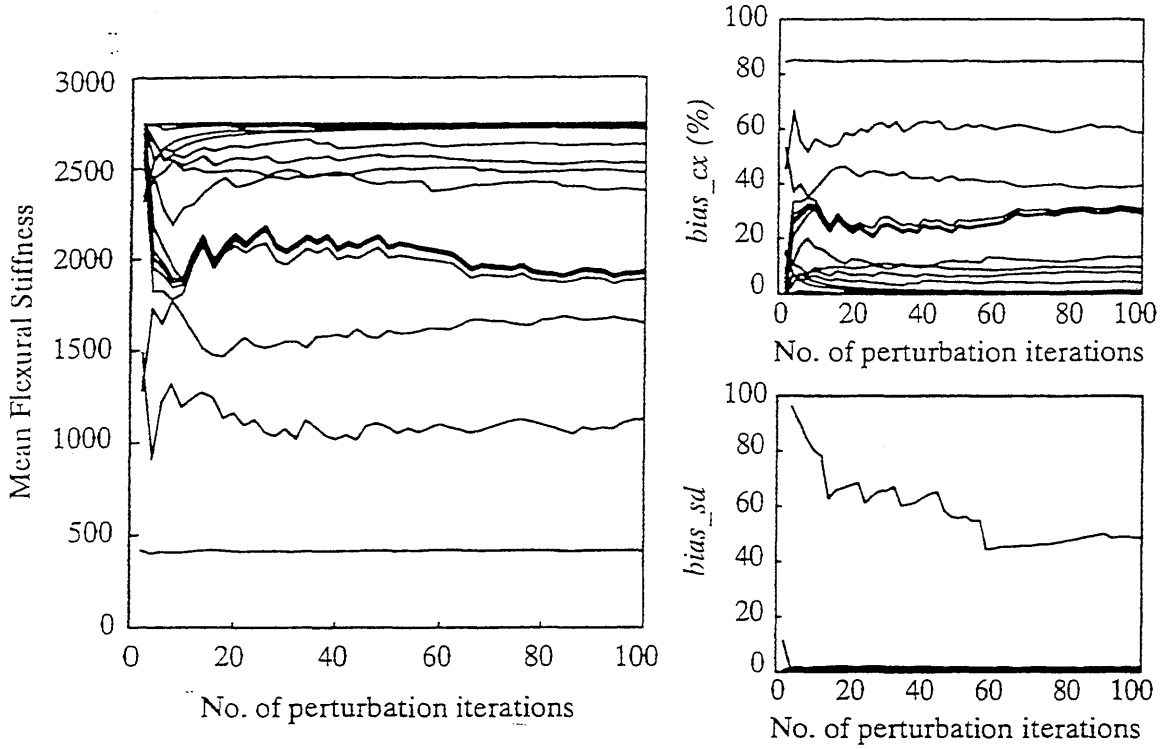

Fig. 5.5 : Variations of mean flexural stiffness and biases for each element with respect to the number of measured data perturbation iterations

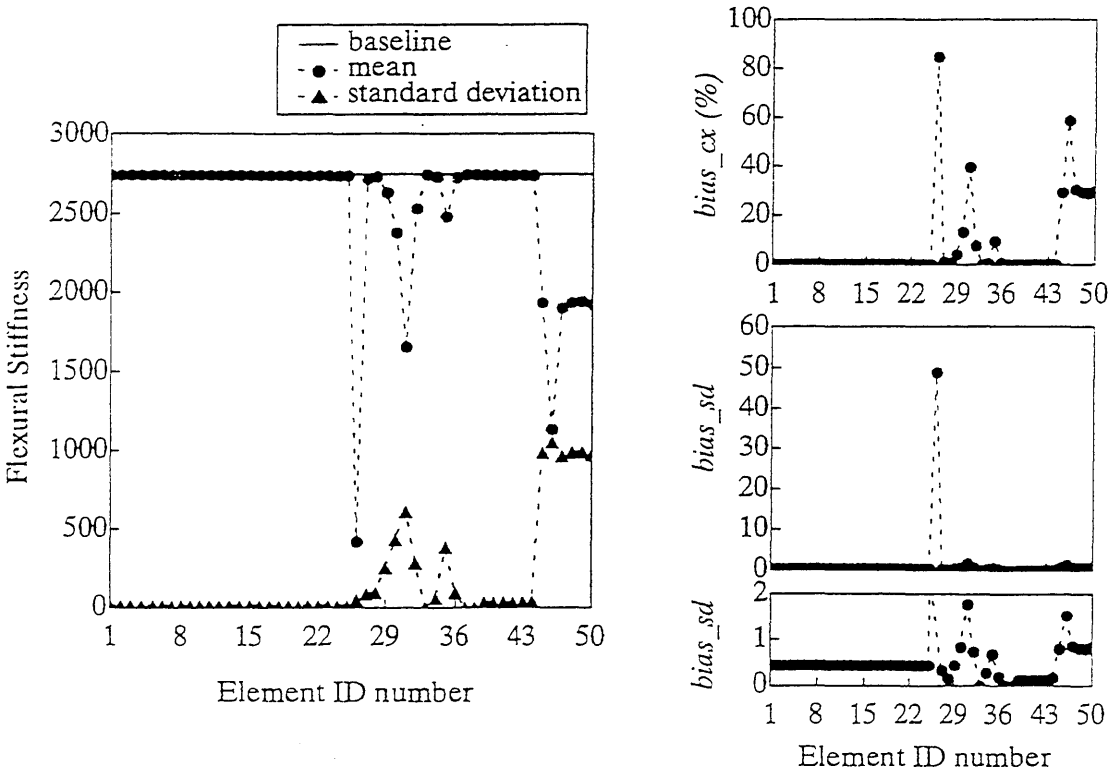

Fig. 5.6 : Damage detection and assessment with 50 Bernoulli beam element model

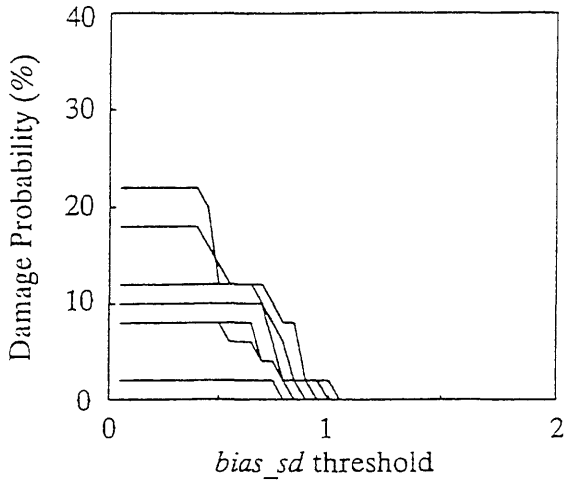

Fig. 5.7 : Variation of damage probability with respect to *bias_sd* damage index threshold for the baseline cantilever structure when *cxlmt*=10%

The computed mean and standard deviation values from 100 measured modal displacement perturbation iterations are drawn in Fig. 5.6. By considering the standard deviations, the figure of the damage index *bias_sd* reveals clearly that element (*26*) is the most possibly cracked element. However, some other elements such as elements (*31*) and (*46*) also seem to be damaged with their relatively high *bias_sd* values compared with the others. To verify their actual damage, the upper limit values for the damage indices should be determined from the simulation study for the baseline structure as suggested in *Chapter Three*. By definition, the upper limit value for the damage index *bias_cx* can be selected as *cxlmt*=10%, the same value as the proportional noise amplitude, and that for the *bias_sd* damage index can be determined from Fig. 5.7 as *sdlmt*=1.1. By the determined upper limit values, we can observe that elements (*31*) and (*46*) might be considered as damaged in addition to element (*26*). The erroneous results in those elements are worth noting even if their large standard deviations reveal their insensitivities with respect to the test conditions. However, the region around element (*26*) can be easily considered as the most highly cracked area and should be investigated first.

Table 5.4 : Measured and computed natural frequencies from different Bernoulli beam models

Number of Bernoulli beam elements †	Frequency (*Hz*)		
	1st	*2nd*	*3rd*
measured	171	987	3034
$n_e = 50$	170	1004	3069
$n_e = 30$	173	1016	3068
$n_e = 20$	174	1034	3006
$n_e = 10$	152	1003	2852

† The used material density $\varrho = 8.587 \times 10^3\ kg/m^3$

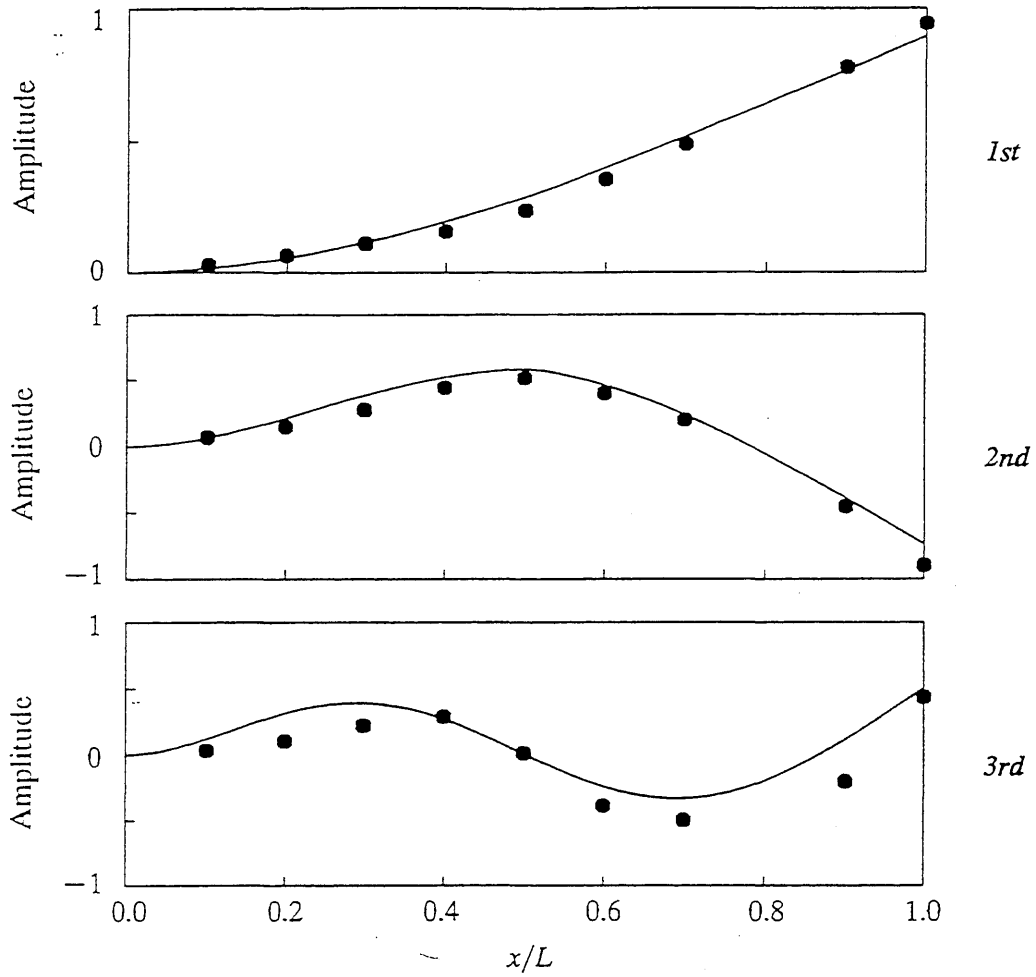

Fig. 5.8 : The computed lowest three mode shapes of the Bernoulli-Euler beam model with 50 elements when the flexural stiffness of the member (*26*) is reduced

With the crack detected in element (*26*) from the reduced flexural stiffness, modal frequencies are computed and summarized in Table 5.4, and the identified modal shapes are compared with the measured data in Fig. 5.8. The computed natural frequencies are generally a little higher than the measured ones in all the three modes but they are very close to each other. From Fig. 5.8, it is observed that the first and second mode shapes are satisfactorily close to the measured data but the the identified third mode still shows a large discrepancy from the measured modal displacements. In the second mode, a little kink of modal displacements around the imposed damaged element (*26*) is observed. However, a kink is not observed in the third mode from the computed mode shape, even though the measured data shows a serious variation of the curvature of the modal curve around the actual crack location. An interesting observation from Fig. 5.6 is that the elements closer to the fixed end than the location of the actually cracked section show almost perfectly undamaged flexural stiffness. All the detected cracked elements by the reduction of the flexural stiffnesses are from the elements located farther from the fixed end than the actual crack.

The model with 50 beam elements can be considered as fairly refined. However, depending on the engineer's choice, a simpler or a more refined model can be selected and used to detect cracks in the cantilever structure. Even though the geometry of the structure and the measured modal displacements are the same for any selected model, the difference in the level of refinements of the model may produce different results in locating the cracks and in assessing the element flexural properties. In the following section, some other models with a number of Bernoulli beam elements less than 50 are studied and their results are compared with those from the 50 Bernoulli beam element model.

5.3.2 Models with smaller than 50 Bernoulli-Euler Beam Elements

A model with 10 Bernoulli-Euler beam elements

A model with 10 Bernoulli beam elements was used to detect cracks and to assess element stiffness properties as the simplest model among the tested cases. Since each Bernoulli beam element has one flexural stiffness parameter, the maximum number of allowable parameter groups is limited by 10 by the number of total member parameters n_{sum}. Since the number n_{sum} is smaller than the given measured information $nmd \times \hat{n}_d = 27$, satisfying the identifiability criterion of Eq. (2.11), the parameter grouping scheme need not be used to identify the system. Each element can have its own parameter group and its flexural stiffness can be estimated directly. However, one may still want to use a grouping scheme, even though the maximum number of parameters is far less than the allowable upper limit. For this case, both approaches resulted in the same identified system.

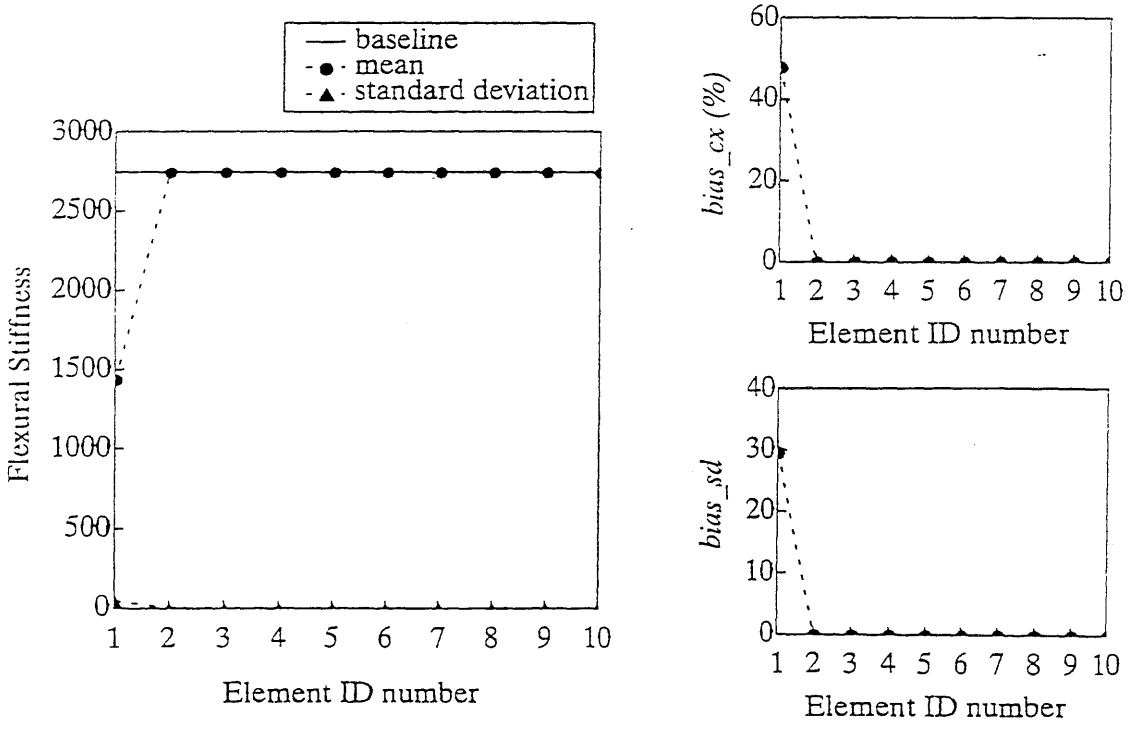

Fig. 5.9 : Damage detection and assessment with 10 Bernoulli beam element model

The identification results from the measured data perturbation iterations drawn in Fig. 5.9 indicate that element (*1*) is detected as the damaged element. The results are completely erroneous compared with the actual situation where the actually cracked section is located in element (*5*). The computed natural frequencies are also much smaller than the measured frequencies in all the three modes as summarized in Table 5.4. These results suggest the possibility of multiple solutions for this case. This case study illustrates that a fairly refined structural model should be selected to locate cracks. Such a simple model cannot provide even a rough idea of the crack location.

A model with 20 Bernoulli-Euler beam elements

For the structural model with 20 Bernoulli beam elements, the total number of parameters n_{sum} is 20, and is less than the available measured information $nmd \times \hat{n}_d = 27$. Thus the identifiability criterion equation of Eq. (2.11) is satisfied. Therefore, the parameter grouping scheme need not be used. Each group can be constructed with a single element and thus each element flexural stiffness parameter can be estimated by a single iteration of the developed algorithm for each measured modal displacement perturbation case.

By applying the measured data perturbation iterations, we can observe from Fig. 5.10 that element (*12*) is detected as the most damaged element. The other seemingly damaged elements, such as element (*2*) and (*19*), might be considered undamaged by observing their relatively high standard

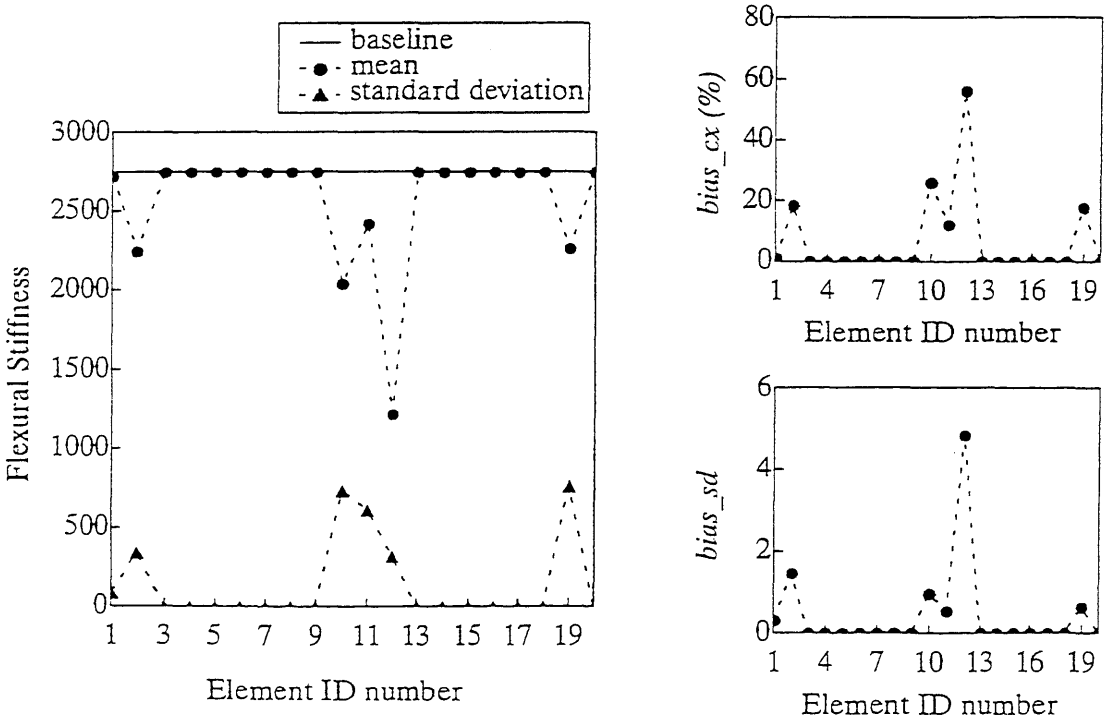

Fig. 5.10 : Damage detection and assessment with 20 Bernoulli beam element model

deviations and their low *bias_sd* damage index values. In this model case, erroneous results are obtained at both boundaries of the cantilever structure, close to the fixed end and close to the free end, in addition to the area around element (*12*). The computed natural frequencies are closer to the measured values than the results from the model with 10 Bernoulli beam elements as summarized in Table 5.4.

A model with 30 Bernoulli-Euler beam elements

Since the maximum number of parameters $n_{sum} = 30$ is larger than the available measured information $nmd \times \hat{n}_d = 27$ for the model with 30 Bernoulli beam elements, the identifiability criterion is not satisfied when each element comprises a single parameter group. If one more displacement component could be measured for each mode, the identifiability criterion would just be satisfied and a unique solution could be obtained. By approximating a modal amplitude for each mode at the equal location of 240 *mm* from the clamped end, we could reduce the computation time without performing the parameter group updating iterations. However, for the current purpose of the research, the amount of measured information is kept consistent without modifying it and thus the parameter group updating scheme is applied. The group updating starts from one group with the uniform baseline undamaged cantilever structure and hierarchically updated up to 27 groups. In this model case, the actual crack is located exactly on node *15*.

By applying the proposed measured data perturbation scheme with the consideration of noise in

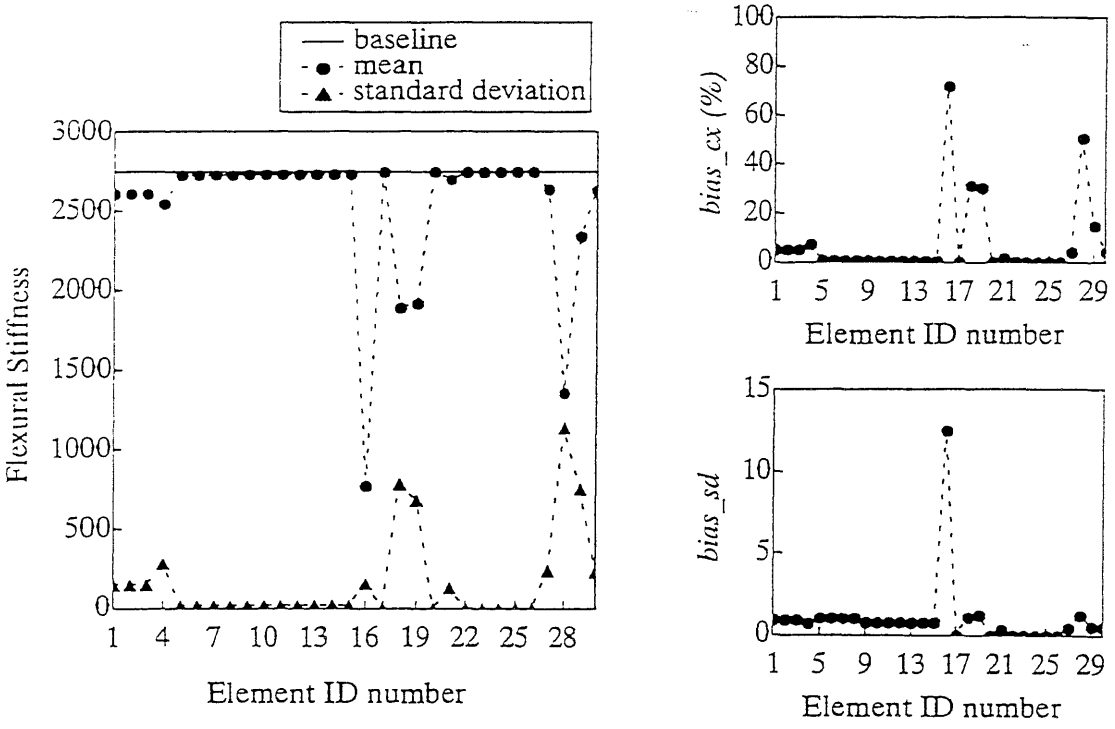

Fig. 5.11 : Damage detection and assessment with 30 Bernoulli beam element model

measurements, we can observe from Fig. 5.11 that element (*16*) is detected as the most highly damaged one. The other elements which seem to be damaged by the estimated flexural stiffness values are discriminated as undamaged by their low *bias_sd* damage index values. The computed natural frequencies summarized in Table 5.4 shows that the first and second frequencies are getting closer to the measured values from the upper values but the computed third natural frequency passes the measured frequency from a lower value in the 20 element case to a higher value in the current case. Comparing with the model cases with 10 and 20 Bernoulli beam elements, this more refined model case reduces the risk of detecting an element close to the fixed end as damaged one. Even though the relative amount of the measured data with respect to the number of beam elements is reduced compared with the 10 and 20 Bernoulli beam model cases, the cracked element can be revealed more clearly by increasing the number of elements.

5.3.3 Comparisons of the Results from the Bernoulli-Euler Beam Models

Four different Bernoulli-Euler beam models with 10, 20, 30, and 50 beam elements have been used to pinpoint the cracked section and to assess the flexural stiffness of the cracked element. Generally, we could observe that the results from a more refined model are better. By increasing the number of Bernoulli beam elements, a single crack is more clearly revealed by a relatively large *bias_sd* value of the detected element compared with those of the other elements. We could also observe that too simple a structural model could not detect a crack close to the actual location. For the simpler models, the error in the identified results compared with the actual values occur close to the fixed end boundary. On the other hand, as a model is more refined, the identification errors come from the part of the cantilever structure farther than the actually cracked section from the fixed end.

The computed natural frequencies for each model case are compared with the measured values in Fig. 5.12. The computed natural frequencies get closer to the measured values as more Bernoulli beam elements are used for representing the cantilever structural system. For a lower mode, the computed natural frequencies of all the tested models match the measured values better. The natural frequencies for the first mode are almost perfectly matched with the measured value in most model cases

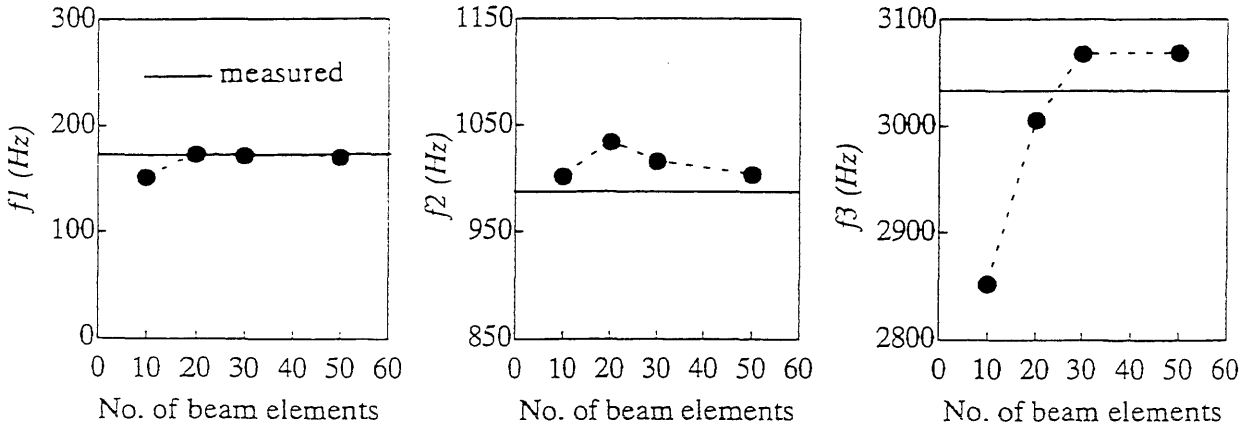

Fig. 5.12 : Comparison of the identified modal frequencies

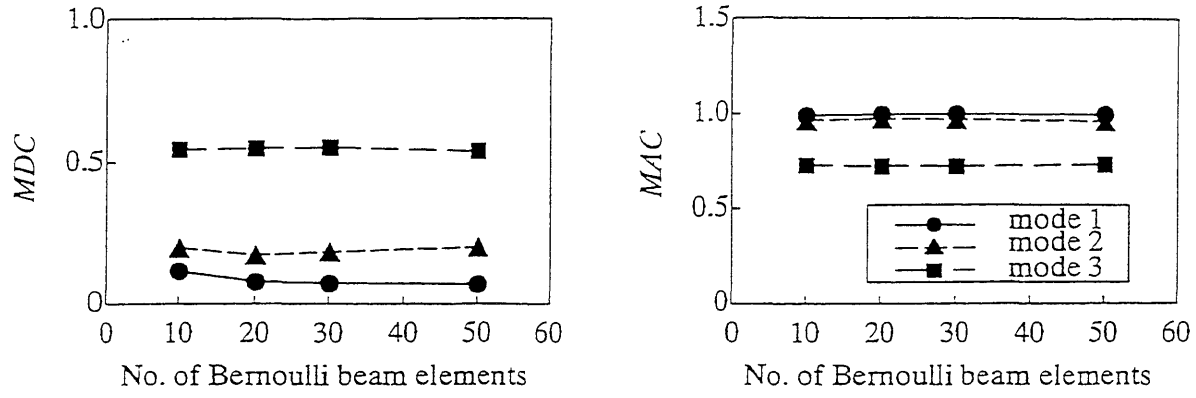

Fig. 5.13 : Errors in the identified modal displacements

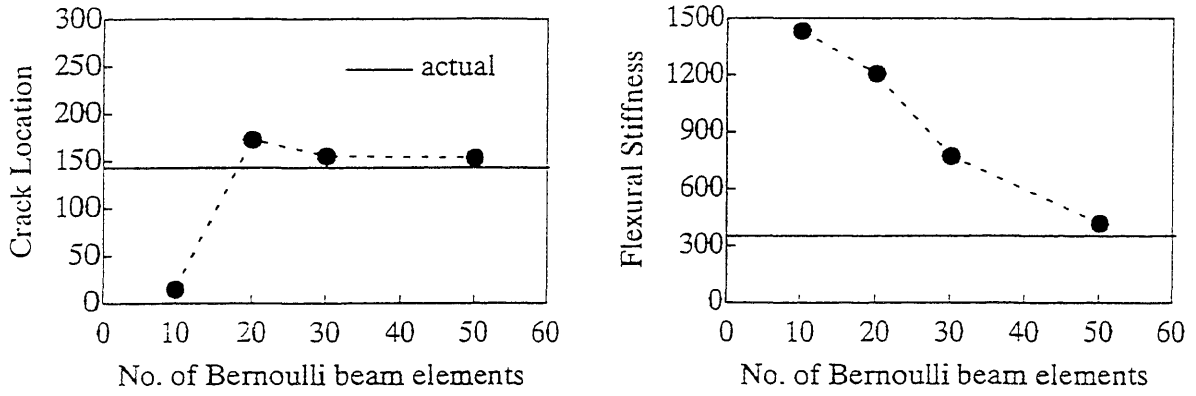

Fig. 5.14 : The estimated crack location and the flexural stiffness of the cracked element

except the model with 10 Bernoulli beam elements. Generally, the errors in the natural frequencies are negligibly small.

The errors in the identified modal displacements compared with the measured mode are investigated in Fig. 5.13. To compare the identified mode shape with the measured modal displacements, two error indicators defined by Eq. (5.1) are computed. From Fig. 5.13, we can observe that those two kinds of indicators are almost constant regardless of the number of Bernoulli beam elements. It is also observed that the identified mode shapes of the first and second modes are satisfactorily close to the measured shapes, but the computed mode shape of the third mode is difficult to match to the measured modal displacements even with a refined Bernoulli beam model.

The primary interest in this study is the location of the detected crack and the estimated flexural stiffness of the cracked element. For the purpose of comparison, the location of the crack is defined as the distance from the fixed end to the middle of the element which was detected as the most likely damaged. The estimated flexural stiffness of the detected element is simply compared with the flexural stiffness of the actually cracked section computed by reducing the sectional depth. Those results are plotted in Fig. 5.14. As more Bernoulli beam elements are used for the model, better results can

be obtained. The detected crack location is close to the actual location even with 20 Bernoulli beam element model, but the flexural stiffness can be correctly estimated with a fairly refined model.

5.3.4 The Effects of the Third Mode

Even though the general results of pinpointing the crack location and of estimating the stiffness properties of the cracked section are satisfactory, the error between the identified and the measured mode shapes of the third mode suggests more studies about the effect of the third mode on the damage detection and assessment results. Two kinds of studies are performed to consider the errors in the third mode. The first study is to detect and assess damage with the measured data for the first and second modes only without using the measured data for the third mode. Through this case study the contribution of higher modes in detecting localized damage may be examined. Another case study is with the use of a higher weight factor for the third mode than those for the other modes. By multiplying a higher weight factor in parameter estimation to the measured response for the third mode, the sharp change of the curvature observed in the third mode around the actual crack region may contribute to a better identification result and thus the discrepancy in the third mode shapes may diminish.

Without using the measured response of the third mode

This case is to detect the crack using the measured data of the first and second modes only. The structural model with 50 Bernoulli beam elements is selected to represent the cantilever beam. Since

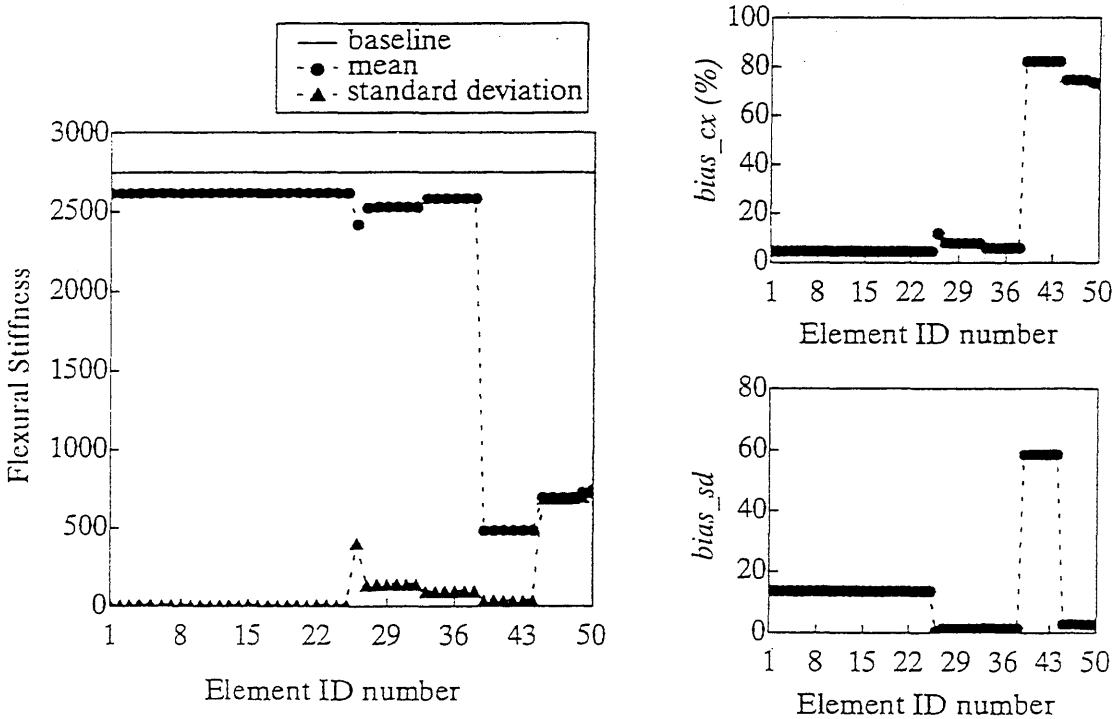

Fig. 5.15 : Damage detection and assessment with 50 Bernoulli beam element model when the measured data for the third mode are not used

the amount of measured data is reduced by eliminating the data from the third mode, the maximum number of parameter groups is limited by $nmd \times \hat{n}_d = 18$ to satisfy the identifiability criterion. Fig. 5.15 shows the identification results from the developed damage assessment algorithm. Damage indices computed from the mean and standard deviation for each element are drawn in the same figure. As discussed in the section 5.3.1, the upper limit value *cxlmt* for the *bias_cx* damage index can be selected by the same values as the proportional measurement error 10%, and the upper limit value *sdlmt* for the *bias_sd* damage index should be determined from the simulation study for the baseline structure but should be around 1.1. From the figures, we can observe that some elements close to the free end are detected as damaged by the upper limit values for both indices. From Fig. 5.15, it is clear that the damage detection results are erroneous without using the measured response of the third mode. This result may indicate that higher modes are required to detect localized damage correctly in a structural system, even if the measured data of those higher modes are difficult to match with the selected structural model or are considered to be polluted with more error.

With the use of a higher weight factor for the third mode

From Fig. 5.15, the importance of the third mode in correctly locating the crack was demonstrated. To reflect the contribution of the third mode, the weight factor for the third mode can be assigned a higher value than those for the other modes. For the current case study, the weight factor for the third mode is assigned arbitrarily as twice that for the first and second modes. All the other

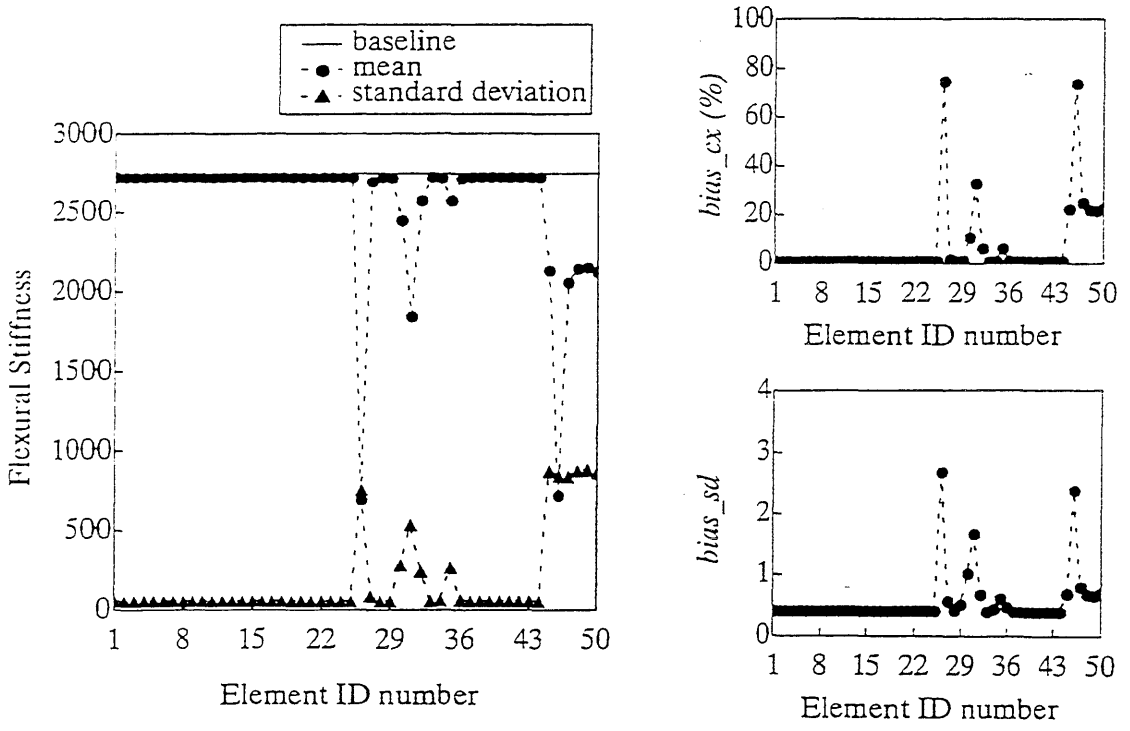

Fig. 5.16 : Damage detection and assessment with 50 Bernoulli beam element model when twice a weight factor for the third mode to the first and second modes are used

conditions of measured data and the structural model are the same as the model study case with 50 Bernoulli beam elements. The identification results from the measured data perturbation iterations are summarized in Fig. 5.16. From the figure, it can be observed that element (*26*) is the most highly damaged element, but some other elements closer to the free and can be also considered as relatively high-damaged ones even with the help of limit values of *cxlmt* and *sdlmt*. The damage index *bias_sd* of element (*26*) is a little higher than those of some other elements but the *bias_sd* values of elements (*31*) and (*46*) are also as high as that of element (*26*). As a conclusion, the results with a higher weight factor for the third mode are worse than the case without altering it. It is more difficult to verify the existence of a single crack in the cantilever beam. The estimated flexural stiffness in element (*26*) is almost the same as that obtained from the case with an equal weight factor for all the modes.

The natural frequencies and the errors in the modal displacements are compared in Fig. 5.17 and Fig. 5.18. In the figures, *dcBE* denotes the 50 Bernoulli beam element model with an equal weight factor for all three modes and *dcW2* is for the case with the weight factor doubled for the third mode. An interesting observation from Fig. 5.17 is that the computed natural frequency of the third mode is much closer to the measured value with the increased weight factor for the third mode. However, the error in the modal displacements of the third mode is still high regardless of the change of the weight factor as shown in Fig. 5.18. The two kinds of error indicators for the modal displacements are

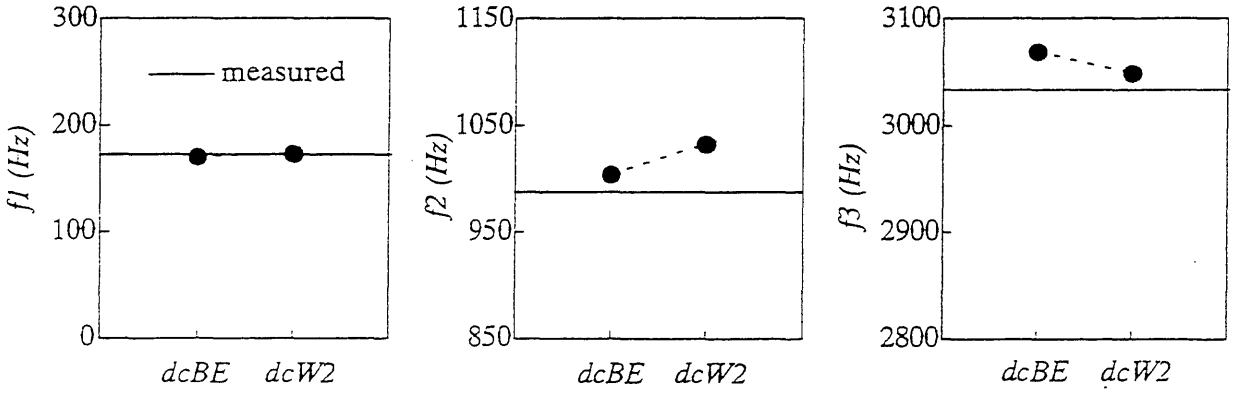

Fig. 5.17 : Comparison of the identified modal frequencies

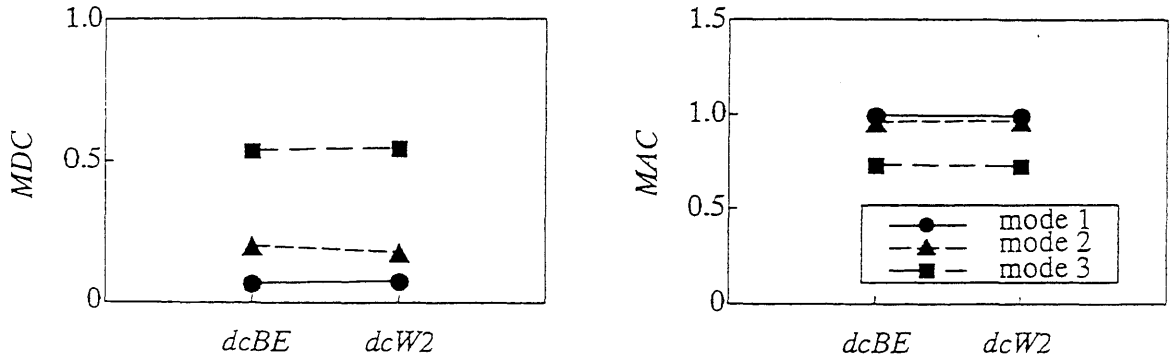

Fig. 5.18 : Errors in modal displacements

almost constant regardless of the different weight factor. Therefore, we can conclude that by changing the weight factor for the third mode the natural frequency can be improved but the identified mode shape of the third mode does not change. In addition, the results in Fig. 5.16 demonstrate that it is more difficult to pinpoint a single cracked section in the cantilever beam. More identification errors are found in the area close to the free end.

5.3.5 Discussion of the Observations from Bernoulli-Euler Beam Models

From the case studies with the Bernoulli-Euler beam models for the cantilever structural system, we have observed a consistent phenomenon that the third mode shape is poorly matched with the measured data, even though the identified natural frequencies are close to the measured values. However, we could also observe that the crack detection result without using the third mode was meaningless from Fig. 5.15. This paradox is hard to interpret but indicates one thing clearly. The current measured data of the third mode is the key to correctly identifying the cracked cantilever system.

An interesting observation from the case studies with the Bernoulli-Euler beam models is that most of the elements detected as cracked are located closer to the free end than the actual crack in the cantilever structure. In other words, the damage detection errors come from the identification mismatch in the area closer to the free end than the location of the actually cracked section. The elements close to the fixed boundary of the cantilever structure were also estimated erroneously, but the estimated flexural stiffnesses of the elements close to the fixed end could be identified as undamaged as a more refined Bernoulli beam model was used. Therefore, we can guess that the vibrational behavior of the part of the cantilever beam closer to the free end than the actually cracked section might be changed after the crack was created. The models with Bernoulli-Euler beam elements may not be adequate, especially for the part farther than the actual cracked section from the fixed end. The significant curvature change of the measured third mode illustrates that more rotational deformation is needed to represent the behavior of the part of the cantilever beam. In the following section, the additional rotation is considered by the shear deformation in the Timoshenko beam.

5.4 Timoshenko Beam Model

Timoshenko beam models rather than Bernoulli-Euler beams are used to represent the cracked cantilever structural system in this section. For the Timoshenko beam model, the shear stiffnesses of the beam elements are the additional parameter type to the flexural stiffnesses. The consideration of the shear effects may be desirable for the cracked cantilever structure, because shear deformation becomes important in studying the modes of vibration of higher frequencies when a vibrating beam is subdivided by nodal cross sections into comparatively short portions (Timoshenko, *et. al.* 1974). We could observe from the Bernoulli beam case studies that the third mode, with a relatively high frequency, plays an important role in identifying the cantilever structural system, but due to the significant curvature change in the measured third mode the identified mode shapes for the third mode by Bernoulli beam models were poorly matched. The additional angular deformation due to shear force is reflected herein without taking account of the rotational masses.

By considering the additional shear deformation, each Timoshenko beam element has two types of stiffness parameters, flexural and shear. When there are more than two types of parameters in an element and when the parameters provide different evaluation of damage for the element, it will be difficult to decide which result is more reliable to determine damage. If we can determine the most reliable parameter type for the structure in advance, we use it for damage detection. If not, we have to determine damage either by combining all the obtained results or by investigating each possibility separately. However, since a reliable parameter may be determined depending on the type of a structure and the location of an element in the structure and since the geometry and topology of the structure are assumed to be known, we may be able to determine a more reliable parameter type for the given structure in advance. A simulation study may be helpful for determining it, too. For the current cracked cantilever structure, a simulation study is carried out in section 5.4.1 to investigate the reliability of flexural and shear parameters.

As a merit of the algorithm, the parameter grouping is still sequentially updated by minimizing the squared model error (*SME*), regardless of the number of different types of parameters in an element. However, a local termination criterion to remove parameters from further modification may depend on the sensitivity of the various parameter type. If a reliable parameter type can be determined in advance, all the parameters in a group can be removed together from further modification when the most reliable parameter satisfies the local termination criterion. However, if we cannot determine a reliable parameter, as a more general approach, the local termination criterion should be applied for each parameter separately and only the parameter satisfying the criterion should be removed from further modification without affecting the remaining parameters in the same group.

As for the Bernoulli beam case studies, four different structural models with 10, 20, 30, and 50 Timoshenko beam elements were studied and their results compared. The computed natural frequencies and the identified mode shapes are compared with the measured responses. The location of the detected cracked section is also compared with the actual location and with the results from the Bernoulli beam models. The same number of perturbation iterations as determined by the Bernoulli beam models is applied to obtain the statistical properties for each element. Because the available amount of measured information is given by $nmd \times \hat{n}_d = 27$ and because there are two parameter types for each group with the flexural stiffness and the shear stiffness, the maximum allowable number of parameter groups is 13.

5.4.1 Reliability of Flexural and Shear Stiffness Parameters

For the current cantilever structure, the flexural deformation is believed to be more dominant than the shear deformation. Therefore, the flexural stiffness parameter may be the more dependable to evaluate damage. To verify the reliability of the flexural stiffness parameter in detecting damage, a simulation study is proposed in this section.

For the Monte Carlo simulation, a structure model with 50 Timoshenko beam elements is considered as shown in Fig. 5.2. We assume that damage is located at element (*24*) with the reduced sectional

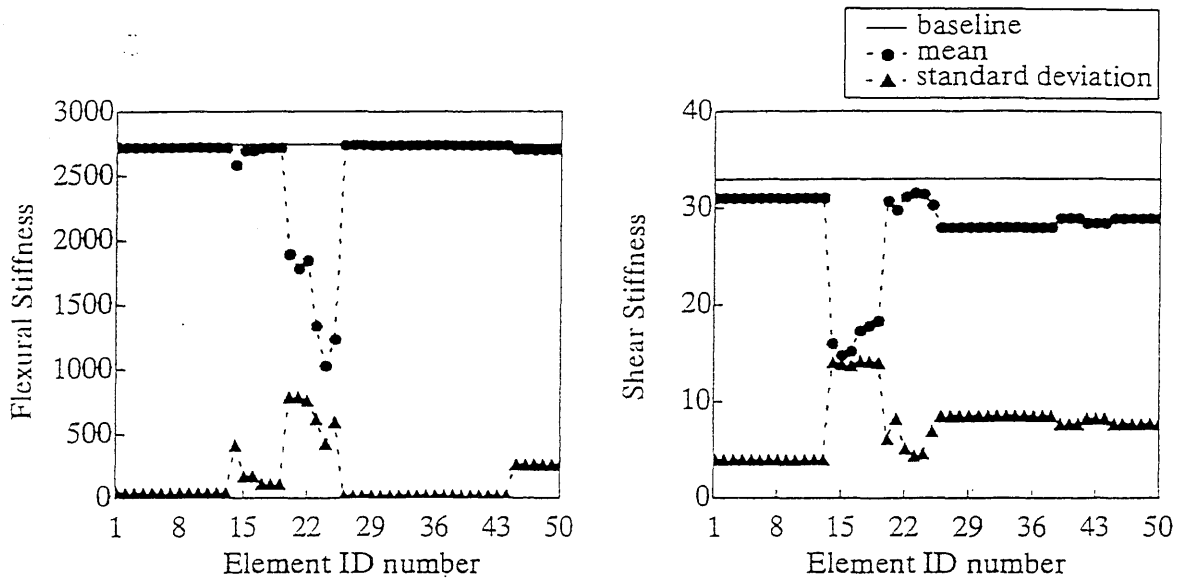

Fig. 5.19 : Averaged element flexural and shear stiffnesses after 50 Monte Carlo trials

thickness by half, as in the real cracked case. We also assume 10% proportional error for the simulated measured data and apply 50 iterations of Monte Carlo simulation to obtain the mean and standard deviation values for each element parameter. The obtained results are plotted in Fig. 5.19 for flexural and shear stiffness separately. At each Monte Carlo trial, if a final estimated stiffness parameter was larger than the baseline value, it was modified with the baseline value. From the figures, we can observe that the flexural stiffnesses can locate a damaged element close to the actual damage zone but the shear stiffnesses erroneously predict damage at other locations. All the estimated shear stiffnesses are lower than the baseline value so that all the elements can be considered damaged when judged from the estimated shear stiffnesses. Another observation is that the standard deviations of shear stiffnesses are relatively large in all the elements. Therefore, we can conclude that damage in the current cantilever structure must be evaluated based on the estimated flexural stiffnesses rather than the estimated shear stiffnesses.

The unreliability of shear stiffnesses in determining damage is also demonstrated by a case study with the real measured data summarized in section 5.1. By assuming that the measured data are exact without considering noise in measurements, the estimated flexural and shear stiffnesses at each updated grouping are summarized in Table 5.5. To obtain the results, the data perturbation scheme was not applied, but the parameter group updating scheme was sequentially applied due to the relatively small measured information. In Table 5.5, the initial grouping has one group with uniform baseline flexural and shear stiffnesses over the structure. As the parameter grouping was updated, the *SME* value reduced, and the process stopped at grouping step 5 when *SME* was not reduced any more by updating grouping 5. In the damage localization process, one can observe that the flexural stiffnesses were modified in the direction of searching for the correct cracked location in element (*24*), but in most of the cases the shear stiffnesses seem to have preferred hitting the constrained upper or lower

Table 5.5 : Estimated flexural and shear stiffnesses at each updated grouping (complete)

Element#	Initial		Grouping 1		Grouping 2		Grouping 3		Grouping 4		Grouping 5	
	EI	*GA*	*EI*	*GA*	*EI*	*GA*	*EI*	*GA*	*EI*	*GA*	*EI*	*GA*
1	2747	32.96	2496	36.26	2982	36.26	2816	36.26	2699	36.26	2618	36.26
2	2747	32.96	2496	36.26	2982	36.26	2816	36.26	2699	36.26	2618	36.26
3	2747	32.96	2496	36.26	2982	36.26	2816	36.26	2699	36.26	2618	36.26
4	2747	32.96	2496	36.26	2982	36.26	2816	36.26	2699	36.26	2618	36.26
5	2747	32.96	2496	36.26	2982	36.26	2816	36.26	2699	36.26	2618	36.26
6	2747	32.96	2496	36.26	2982	36.26	2816	36.26	2699	36.26	2618	36.26
7	2747	32.96	2496	36.26	2982	36.26	2816	36.26	2699	36.26	2618	36.26
8	2747	32.96	2496	36.26	2982	36.26	2816	36.26	2699	36.26	2618	36.26
9	2747	32.96	2496	36.26	2982	36.26	2816	36.26	2699	36.26	2618	36.26
10	2747	32.96	2496	36.26	2982	36.26	2816	36.26	2699	36.26	2618	36.26
11	2747	32.96	2496	36.26	2982	36.26	2816	36.26	2699	36.26	2618	36.26
12	2747	32.96	2496	36.26	2982	36.26	2816	36.26	2699	36.26	2618	36.26
13	2747	32.96	2496	36.26	2982	36.26	2816	36.26	2699	36.26	2618	36.26
14	2747	32.96	2496	36.26	1650	36.26	3021	3.40	3021	1.00	3021	1.39
15	2747	32.96	2496	36.26	1650	36.26	3021	3.40	3021	1.58	3021	17.69
16	2747	32.96	2496	36.26	1650	36.26	3021	3.40	3021	1.00	3021	1.04
17	2747	32.96	2496	36.26	1650	36.26	3021	3.40	3021	1.00	3021	32.31
18	2747	32.96	2496	36.26	1650	36.26	3021	3.40	3021	17.78	3021	36.26
19	2747	32.96	2496	36.26	1650	36.26	3021	3.40	3021	36.26	3021	32.52
20	2747	32.96	2496	36.26	1650	36.26	1123	36.26	1378	36.26	3020	36.26
21	2747	32.96	2496	36.26	1650	36.26	1123	36.26	1378	36.26	3020	36.26
22	2747	32.96	2496	36.26	1650	36.26	1123	36.26	1378	36.26	3020	36.26
23	2747	32.96	2496	36.26	1650	36.26	1123	36.26	1378	36.26	910	36.26
24	2747	32.96	2496	36.26	1650	36.26	1123	36.26	1378	36.26	910	36.26
25	2747	32.96	2496	36.26	1650	36.26	1123	36.26	1378	36.26	910	36.26
26	2747	32.96	2742	36.26	3021	36.26	2945	36.26	2904	36.26	2754	36.26
27	2747	32.96	2742	36.26	3021	36.26	2945	36.26	2904	36.26	2754	36.26
28	2747	32.96	2742	36.26	3021	36.26	2945	36.26	2904	36.26	2754	36.26
29	2747	32.96	2742	36.26	3021	36.26	2945	36.26	2904	36.26	2754	36.26
30	2747	32.96	2742	36.26	3021	36.26	2945	36.26	2904	36.26	2754	36.26
31	2747	32.96	2742	36.26	3021	36.26	2945	36.26	2904	36.26	2754	36.26
32	2747	32.96	2742	36.26	3021	36.26	2945	36.26	2904	36.26	2754	36.26
33	2747	32.96	2742	36.26	3021	36.26	2945	36.26	2904	36.26	2754	36.26
34	2747	32.96	2742	36.26	3021	36.26	2945	36.26	2904	36.26	2754	36.26
35	2747	32.96	2742	36.26	3021	36.26	2945	36.26	2904	36.26	2754	36.26
36	2747	32.96	2742	36.26	3021	36.26	2945	36.26	2904	36.26	2754	36.26
37	2747	32.96	2742	36.26	3021	36.26	2945	36.26	2904	36.26	2754	36.26
38	2747	32.96	2742	36.26	3021	36.26	2945	36.26	2904	36.26	2754	36.26
39	2747	32.96	2742	36.26	3021	36.26	2945	36.26	2904	36.26	2754	36.26
40	2747	32.96	2742	36.26	3021	36.26	2945	36.26	2904	36.26	2754	36.26
41	2747	32.96	2742	36.26	3021	36.26	2945	36.26	2904	36.26	2754	36.26
42	2747	32.96	2742	36.26	3021	36.26	2945	36.26	2904	36.26	2754	36.26
43	2747	32.96	2742	36.26	3021	36.26	2945	36.26	2904	36.26	2754	36.26
44	2747	32.96	2742	36.26	3021	36.26	2945	36.26	2904	36.26	2754	36.26
45	2747	32.96	2742	36.26	3021	36.26	2945	36.26	2904	36.26	2754	36.26
46	2747	32.96	2742	36.26	3021	36.26	2945	36.26	2904	36.26	2754	36.26
47	2747	32.96	2742	36.26	3021	36.26	2945	36.26	2904	36.26	2754	36.26
48	2747	32.96	2742	36.26	3021	36.26	2945	36.26	2904	36.26	2754	36.26
49	2747	32.96	2742	36.26	3021	36.26	2945	36.26	2904	36.26	2754	36.26
50	2747	32.96	2742	36.26	3021	36.26	2945	36.26	2904	36.26	2754	36.26
SME	0.882		0.828		0.760		0.370		0.361		0.351	

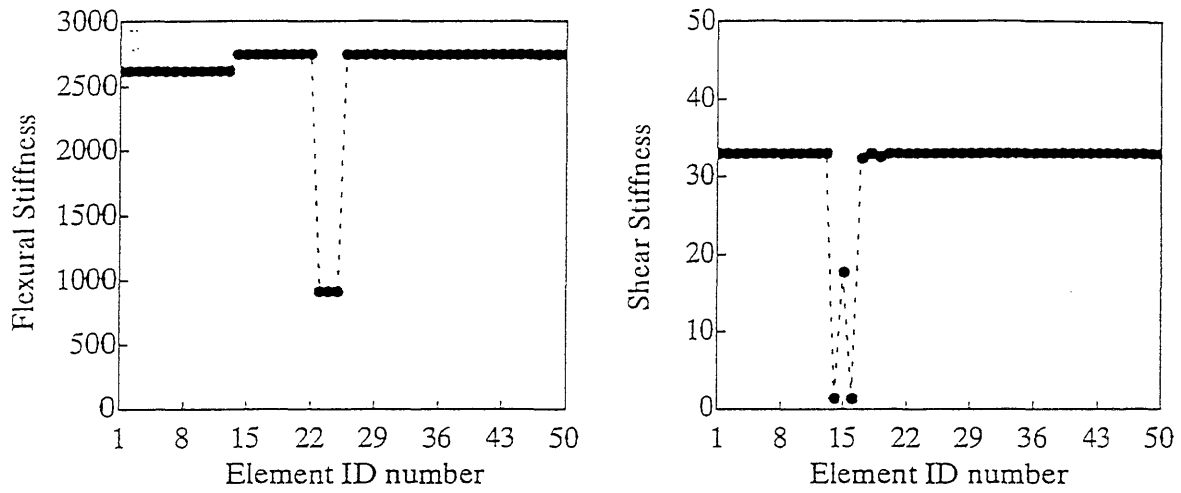

Fig. 5.20 : Estimated element flexural and shear stiffnesses when the measured data are assumed to be noise-free

bound. The imposed lower and upper bounds for the shear stiffness with the baseline value of 32.96 *MN* were 1.0 *MN* and 36.26 *MN* for the case study. The fact that the shear stiffnesses hit the upper bound frequently may be indicative of the insensitivity of the shear stiffnesses in the optimization process. Therefore, we can conclude again from the observations that the shear stiffnesses are unreliable compared with the flexural stiffnesses for localizing damage in the current cantilever structure and that local termination should be based on the variation in the flexural stiffnesses.

Up to grouping step 5 in Table 5.5, none of the estimated parameters could be fixed with estimated values or baseline value, because their changes could not satisfy the local termination criterion or their estimated values were higher than the baseline value. A parameter whose estimated value was higher than the baseline value was left for further modification in the algorithm. After the damage localization process was completed by grouping step 5, elements with their parameters higher than the baseline value were changed to the baseline value. Those finally corrected flexural and shear stiffnesses are shown in Fig. 5.20. From the figure, we can observe that the actually damaged element (*24*) can be more accurately identified by the figure for the flexural stiffnesses. Some elements nearby the fixed boundary also show a possibility of light damage if damage is evaluated by comparing the estimated flexural stiffness with the baseline flexural stiffness value. Even though the measured data are assumed to be noise-free, the identified crack location by the estimated flexural stiffnesses is quite accurate but the area detected as damaged is a little wide.

To obtain the results in Table 5.5 and thus Fig. 5.20, the current algorithm updates grouping by subdividing a group in half or completely depending on the available amount of measured information. For example, at grouping step 4 in Table 5.5, we can observe that the group with elements (*14*)–(*19*) at grouping step 3 could be subdivided completely by comprising each group with an element. The current case study can allow the number of groups up to 13 because the available amount of measured information is given by $nmd \times \hat{n}_d = 27$ and because there are two parameter types for

Table 5.6 : Estimated flexural and shear stiffnesses at each updated grouping (binary)

Element#	Initial		Grouping 1		Grouping 2		Grouping 3		Grouping 4	
	EI	*GA*	*EI*	*GA*	*EI*	*GA*	*EI*	*GA*	*EI*	*GA*
1	2747	32.96	2496	36.26	2982	36.26	2816	36.26	2657	36.26
2	2747	32.96	2496	36.26	2982	36.26	2816	36.26	2657	36.26
3	2747	32.96	2496	36.26	2982	36.26	2816	36.26	2657	36.26
4	2747	32.96	2496	36.26	2982	36.26	2816	36.26	2657	36.26
5	2747	32.96	2496	36.26	2982	36.26	2816	36.26	2657	36.26
6	2747	32.96	2496	36.26	2982	36.26	2816	36.26	2657	36.26
7	2747	32.96	2496	36.26	2982	36.26	2816	36.26	2657	36.26
8	2747	32.96	2496	36.26	2982	36.26	2816	36.26	2657	36.26
9	2747	32.96	2496	36.26	2982	36.26	2816	36.26	2657	36.26
10	2747	32.96	2496	36.26	2982	36.26	2816	36.26	2657	36.26
11	2747	32.96	2496	36.26	2982	36.26	2816	36.26	2657	36.26
12	2747	32.96	2496	36.26	2982	36.26	2816	36.26	2657	36.26
13	2747	32.96	2496	36.26	2982	36.26	2816	36.26	2657	36.26
14	2747	32.96	2496	36.26	1650	36.26	3021	3.40	3021	36.26
15	2747	32.96	2496	36.26	1650	36.26	3021	3.40	3021	36.26
16	2747	32.96	2496	36.26	1650	36.26	3021	3.40	3021	36.26
17	2747	32.96	2496	36.26	1650	36.26	3021	3.40	3021	36.26
18	2747	32.96	2496	36.26	1650	36.26	3021	3.40	3021	36.26
19	2747	32.96	2496	36.26	1650	36.26	3021	3.40	3021	36.26
20	2747	32.96	2496	36.26	1650	36.26	1123	36.26	3021	36.26
21	2747	32.96	2496	36.26	1650	36.26	1123	36.26	3021	36.26
22	2747	32.96	2496	36.26	1650	36.26	1123	36.26	3021	36.26
23	2747	32.96	2496	36.26	1650	36.26	1123	36.26	782	36.26
24	2747	32.96	2496	36.26	1650	36.26	1123	36.26	782	36.26
25	2747	32.96	2496	36.26	1650	36.26	1123	36.26	782	36.26
26	2747	32.96	2742	36.26	3021	36.26	2945	36.26	2733	36.26
27	2747	32.96	2742	36.26	3021	36.26	2945	36.26	2733	36.26
28	2747	32.96	2742	36.26	3021	36.26	2945	36.26	2733	36.26
29	2747	32.96	2742	36.26	3021	36.26	2945	36.26	2733	36.26
30	2747	32.96	2742	36.26	3021	36.26	2945	36.26	2733	36.26
31	2747	32.96	2742	36.26	3021	36.26	2945	36.26	2733	36.26
32	2747	32.96	2742	36.26	3021	36.26	2945	36.26	2733	36.26
33	2747	32.96	2742	36.26	3021	36.26	2945	36.26	2733	36.26
34	2747	32.96	2742	36.26	3021	36.26	2945	36.26	2733	36.26
35	2747	32.96	2742	36.26	3021	36.26	2945	36.26	2733	36.26
36	2747	32.96	2742	36.26	3021	36.26	2945	36.26	2733	36.26
37	2747	32.96	2742	36.26	3021	36.26	2945	36.26	2733	36.26
38	2747	32.96	2742	36.26	3021	36.26	2945	36.26	2733	36.26
39	2747	32.96	2742	36.26	3021	36.26	2945	36.26	2733	36.26
40	2747	32.96	2742	36.26	3021	36.26	2945	36.26	2733	36.26
41	2747	32.96	2742	36.26	3021	36.26	2945	36.26	2733	36.26
42	2747	32.96	2742	36.26	3021	36.26	2945	36.26	2733	36.26
43	2747	32.96	2742	36.26	3021	36.26	2945	36.26	2733	36.26
44	2747	32.96	2742	36.26	3021	36.26	2945	36.26	2733	36.26
45	2747	32.96	2742	36.26	3021	36.26	2945	36.26	2733	36.26
46	2747	32.96	2742	36.26	3021	36.26	2945	36.26	2733	36.26
47	2747	32.96	2742	36.26	3021	36.26	2945	36.26	2733	36.26
48	2747	32.96	2742	36.26	3021	36.26	2945	36.26	2733	36.26
49	2747	32.96	2742	36.26	3021	36.26	2945	36.26	2733	36.26
50	2747	32.96	2742	36.26	3021	36.26	2945	36.26	2733	36.26
SME	0.882		0.828		0.760		0.370		0.361	

each group with the flexural stiffness and the shear stiffness. Another alternative group updating scheme can be realized by subdividing a group always in half as shown in Table 5.6. The binary grouping scheme seems to be better for the current case with a smaller number of group updating steps and a better estimation of flexural stiffnesses for the around elements of the actually damaged element (*24*). However, the best group updating scheme may be case-dependent. Generally, we can say that a binary group updating scheme is more conservative. The number of groups increases only by one at every group updating and thus the number of parameter groups can be controlled in a more rational manner. However, how to divide a group in half is a problem in both group updating schemes. For a line structure like the current cantilever structure, it may not be difficult to decide how to divide a group in half, because the element number usually matches with the location of the element in the structure. However, for usual civil structures, the number of combinations of binary subgroupings for a group is large with even a small number of elements. Depending on the choice of a binary grouping, the objective function error may or may not reduce. Compared with the binary grouping, the complete subgrouping may be more radical by increasing the number of groups rapidly whenever the amount of measured information allows it. Since the squared model error (*SME*) controls the number of groups and the parameter grouping can be updated only when *SME* reduces, it may be possible that a new grouping with a sudden increase in the number of groups may have a larger *SME* value than the previous grouping case. However, regardless of the increased number of groups, if a damaged element exists within a group and the group can be subdivided completely by making the damaged element with a single group, *SME* will always reduce. In other words, *SME* can reduce considerably when a damaged element is singled out. If a group does not contain any damaged elements, the group divided even in half should not produce a reduced *SME*. Therefore, the current algorithm follows the complete subgrouping rather than the binary group updating and has produced good results from the tested cases.

5.4.2 A Model with 50 Timoshenko Beam Elements

In this section, a structural model with 50 Timoshenko beam elements is studied. The model with 50 Timoshenko beam elements is the most refined model among the current case studies with Timoshenko beam models. Since the maximum allowable number of parameter groups was determined as 13, the parameter grouping scheme must be applied. The initial number of parameter groups starts from a single group because the member properties of the uncracked baseline cantilever structure are uniform over the whole length of the structure, and can be subdivided sequentially up to 13 groups.

By applying the measured modal displacement perturbation iterations, almost the same identification results of the flexural stiffnesses are obtained as shown in Fig. 5.21. By considering the statistical properties of the mean and the standard deviations, two damage indices are computed for each element in the figure. From the figures for the damage indices, the three elements (*23*), (*24*), and (*25*) are detected as damaged elements. Relatively high values of *bias_sd* damage index in the elements near the fixed end are due to the small values of the standard deviations. However, the possibility of damage in those elements can be discounted when the low values of the *bias_cx* damage index in those

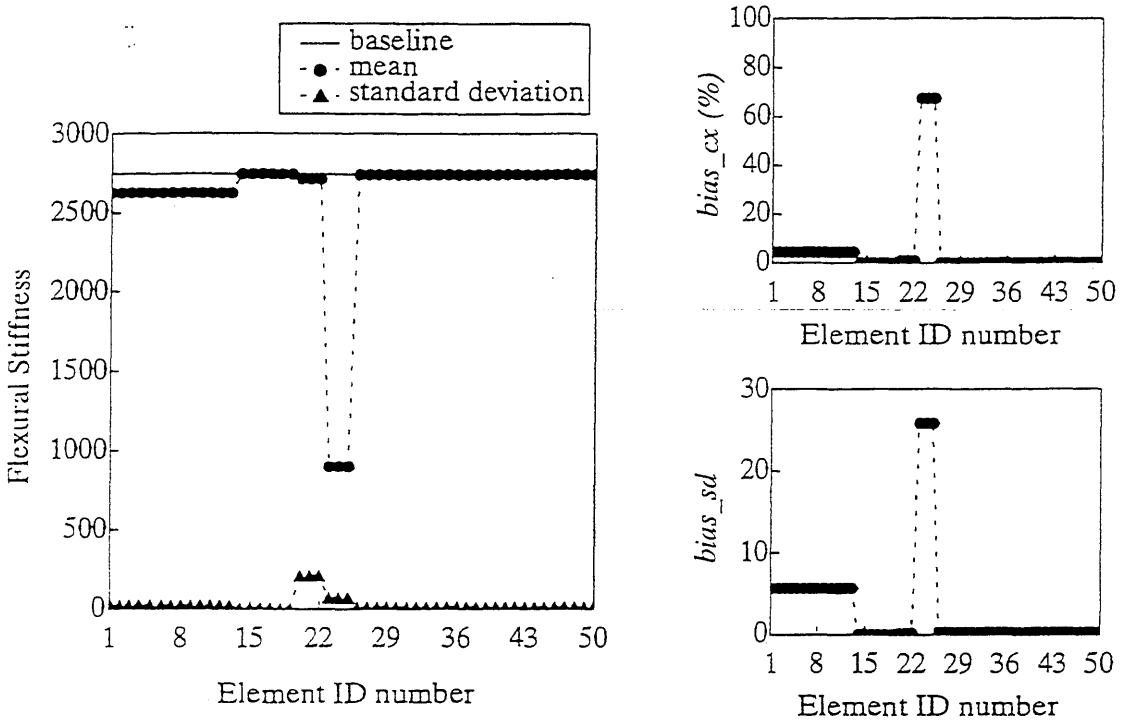

Fig. 5.21 : Damage detection and assessment with 50 Timoshenko beam element model

elements are considered. Since the actually cracked section is in element (*24*) for this Timoshenko beam model, the location of crack is almost exactly identified for this 50 Timoshenko beam element model. A big difference from the case study with 50 Bernoulli beam elements as shown in Fig. 5.6 is that the flexural stiffnesses of the elements located farther than the actually cracked section from the fixed end are well identified by the Timoshenko beam model, while those elements in Bernoulli beam models were often difficult to correctly identify. Therefore, we may conclude that the behavior of the cracked cantilever beam may be better represented by the Timoshenko beam rather than the Bernoulli beam models.

The computed natural frequencies by the reduced flexural stiffnesses for elements (*23*), (*24*), and (*25*) are summarized in Table 5.7, and the identified mode shapes are compared with the normalized

Table 5.7 : Measured and computed natural frequencies from different Timoshenko beam models

Number of Timoshenko beam elements †	Frequency (*Hz*)		
	1st	*2nd*	*3rd*
measured	171.0	987	3034
$n_e = 50$	172.5	1001	3013
$n_e = 30$	176.3	1046	3016
$n_e = 20$	175.9	1033	2997
$n_e = 10$	161.5	1028	2849

† The used material density $\varrho = 8.303 \times 10^3\ kg/m^3$

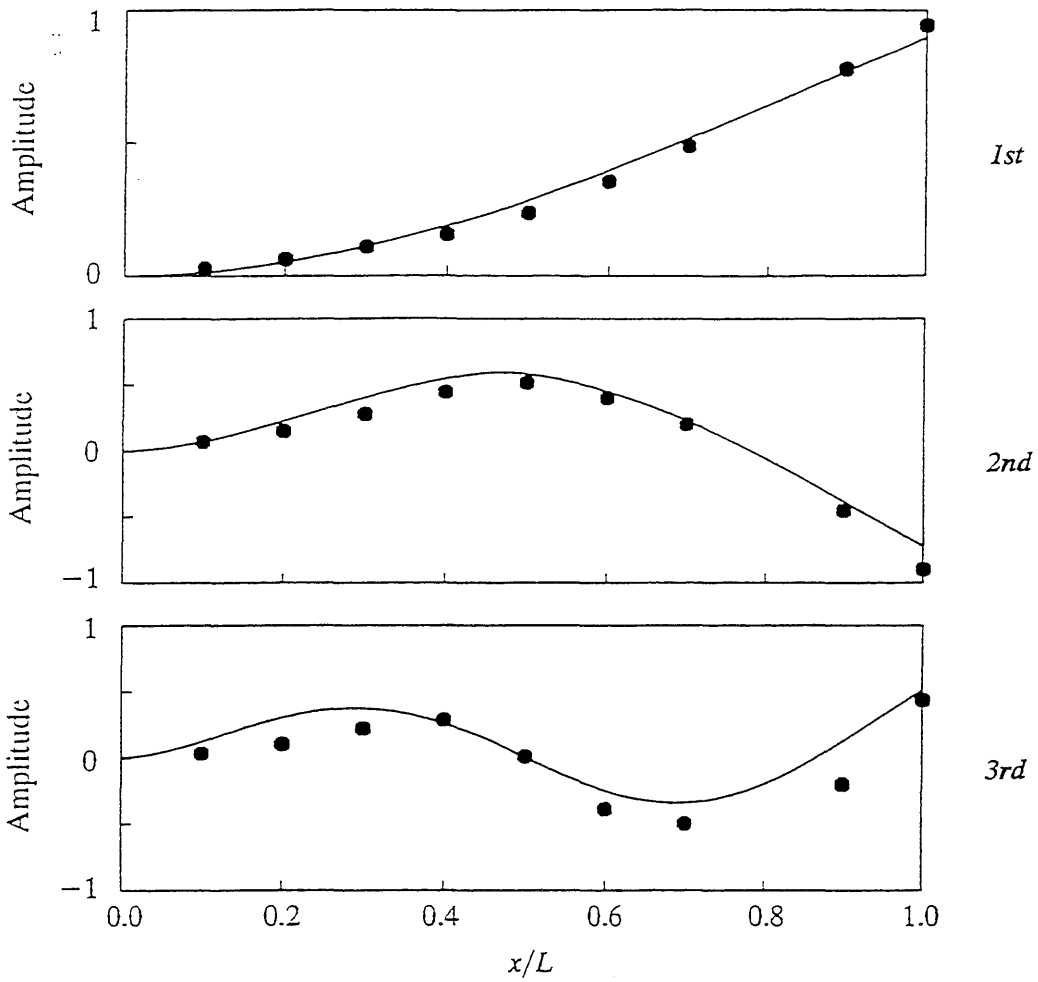

Fig. 5.22 : The computed lowest three mode shapes of the Timoshenko beam model when the stiffnesses of the member (23), (24), and (25) are reduced as identified

measured modal displacements in Fig. 5.22. From Table 5.7, we can observe that the identified natural frequencies for all the three modes are very close to the measured ones. However, the identified mode shape of the third mode in Fig. 5.22 is still distant from the measured displacements as for the Bernoulli beam models. The mode shape of the third mode does not match the measured data well for either type of beam model. The computed modal displacement errors are plotted in Fig. 5.27.

5.4.3 Models with smaller than 50 Timoshenko Beam Elements

A model with 10 Timoshenko beam elements

A model with 10 Timoshenko beam elements was used to detect cracks and to assess element stiffness properties as the simplest model among the tested cases. Since each Timoshenko beam element has flexural and shear stiffness parameters, the maximum number of allowable parameter groups is 20 according to the number of total member parameters n_{sum}. Since the number n_{sum} is smaller than the given measured information $nmd \times \hat{n}_d = 27$, the parameter grouping scheme need not be used

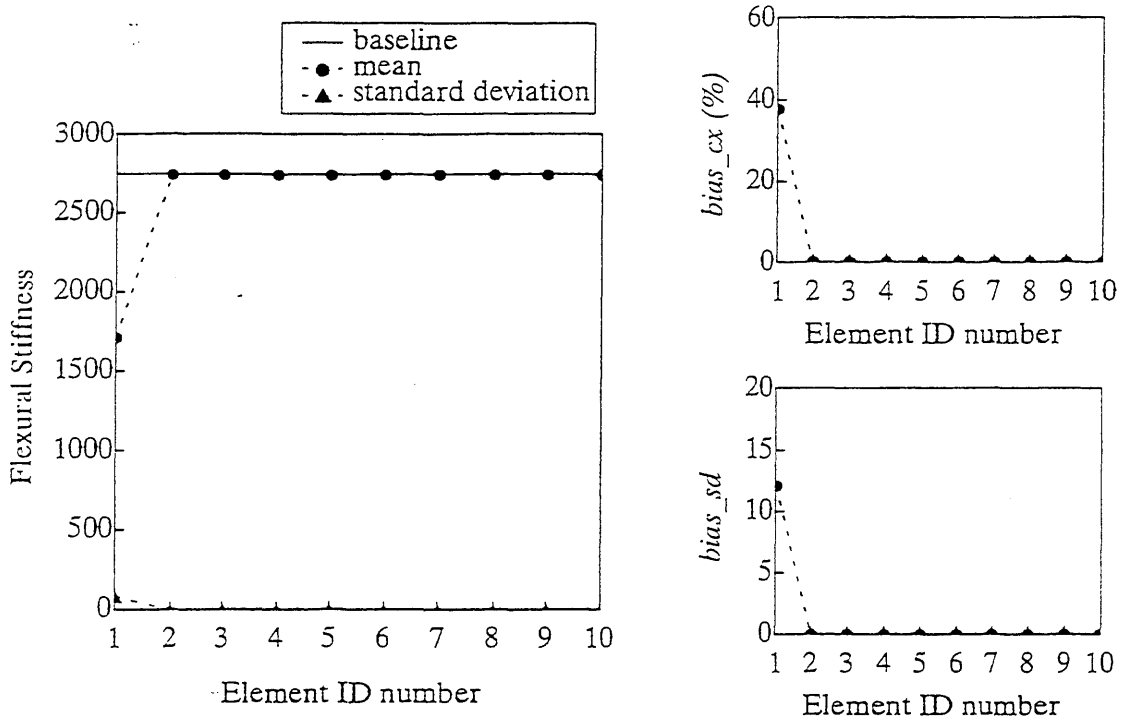

Fig. 5.23 : Damage detection and assessment with 10 Timoshenko beam element model

to identify the system. Each element can comprise a parameter group and its flexural and shear stiffnesses can be estimated directly.

The identified results from the measured data perturbation iterations are shown in Fig. 5.23. As for the Bernoulli beam case with 10 elements, a completely erroneous location of the crack is detected. Its identified natural frequencies are also distant from the measured values as summarized in Table 5.7. Again, this simple model is unable to assess the damage.

A model with 20 Timoshenko beam elements

A little more refined model with 20 Timoshenko beam elements was also studied. Since the maximum number of parameters can be 40 with two parameters for each element, the parameter grouping scheme must be used to satisfy the identifiability criterion of Eq. (2.11). Starting from one group with the uniform undamaged stiffness properties, the beam can be subdivided up to 13 groups. The identified flexural stiffness for each element is plotted in Fig. 5.24. The shear stiffnesses are not drawn here due to its incapability of detecting the cracked section as shown in Fig. 5.20. From Fig. 5.24, we can observe that element (*11*) is the only damaged element. Relatively higher *bias_sd* damage index value of the elements close to the fixed end are due to relatively small standard deviations compared with the difference between the estimated and baseline flexural stiffness, and thus those elements can be considered as undamaged by investigating the *bias_cx* damage index values. Since the actual crack is located in element (*10*), a little error in locating the crack can be observed but the existence of a single

crack is clear. The computed natural frequencies by a model with the reduced flexural stiffness for element (*11*) are close to the measured frequencies as shown in Table 5.7.

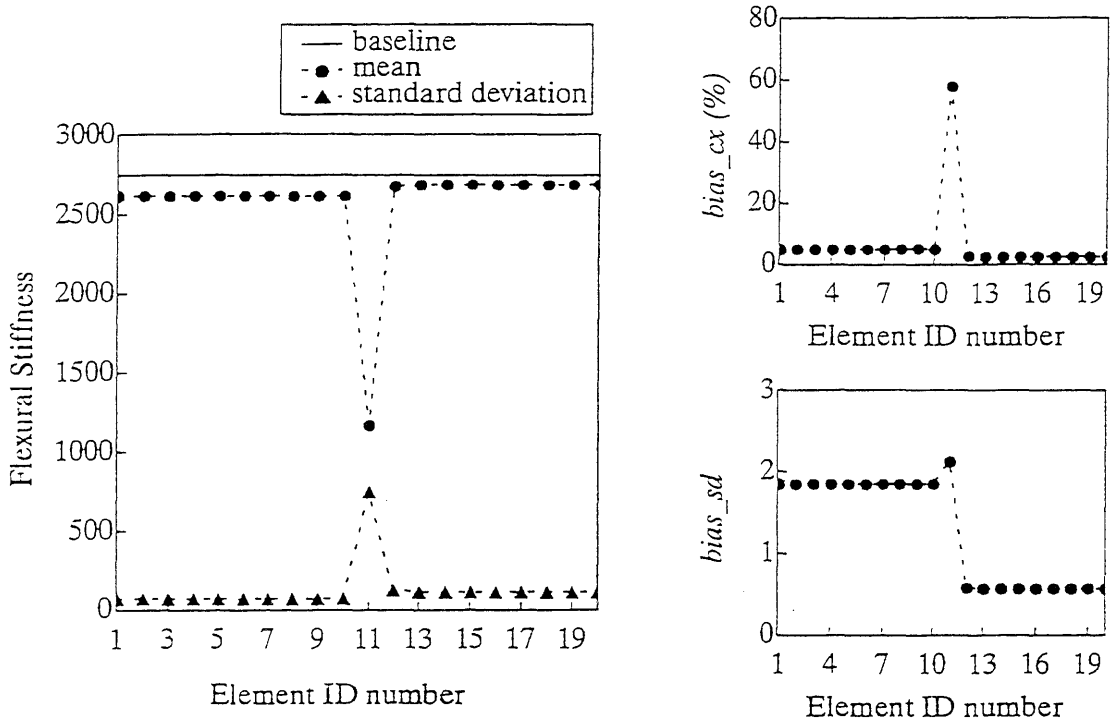

Fig. 5.24 : Damage detection and assessment with 20 Timoshenko beam element model

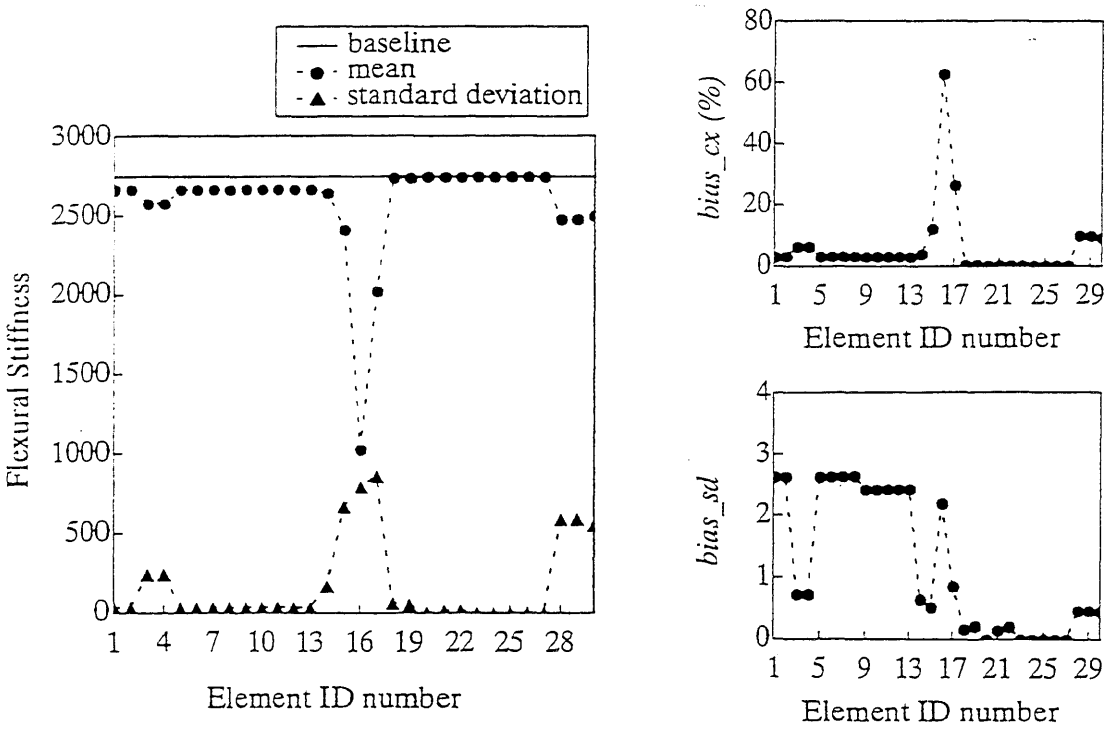

Fig. 5.25 : Damage detection and assessment with 30 Timoshenko beam element model

A model with 30 Timoshenko beam elements

A model with 30 Timoshenko beam element model also requires the parameter grouping scheme due to its relatively large number of total element parameters compared with the maximum allowable number of parameters $nmd \times \hat{n}_d = 27$ from the measured information. The parameter group can be subdivided up to 13 groups without violating the identifiability criterion. The estimated flexural stiffnesses from the measured data perturbation iterations are shown in Fig. 5.25. From the figure, we can observe that element (*16*) can be considered as the single damaged element by evaluating the computed damage indices. The actual cracked section is located directly on node *15* which connects element (*14*) and (*15*). The estimated flexural stiffness is larger than the estimated value by the 30 Bernoulli beam element model due to the effect of the shear deformation.

5.4.4 Comparisons of the Results from the Timoshenko Beam Models

The computed modal properties from the identified damaged cantilever structural system by the Timoshenko beam models are compared with the measured responses in Fig. 5.26 and Fig. 5.27. The identified location of a cracked section is compared with the actual crack location in Fig. 5.28. From

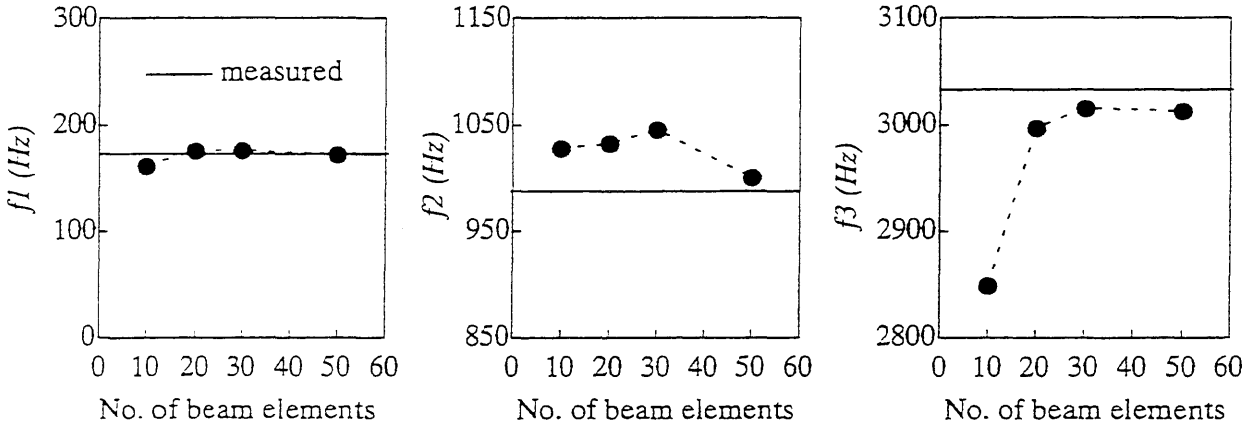

Fig. 5.26 : Comparison of the identified modal frequencies

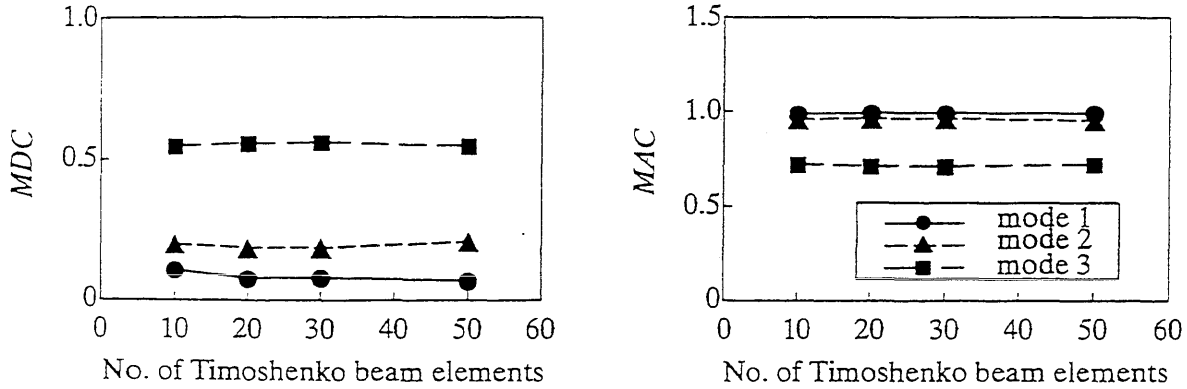

Fig. 5.27 : Errors in modal displacements

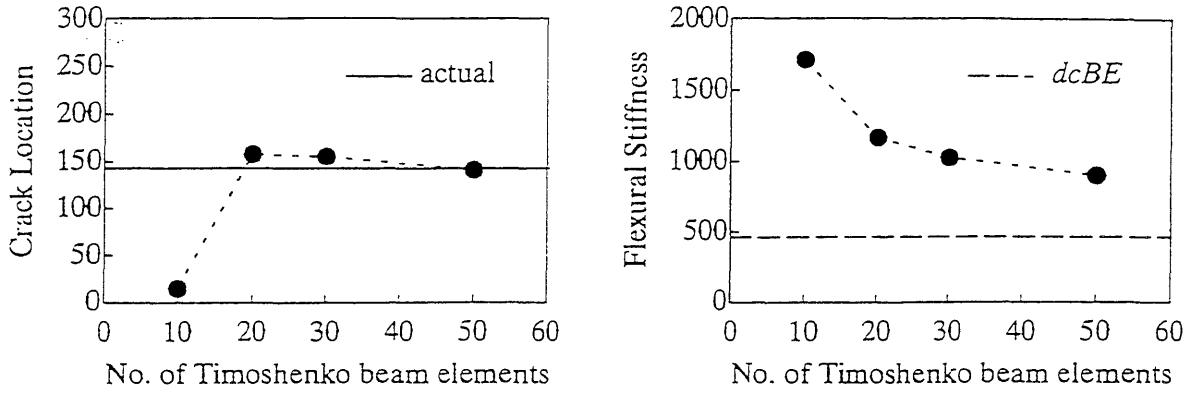

Fig. 5.28 : The estimated crack location and the flexural stiffness of the cracked element

the figures, we can observe that the identified results improve with more Timoshenko beam elements in the structural model and the cracked section location can be almost exactly pinpointed by the developed algorithm. The computed natural frequencies are very close to the measured frequencies in all the three modes, but the identified mode shape of the third mode is hard to match to the measured mode even with such a refined model with 50 Timoshenko beam elements. The estimated flexural stiffness of the detected cracked element seems to approach a certain value which is higher than the estimated flexural stiffness by 50 Bernoulli beam element model denoted by *dcBE* with a dotted line in the figure.

5.5 Summary

To compare the results from the Bernoulli and Timoshenko beam models, the results obtained from 50 beam elements for both Bernoulli and Timoshenko beams are compared in Fig. 5.29 and Fig. 5.30. In the figures, *dcBE* denotes the identified results from the model with 50 Bernoulli-Euler beam elements and *dcTS* is the results from the structural model with 50 Timoshenko beam elements. From the figures we can observe that both identified models predict almost the same natural frequencies and mode shapes for all the three modes. The computed natural frequencies of all the three modes by the Timoshenko beam model are closer to the measured frequencies, but the relative errors are negligible. About the mode shape, the third mode is hard to match regardless of the selected beam model type.

The cracked section can be more closely located by using the Timoshenko beam model as shown in Fig. 5.31. In addition, the results from the Timoshenko beam models were able to indicate the existence of a single crack clearly while the identification results from the Bernoulli beam models left a little ambiguity of deciding if there are some other damaged elements or not. All the misinterpreted damaged elements identified from the Bernoulli beam models are from the elements located nearer the free end than the actually cracked section as shown in Fig. 5.6. Those elements could be clearly evaluated as undamaged by Timoshenko beam models. This comparison may demonstrate that the

deformational behavior of the part of the cantilever structure beyond the actually cracked section can be better represented by considering shear deformation in addition to the flexural deformation. For the structural part closer to the fixed end, the Bernoulli beam models could produce better estimations of flexural stiffnesses than the Timoshenko beam models, but the identified values from the Timoshenko beam models are also close enough to the baseline value. The identified flexural stiffness at the detected damaged element in the Timoshenko beam model shows a relatively higher value than that obtained from the Bernoulli beam model (Fig. 5.31), because the shear stiffness afford more flexibility in representing the behavior of the cantilever beam. For both models, if too simplified a model

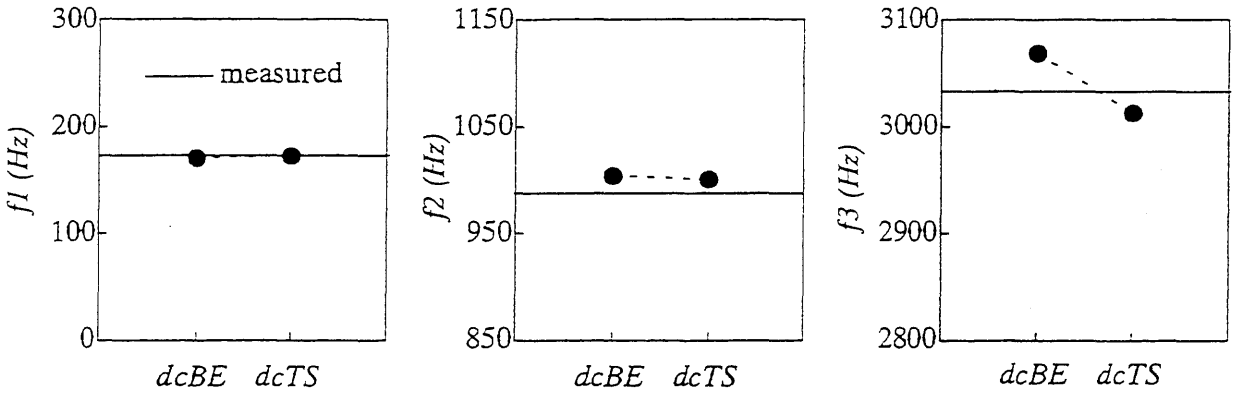

Fig. 5.29 : Errors in modal frequencies

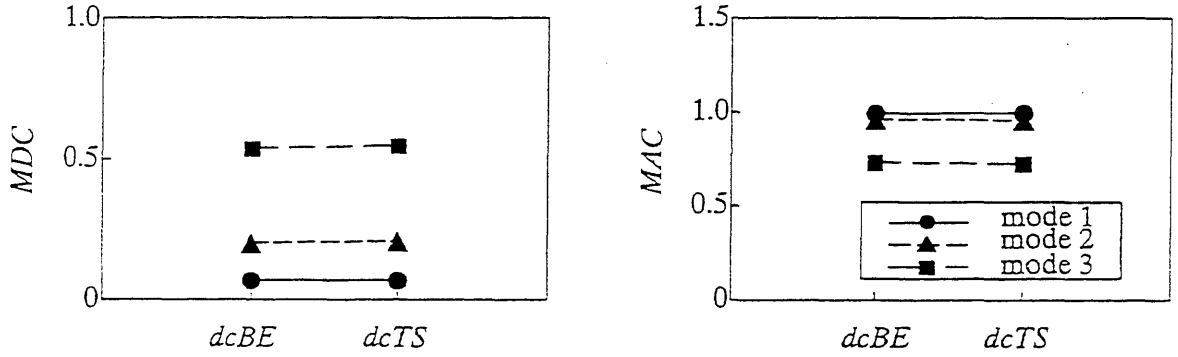

Fig. 5.30 : Errors in modal displacements

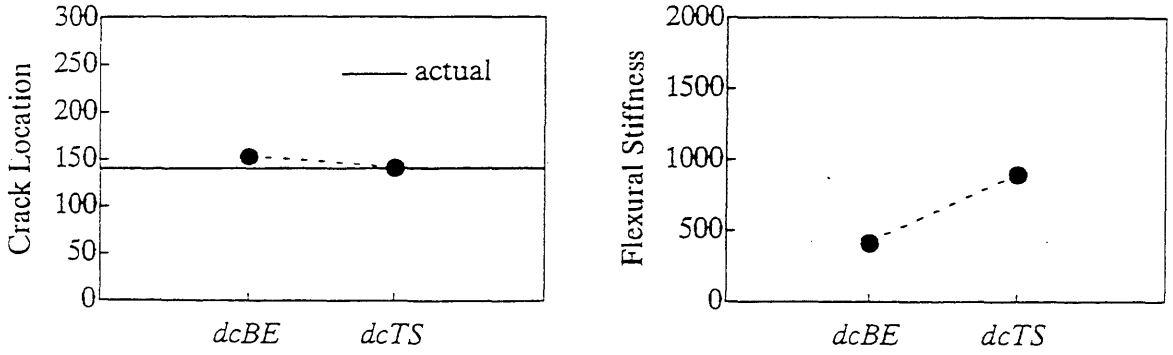

Fig. 5.31 : The estimated crack location and the flexural stiffness of the cracked element

is used to detect the crack in the cantilever structure, it has been observed that the identification error around the fixed boundary is considerable. As a more refined model is selected, the errors near the fixed and free boundaries diminish.

To determine damage by the computed damage indices, the upper limit values *cxlmt* and *sdlmt* for the damage indices are obtained from the simulation study of the baseline structure. However, the use of the upper limit values for the damage indices seems not to be as effective in the current beam case studies as the cases for the truss structure in *Chapter Three*. Without using the upper limit values, the single cracked element could be identified easily from the case studies. If there are multiple cracked sections in the cantilever beam, however, the use of the upper limit values for the damage indices may be still useful in detecting those damaged elements.

For both of Bernoulli and Timoshenko beam models, parameter group updating has been performed in the direction that minimizes the squared model error (*SME*). In other words, the parameter grouping is updated sequentially to minimize an objective error function regardless of the number of different types of parameters in an element. In addition to increasing the number of unknowns by updating parameter grouping, the localization algorithm also allows a parameter to be removed from further modification as described in *Chapter Two*. When there is only one parameter type in each element, the variation of the parameter can be watched by the local termination criterion. However, when there exist more than two different types of parameters in an element, the current algorithm uses the most reliable parameter type for the local termination criterion (this must be specified in advance), and eliminates all the parameters in the group from further modification only when the reliable parameter satisfies the local termination criterion. The cantilever structure studied in this chapter uses the flexural stiffness for this purpose because the shear stiffnesses were thought to be less reliable. However, in general, it may be difficult to deduce which parameter type is more essential to characterize the behavior of a given structure. Therefore, when it is impossible to identify a reliable parameter type, we may need to watch the variations of all the types of parameters concurrently and must apply a local termination criterion separately for each parameter without relating it to the remaining parameters in the same group.

To define a structural model for a continuous structure such as the cantilever structure, finite elements with an equal size are best used for the structural model because the locations of damaged elements in the structure are unknown. A fairly refined finite element model should be selected to produce good identification results. However, it is difficult to verify how many elements are needed to construct the refined model. To overcome this difficulty, one could equip the algorithm with an adaptive mesh generation scheme. By updating the finite element model adaptively, elements around cracks could be finer to localize damaged regions, and thus the model might represent the behavior of the continuous structural system better. The undamaged area will have a relatively rough finite element mesh compared with the possibly damaged area. To apply adaptive mesh generation, some criteria must be established to decide which elements are subjected to division for localizing damage in a continuous structure. The geometry of the structure does not change after updating the finite ele-

ment model, and only the physical properties would be altered. An advantage of using the adaptive mesh generation for localizing damage is that we do not have to worry about the selection of the initial refined finite element model for the damage assessment algorithm. However, this approach would require some additional computation for updating the finite element model. The merit of using the adaptive mesh generation approach is not so apparent compared with the current approach by defining a well refined model with an equal size of finite element from the beginning. Which approach leads to better results may be case-dependent. Nevertheless, it will be interesting to see the damage localization and assessment results by using an adaptive finite element mesh generation scheme for those continuous structural systems.

Chapter Six

Conclusions

A new damage detection and assessment algorithm was proposed and tested by some case studies. System identification is used as one of the main concepts in developing the algorithm, and an output error estimator was implemented to estimate the unknown structural parameters. A nonlinear constrained optimization problem is solved for the optimal structural parameters. The structural system is represented by a finite element model with known topology and geometry, and thus the constitutive parameters parameterized in terms of kernel matrices are the unknowns to be estimated. Measured responses of the structure are used to detect damage and to assess the damaged member properties. As formulated, static and modal responses are the two types of measured responses which have been implemented in the current algorithm.

We have assumed that the baseline property of the undamaged structure and the amplitude of noise in the measured data are known. Damage is defined as the reduction of the estimated structural parameters compared with the baseline values. We have also assumed that a well refined finite element model is defined, and that the selected finite element model is linear in its response. In detecting damage with modal response, only the stiffness parameters are investigated and the mass components are assumed to be known.

In developing the current damage assessment algorithm, the sparseness and noise in measured data were the main concerns to the success of the algorithm because they are inevitable characteristics of the measured data from civil structures. Even though we have enough measured information to satisfy the identifiability criteria in using the implemented output error estimator, one must account for noise in measurements in estimating unknown parameters. Statistical evaluation of the estimated parameters is a desirable approach to achieve more reliable results against the randomness of noise in measurements.

The parameter grouping scheme is applied to overcome severe sparseness in the measured data. The scheme is especially effective when not enough measured information is available. By using the parameter grouping scheme, the defined finite element model need not be simplified or the measured data need not be expanded to make the system of equations solvable. Since the baseline property is

assumed known and since damaged parts are hidden in some parameter groups, each of which consists of a number of structural members, the parameter groups are sequentially updated to localize the damaged parts in a structure starting from the baseline grouping. The allowed depth of the hierarchical subdivision in a complex structure depends on the quantity of measured information. The systematic subdivision procedure by comparing the squared model errors is proposed and the termination criteria are implemented in the developed algorithm. However, in the case when the measured data are enough to satisfy the identifiability criterion so that each member can compose a single group, the parameter grouping scheme and thus the parameter group updating scheme need not be used in localizing damage.

Even if there are more than two different types of parameters in a parameter group, the parameter grouping is updated sequentially as far as the squared model error reduces. The current algorithm removes all the parameters in a group at the same time from further modifications when the most reliable and essential parameter in the group satisfies a local termination criterion, simply by assuming that the essential deformational behavior of a given structure is known as uniform all over the structure. However, when it is difficult to determine the reliable parameter type in a structure and the essential property may vary depending on locations inside a structure, a more general approach must be considered. A possible way is to apply a local termination criterion separately for each parameter without relating it to the remaining parameters in the same group. Through a data perturbation iterations, the sensitivity of each parameter in an element can be investigated and damage can be detected by investigating the results from the behaviors of all the parameters in an element.

To consider noise in the measured data, the measured data perturbation scheme is proposed. Through the tested case studies, it has been observed that the measured data perturbation scheme can evaluate the sensitivity of the member parameters satisfactorily and thus provide a good statistical basis for assessing damage in the structure. Two damage indices computed from the measured data perturbation iterations are used to describe the statistical properties of the estimated member parameters. The upper limit values for the two damage indices obtained from the simulation study for the baseline structure are used to determine damage in a structural system. The upper limit values have proven useful when there are multiple damaged members in a structure.

The procedure of determining the upper limit values for the damage indices of each member was illustrated by the simulation studies for the bowstring truss structure with the static response in *Chapter Three*. It was observed that the determined limit values are effective in detecting damage in the structure if the damage is significant enough to be seen above the noise. There is always a small probability of interpreting actually undamaged members as damaged or of interpreting actually damage members as undamaged. In most cases, however, those actually undamaged but detected as damaged members have been observed to have relatively high standard deviations from the measured data perturbation iterations, and thus their *bias_sd* damage indices could be a little higher than but close to the determined upper limit value *sdlmt*. In all the cases studied, the most severely damaged member could be always successfully identified as damaged. Therefore, damage should be determined based

on the detection results by the upper limit values for the damage indices and the sensitivity investigation of the parameters.

As one of the fundamental assumptions for the developed damage assessment algorithm, the baseline structure is defined as the structure whose topology and geometry are the same as the existing structure and whose member properties are known with the undamaged baseline properties. In real cases, the baseline properties may be determined in either of two ways. The first way of defining the baseline values is by testing the original undamaged structure before the structure experiences any severe loading. The identified properties from the undamaged structure can be used as the baseline properties which can well represent the behavior of the undamaged structure. However, if the measured data for the original undamaged structure are not available, as an alternative, the design properties may be used as the baseline values if they are available. In this case, the appropriateness of the defined structural model can be a problem, because the model cannot be verified. For cases when some information on the undamaged structural system is not available, the existing structure should be identified, and the existing structure should be analyzed with the identified member properties. In this case, damage in each member cannot be assessed, but instead the serviceability of the structure can be evaluated.

One of the advantages of the developed algorithm is that the algorithm can evaluate the sensitivity of each structural member parameter simultaneously with the process of the damage detection. In other words, the sensitivity of the members need not be determined separately before trying to detect damage in the structure. Therefore, damage in all the structural members is evaluated regardless of their sensitivities at first and then damage is detected. This approach of detecting damage is much more reasonable because damage can occur even in an insensitive member and because the insensitivity of a structural member is not an inherent characteristic of the member but rather dependent on the loading and measurement conditions. From the simulation studies for the bowstring truss structure with static response, it has been observed that damage in the insensitive members can also be detected successfully by the algorithm. However, such damage might be difficult to detect if the noise level is high.

From the case studies, it has been proved that the developed damage assessment algorithm can detect and assess damage in a structural system successfully even under sparse and noisy measured data. However, the biggest disadvantage of the algorithm seems to be the computation time. Due to a number of iterations involved in the algorithm, the burden of computation increases as the number of finite elements increases in the structural model. Especially the computation time for the simulation study for the baseline structure will be extremely large if a structure is complex with a large number of degrees of freedom in its finite element model. However, the simulation study for the baseline structure can be carried out once if the topology and the geometry of the structure is known and as far as the measuring and loading conditions are kept the same in any test inference. In addition, an improvement can still be achieved if we make some effort at optimizing the algorithm. Even if it takes some hours of detecting the damaged members in a complex civil structure, if the detection and assess-

ment results are superior, we would rather spend some more computation time than obtain useless results in a few seconds. *Do we really have the cases when we have to judge damage in a structure in a few minutes?* If not, we may not have to worry about the computational burden. The time efficiency cannot be the main issue in developing a reliable damage detection and assessment algorithm.

For the continuous structural systems such as the beam structure, the number of finite elements plays an important role in detecting damaged parts correctly as shown from the case studies in *Chapter Five*. For the current algorithm, since the finite element model is assumed to be well defined, the model cannot be refined during the damage detection process. The finite element model is constructed by elements with an equal size, because the actual locations of damage are not known. Therefore, for the developed damage assessment algorithm, a well refined finite element model must be defined first to reduce the modeling error. When a relatively unrefined finite element model was used in the case studies with modal response, the estimated parameters in the members nearby the structure boundaries were erroneous.

The current algorithm uses static or modal measured response to detect and assess damage in a structural system. To investigate existing structures, the process with modal responses seems to be more practical. However, for civil structures, it seems to be true that seismic time history data are also popular. To use those seismic measured data, the developed algorithm should be extended to accommodate the time dependent measured response. A possible advantage in using the time history measured response may be that the measured data perturbation scheme may not be necessary, because a number of sets of measured data can be obtained by dividing data into a number of time windows. One restriction of using the ideas in the developed algorithm with the seismic response may be that the baseline information should be available. Nonlinearity of a structural behavior by seismic loadings should be also considered. The undamaged structure should be identified to provide the baseline properties which can be used to determine damage after severe loadings on the structure. In practice, after-shock data would be useful.

The current algorithm does not concern the optimal measuring locations to provide a best damage detection result. The algorithm rather investigates the member sensitivity with respect to the given measured degrees of freedom and load or mode cases. It intends to identify a structural system well with any given measured information on a statistical basis. However, because the baseline structure is given, it may be possible to determine the optimal measuring locations by simulation studies for the baseline structure before the field tests. The optimal measuring locations may not be an inherent property of the defined structure, but may be dependent on the applied load or mode cases. The study of finding the optimal measuring locations is beyond the current research scope but may be an interesting future topic.

Appendix

Decomposition of Element Stiffness Matrices by Constitutive Parameters and Kernel Matrices

The purpose of this appendix is to illustrate how element stiffness matrices can be expressed in terms of constitutive parameters and kernel matrices. We summarize the formulations of the element stiffness matrices for a truss bar element, a Bernoulli-Euler beam element, and a Timoshenko beam element. A general form of the decomposed stiffness matrix for finite elements is briefly reviewed. The stiffness matrices for the truss bar and the Bernoulli-Euler beam element are linear with respect to their constitutive parameters, while the stiffness matrix for the Timoshenko beam element is non-linear with respect to its parameters.

A.1 Stiffness Parameter Decomposition for Numerically Integrated Elements

A general integral form for the element stiffness matrix $K^e(n_d^e \times n_d^e)$ can be described as follows:

$$K^e(x^e) = \int_{\Omega^e} B^{eT}(\xi) E^e(\xi, x^e) B^e(\xi) d\xi \tag{A.1}$$

where $x^e(n_d^e \times 1)$ is a vector of element constitutive parameters, Ω^e is the spatial domain of the element, $B^e(n_\varepsilon^e \times n_d^e)$ is a strain–displacement matrix, and $E^e(n_\varepsilon^e \times n_\varepsilon^e)$ is element constitutive matrix. For the matrix dimensions, n_d^e is the number of displacement degrees of freedom associated with the element and n_ε^e is the number of strain components for the element.

The integral of the element stiffness matrix of Eq. (A.1) can be computed numerically by the Gaussian quadrature as:

$$K^e(x^e) = \sum_{m=1}^{n_{GP}^e} w_m \, B^{eT}(\xi_m) E^e(\xi_m, x^e) B^e(\xi_m) \tag{A.2}$$

spect to EI and GA. Therefore, the first kernel matrix for the axial stiffness is the same as Eq. (A.7), and the decomposed second and third kernel matrices with their corresponding constitutive parameter functions are defined by:

$$z_2^e(x_2^e, x_3^e) = a = \frac{l^2 EI \cdot GA}{l^2 GA + 12\zeta EI}$$

$$G_2^e(x_2^e, x_3^e) = \frac{1}{l^3}\begin{bmatrix} 0 & 0 & 0 & 0 & 0 & 0 \\ 0 & 12 & 6l & 0 & -12 & 6l \\ 0 & 6l & 4l^2 & 0 & -6l & 2l^2 \\ 0 & 0 & 0 & 0 & 0 & 0 \\ 0 & -12 & -6l & 0 & 12 & -6l \\ 0 & 6l & 2l^2 & 0 & -6l & 4l^2 \end{bmatrix} \begin{matrix} u_1 \\ w_1 \\ \theta_1 \\ u_2 \\ w_2 \\ \theta_2 \end{matrix} \tag{A.13}$$

$$z_3^e(x_2^e, x_3^e) = ag = \frac{\zeta l^2 (EI)^2}{l^2 GA + 12\zeta EI}$$

$$G_3^e(x_2^e, x_3^e) = \frac{1}{l^3}\begin{bmatrix} 0 & 0 & 0 & 0 & 0 & 0 \\ 0 & 0 & 0 & 0 & 0 & 0 \\ 0 & 0 & 12 & 0 & 0 & -12 \\ 0 & 0 & 0 & 0 & 0 & 0 \\ 0 & 0 & 0 & 0 & 0 & 0 \\ 0 & 0 & -12 & 0 & 0 & 12 \end{bmatrix} \begin{matrix} u_1 \\ w_1 \\ \theta_1 \\ u_2 \\ w_2 \\ \theta_2 \end{matrix} \tag{A.14}$$

References

Abel-Ghaffar, A.M., A.M. Niazy, and S.F. Masri (1993), "Analysis of the seismic records of a suspension bridge," *Structural Engineering in Natural Hazards Mitigation, Vol.* 1, *ASCE*, ed. by A.H-H. Ang and R. Villaverde, 1509–1514.

Agbabian, M.S., S.F. Masri, R.K. Miller, and T.K. Caughey (1991), "System identification approach to detection of structural changes," *J. of Eng. Mech., ASCE*, 117(2), February, 370–390.

Akaike, H. (1972), "Information theory and an extension of the maximum likelihood principle," *Proc. of the 2nd International Symposium on Information Theory*, B.N. Petrov and F. Csaki (ed), Akademiai Kiado, Budapest, 267–281.

Alcoe, D.J. and K.D. Hjelmstad (1992), "Identification of parametric finite element models using experimental modal data," *Structural Research Series No. 566, Dept. of Civil Eng., Univ. of Illinois at Urbana–Champaign*, January.

Ang, A.H.S. and W.H. Tang (1975), *Probability concepts in engineering planning and design, Vol.I*, John Wiley & Sons, Inc., New York, N.Y.

Ashby, M.F. and D.R.H. Jones (1980), *Engineering materials 1: an introduction to their properties and applications*, Pergamon Press.

Banan, M.–R. and K.D. Hjelmstad (1993), "Identification of structural systems from measured response," *Structural Research Series No. 579, Dept. of Civil Eng., Univ. of Illinois at Urbana–Champaign*, May.

Barron, A.R. (1984), "Predicted squared error: A criterion for automatic model selection," *Self-organizing Methods in Modeling*, S.J. Falow ed., Marcel Dekker, N.Y.

Berman, A. and E.J. Nagy (1983), "Improvement of a large analytical model using test data," *AIAA J.*, 21(8), August, 1168–1173.

Bray, D.E. and R.K. Stanley (1989), *Nondestructive evaluation: A tool for design, manufacturing, and service*, McGraw-Hill Co.

Cawley, P. and R.D. Adams (1979), "The location of defects in structures from measurements of natural frequencies," *J. of Strain Analysis*, 14(2), 49–57.

Chen, J. and J.A. Garba (1988), "On-orbit damage assessment for large space structures," *AIAA J.*, 26(9), September, 1119–1126.

Chou, C. and C. Wu (1990), "System identification and damage localization of dynamic structures," *AIAA Dynamics Specialists Conference*, San Diego, April, 113–120.

Clark, S.J. (1989), "Member stiffness estimation in linear structures from static and vibrational response," *Document No. 89–22–01, Advanced Construction Technology Center, Newmark C.E. Lab., Univ. of Illinois at Urbana–Champaign*, August.

Cook, R.D., D.S. Malkus, and M.E. Plesha (1989), *Concepts and applications of finite element analysis*, 3rd ed., John Wiley & Sons, New York.

Crandall, S.H. and W.D. Mark (1963), *Random Vibration in Mechanical Systems*, Academic Press Inc., New York.

Douglas, B.M. and W.H. Reid (1982), "Dynamic tests and system indentification of bridges," *J. of Structural Division, ASCE, Vol.* 108, October, 2295–2312.

Dzemyda, G. and E. Senkiene (1990), "Simulated annealing for parameter grouping," *Information Theory: Statistical decision function, Random processes, Trans. of the 11th Prague Conference, VolA*, Kluwer Academic pb.

Ewins, D.J. (1984), *Modal testing: theory and practice*, John Wiley & Sons, Inc., New York, N.Y.

Eykhoff, P. (1974), *System identification, parameter and state estimation*, John Wiley & Sons, Inc., New York, N.Y.

Freed, A.M. and C.C. Flanigan (1991), "A comparison of test–analysis model reduction methods," *Sound and Vibration*, March, 30–35.

Gardner-Morse, M.G. and D.R. Huston (1993), "Modal identification of cable-stayed pedestrian bridge," *J. of Structural Eng., ASCE*, 119(11), November, 3384–3404.

Guyan, R.J. (1965), "Reduction of stiffness and mass matrices," *AIAA J.*, 3(2), February, 380.

Hajela, P. and F.J. Soeiro (1990a), "Structural damage detection based on static and modal analysis," *AIAA J.*, 28(6), June, 1110–1115.

Hajela, P. and F.J. Soeiro (1990b), "Recent developments in damage detection based on system identification methods," *Structural Optimization, Springer–Velag*, 2, 1–10.

Hjelmstad, K.D., S.L. Wood, and S.J. Clark (1990), "Parameter estimation in complex linear structures," *Structural Research Series No. 557, Dept. of Civil Eng., Univ. of Illinois at Urbana–Champaign*, December.

Hoff, C. (1989), "The use of reduced finite element models in system identification," *Earthquake Eng. and Structural Dynamics, Vol.* 18, 875–887.

Irons, B.M. (1981), "Dynamic reduction of structural models," *ST5*, 1023–1024.

Jones, N.P. and J.M. Thompson (1993), "Ambient vibration survey: sunshine skyway bridge," *Structural Engineering in Natural Hazards Mitigation, Vol.* 1, *ASCE*, ed. by A.H-H. Ang and R. Villaverde, 1521–1526.

Kammer, D.C., B.M. Jensen, and D.R. Mason (1989), "Test–analysis correlation of the space shuttle solid rocket motor center segment," *J. of Spacecraft, Vol.* 26, July–August, 266–273.

Kammer, D.C. and C.C. Flanigan (1991), "Development of test–analysis models for large space structures using substructure representations," *J. of Spacecraft, Vol.* 28, March–April, 244–250.

Kaouk, M. and D.C. Zimmerman (1993), "Structural damage assessment using a generalized minimum rank perturbation theory," *The 34th AIAA/ASME/ASCE/AHS/ASC Structures, Structural Dynamics, and Material Conference*, La Jolla, CA, 1529–1538.

Kim, H.M. and T.J. Bartkowicz (1993), "Damage detection and health monitoring of large space structures," *The 34th AIAA/ASME/ASCE/AHS/ASC Structures, Structural Dynamics, and Material Conference*, La Jolla, CA, 3527–3533.

Lim, T.W. (1990), "Submatrix approach to stiffness matrix correction using modal test data," *AIAA J.*, 28(6), June, 1123–1130.

Linder, D.K., G. Twitty, and R. Goff (1993), "Damage detection, location, and estimation for large truss structures," *The 34th AIAA/ASME/ASCE/AHS/ASC Structures, Structural Dynamics, and Material Conference*, La Jolla, CA, 1538–1548.

Lintermann, C. (1986), *Impact testing and finite element representation of a cable-stayed pedestrian bridge*, M.S. thesis, The Univ. of Vermont, October.

Mazurek, D.F., and J.T. DeWolf (1990),"Experimental study of bridge monitoring technique," *J. of Structural Eng., ASCE*, 116(9), September, 2532–2549.

Natke, H.G. (1982), "Identification of vibrating structures: An introduction," *CISM courses and lectures No. 272, 'Identification of vibrating structures,'* ed. by H.G. Natke, 1–14, *Springer–Velag*, NY.

Natke, H.G. (1989), "Identification approaches in damage detection and diagnosis," *DIAGNOSTICS'89*, Politechnike Pozuanska, 99–110.

Natke, H.G. and C. Cempel (1991), "Fault detection and localization in structures: A discussion," *Mathematical Systems and Signal Processing*, 5(5), 345–356.

Pandey, A.K., M. Biswas, and M.M. Samman (1991), "Damage detection from changes in curvature mode shape," *J. of Sound and Vibration*, 145(2), 321–332.

Paz, M. (1984), "Dynamic condensation," *AIAA J.*, 22(5), May, 724–727.

Raghavendrachar, M. and A.E. Aktan (1992), "Flexibility by multireference impact testing for bridge diagnostics," *J. of Structural Eng., ASCE*, 118(8), August, 2186–2203.

Ricles, J.M. and J.B. Kosmatka (1992), "Damage detection in elastic structures using vibratory residual forces and weighted sensitivity," *AIAA J.*, 30(9), September, 2310–2316.

Rizos, P.F., N. Asparathos, and A.D. Dimarogonas (1990), "Identification of crack location and magnitude in a cantilever beam from the vibration modes," *J. of Sound and Vibration*, 138(3), 381–388.

Sage, A.P. (1972), "System identification – history, methodology, future prospects," *System Identification of Vibrating Structure*, ed. by Pilkey and Cohen, *ASME*, New York, N.Y.

Salane, H.J. and J.W. Baldwin Jr. (1990), "Identification of modal properties of bridges," *J. of Structural Eng., ASCE*, 116(7), July, 2008–2021.

Sanayei, M. and R. Nelson (1987), "Identification of structural element stiffnesses from incomplete static test data," *paper No. 861793, Society of Automotive Engineers*.

Sanayei, M. and O. Onipede (1991),"Damage assessment of structures using static test data," *AIAA J.*, 29(7), 1174–1179.

Sanayei, M. and S.F. Scampoli (1991), "Structural element stiffness identification from static test data," *J. of Engineering Mechanics, ACSE*, 117(5), May, 1021–1036.

Sanayei, M., O. Onipede, and S.R. Babu (1992),"Selection of noisy measurement locations for error reduction in static parameter identification," *AIAA J.*, 30(9), September, 2299–2309.

Smith, S.W. and C.A. Beattie (1990), "Simultaneous expansion and orthogonalization of measured modes for structure identification," *AIAA Dynamics Specialist Conference*, Long Beach, CA, April 5–6, 261–270.

Springer, W.T., K.L. Mawrence, and T.J. Lawley (1988), "Damage assessment based on the structural frequency–response function," *Experimental Mechanics*, March, 34–37.

Stubbs, N., T.H. Broome, and R. Osegueda (1990a), "Nondestructive construction error detection in large space structures," *AIAA J.*, 28(1), January, 146–152.

Stubbs, N., T.H. Broome, and R. Osegueda (1990b), "Global non-destructive damage evaluation in solids," *The International J. of Analytical and Experimental Modal Analysis*, 5(2), April, 67–79.

Stubbs, N., T.H. Broome, and R. Osegueda (1990c), "Global damage detection in solids – experimental verification," *The International J. of Analytical and Experimental Modal Analysis*, 5(2), April, 81–97.

where n_{GP}^e is the number of Gauss points in the element and w_m is the weight factor associated with the mth Gauss point ξ_m.

In Eq. (A.2), only the matrix $E^e(n_\varepsilon^e \times n_\varepsilon^e)$ contains the constitutive parameters $x^e(n_d^e \times 1)$, and can be decomposed as follows:

$$E^e(\xi_m, x^e) = \sum_{p=1}^{\Pi_e} z_p^e(x^e) D_p^e(\xi_m) \tag{A.3}$$

where Π_e is the number of parameter types in the element and $D_p^e(n_\varepsilon^e \times n_\varepsilon^e)$ is the material kernel matrix associated with the pth element constitutive parameter function, $z_p^e(x^e)$, in the element. If the matrix $E^e(n_\varepsilon^e \times n_\varepsilon^e)$ is linear with respect to the decomposed element parameter function, $z_p^e(x^e)$ is equal to x_p^e as the pth parameter in the element.

By substituting the decomposed matrix of material stiffnesses of Eq. (A.3) into Eq. (A.2), a final form of the element stiffness matrix which is decomposed by stiffness parameter functions and the kernel matrices $G_p^e(n_d^e \times n_d^e)$ can be obtained as follows:

$$K^e(x^e) = \sum_{p=1}^{\Pi_e} z_p^e(x^e) G_p^e = \sum_{p=1}^{\Pi_e} z_p^e(x^e) \underline{\left[\sum_{m=1}^{n_{GP}^e} w_m \, B^{e^T}(\xi_m) D_p^e(\xi_m) B^e(\xi_m) \right]} \tag{A.4}$$

A.2 Stiffness Parameter Decomposition for Frame Elements

For frame elements such as truss bar, Bernoulli-Euler beam element, and Timoshenko beam element, explicit forms of element stiffness matrices can be obtained. In this section, the decomposition of those explicit element stiffness matrices with stiffness parameter functions and kernel matrices are summarized.

A general description of displacements of planar truss and beam elements is shown in Fig. A.1. The maximum number of displacement components in an element, n_d^e, is equal to 6. The number of strain components for an element, n_ε^e, varies depending on the element type.

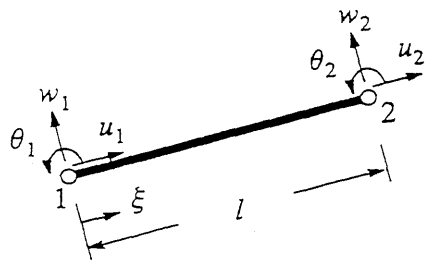

Fig. A.1 Displacements of planar truss and beam elements

The explicit form of the element stiffness matrices can be also expressed by a similar form to the implicit form of Eq. (A.4) as:

$$K^e(x^e) = \sum_{p=1}^{\Pi_e} z_p^e(x^e) G_p^e \tag{A.5}$$

Truss Bar

When a two-node truss element is considered as shown in Fig. A.1, the element stiffness matrix $K^e(6 \times 6)$ can be expressed as:

$$K^e(x^e) = \frac{EA}{l} \begin{bmatrix} 1 & 0 & 0 & -1 & 0 & 0 \\ 0 & 0 & 0 & 0 & 0 & 0 \\ 0 & 0 & 0 & 0 & 0 & 0 \\ -1 & 0 & 0 & 1 & 0 & 0 \\ 0 & 0 & 0 & 0 & 0 & 0 \\ 0 & 0 & 0 & 0 & 0 & 0 \end{bmatrix} \begin{matrix} u_1 \\ w_1 \\ \theta_1 \\ u_2 \\ w_2 \\ \theta_2 \end{matrix} \tag{A.6}$$

where E is the elastic modulus, A is the cross sectional area, and l is the length of the element. From Eq. (A.6), there is only one parameter with $x_1^e = EA$, and the element stiffness matrix is linear with respect to the stiffness parameter. Therefore, the kernel stiffness matrix for the axial stiffness parameter is defined by

$$G^e = \frac{1}{l} \begin{bmatrix} 1 & 0 & 0 & -1 & 0 & 0 \\ 0 & 0 & 0 & 0 & 0 & 0 \\ 0 & 0 & 0 & 0 & 0 & 0 \\ -1 & 0 & 0 & 1 & 0 & 0 \\ 0 & 0 & 0 & 0 & 0 & 0 \\ 0 & 0 & 0 & 0 & 0 & 0 \end{bmatrix} \begin{matrix} u_1 \\ w_1 \\ \theta_1 \\ u_2 \\ w_2 \\ \theta_2 \end{matrix} \tag{A.7}$$

Bernoulli-Euler Beam Element

A two-node Bernoulli-Euler beam element which has also 6 displacement components is considered. Its deformational behavior is shown in Fig. A.2. The assumptions to create the Bernoulli-Euler beam element are: (*1*) cross sections remain plane, (*2*) angular rotation is equal to the slope of the beam mid-surface, and (*3*) the following displacement continuity conditions are satisfied between adjacent finite elements.

$$\begin{aligned} w^- &= w^+ \\ \frac{dw}{d\xi}^- &= \frac{dw}{d\xi}^+ \end{aligned} \tag{A.8}$$

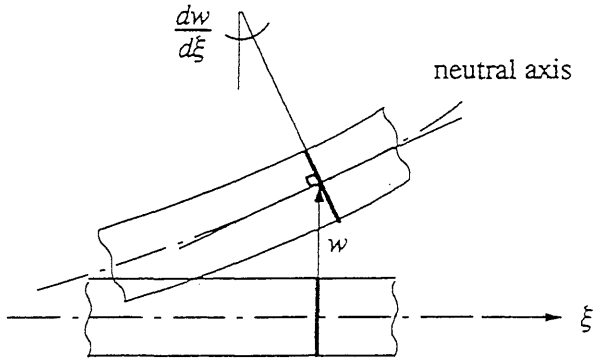

Fig. A.2 Deformation Behavior of Bernoulli-Euler Beam

The explicit form of the element stiffness matrix is given by:

$$K^e(x^e) = \frac{1}{l^3}\begin{bmatrix} l^2EA & 0 & 0 & -l^2EA & 0 & 0 \\ 0 & 12EI & 6lEI & 0 & -12EI & 6lEI \\ 0 & 6lEI & 4l^2EI & 0 & -6lEI & 2l^2EI \\ -l^2EA & 0 & 0 & l^2EA & 0 & 0 \\ 0 & -12EI & -6lEI & 0 & 12EI & -6lEI \\ 0 & 6lEI & 2l^2EI & 0 & -6lEI & 4l^2EI \end{bmatrix} \begin{matrix} u_1 \\ w_1 \\ \theta_1 \\ u_2 \\ w_2 \\ \theta_2 \end{matrix} \tag{A.9}$$

In Eq. (A.9), there are two types of parameters, $x_1^e = EA$ and $x_2^e = EI$, where I is the second moment of the cross sectional area. The element stiffness matrix is linear with respect to the axial stiffness parameter EA and the flexural stiffness parameter EI. By decomposing the stiffness parameters, a kernel matrix can be defined for each type of parameter. The first kernel matrix for the axial stiffness EA is already given by Eq. (A.7), and the second kernel matrix for the flexural stiffness EI can be defined as follows:

$$G_2^e = \frac{1}{l^3}\begin{bmatrix} 0 & 0 & 0 & 0 & 0 & 0 \\ 0 & 12 & 6l & 0 & -12 & 6l \\ 0 & 6l & 4l^2 & 0 & -6l & 2l^2 \\ 0 & 0 & 0 & 0 & 0 & 0 \\ 0 & -12 & -6l & 0 & 12 & -6l \\ 0 & 6l & 2l^2 & 0 & -6l & 4l^2 \end{bmatrix} \begin{matrix} u_1 \\ w_1 \\ \theta_1 \\ u_2 \\ w_2 \\ \theta_2 \end{matrix} \tag{A.10}$$

Timoshenko Beam Element

A two-node Timoshenko beam element with 6 displacement components is considered as shown in Fig. A.2. Its deformational behavior is described in Fig. A.3. The assumptions to create the Timoshenko beam element are: (*1*) a plane section originally normal to the neutral axis remains plane, but

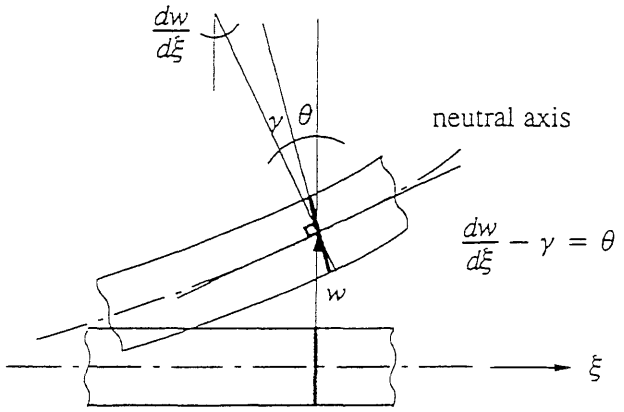

Fig. A.3 Deformation Behavior of Timoshenko Beam

does not necessarily coincide with the neutral axis because of shear deformation, (*2*) total rotation is the sum of the rotation of tangent to the neutral axis and the shear deformation, and thus the relation between the rotations is given by $\frac{dw}{d\xi} = \theta + \gamma$, and (*3*) the following displacement continuity conditions are satisfied between adjacent finite elements.

$$\begin{aligned} w^- &= w^+ \\ \theta^- &= \theta^+ \end{aligned} \tag{A.11}$$

The explicit form for the element stiffness matrix is given by:

$$K^e(x^e) = \frac{1}{l^3}\begin{bmatrix} l^2EA & 0 & 0 & -l^2EA & 0 & 0 \\ 0 & 12a & 6la & 0 & -12a & 6la \\ 0 & 6la & (4l^2+12g)a & 0 & -6la & (2l^2-12g)a \\ -l^2EA & 0 & 0 & l^2EA & 0 & 0 \\ 0 & -12a & -6la & 0 & 12a & -6la \\ 0 & 6la & (2l^2-12g)a & 0 & -6la & (4l^2+12g)a \end{bmatrix} \begin{matrix} u_1 \\ w_1 \\ \theta_1 \\ u_2 \\ w_2 \\ \theta_2 \end{matrix} \tag{A.12}$$

where $a = \dfrac{l^2EI}{l^2 + 12g}$

$g = \zeta\dfrac{EI}{GA}$

where ζ is a shape factor for the given section of a structure, which is computed by assuming a constant shear strain γ and a parabolic variation of shear stresses through thickness. For a rectangular section, the value of ζ is equal to $\frac{6}{5}$.

In Eq. (A.12), there are three types of parameters, $x_1^e = EA$, $x_2^e = EI$, and $x_3^e = GA$. The element stiffness matrix is linear with respect to the axial stiffness parameter EA, but nonlinear with re-

Tavares, R., J.B. Kosmatka, J. Ricles, and A. Wicks (1993), "Using experimental modal data to detect damage in a space truss," *The 34th AIAA/ASME/ASCE/AHS/ASC Structures, Structural Dynamics, and Material Conference*, La Jolla, CA, 1556–1564.

Timoshenko, S., D.H. Young, and W. Weaver, Jr. (1974), *Vibration problems in engineering*, 4th ed., John Wiley & Sons, Inc., New York, N.Y.

Vandier, J.K. (1975), "Detection of structural failure on fixed platforms by measurement of dynamic response," *The 7th Offshore Technology Conference*, Houston, TX, May 5–8, 243–251.

Yao, G.C., K.C. Chang, and G.C. Lee (1992), "Damage diagnosis of steel frames using vibrational signature analysis," *ASCE, J. Eng. Mech.*, 118(9), September, 1949–1961.

Yen, W-H. and T.T. Baber (1993), "Ambient vibration response of a long span bridge," *Structural Engineering in Natural Hazards Mitigation, Vol.* 1, *ASCE*, ed. by A.H-H. Ang and R. Villaverde, 1551–1556.

Yuen, M.M.F. (1985), "A numerical study of the eigenparameters of a damaged cantilever," *J. of Sound and Vibration*, 103(3), 301–310.

Zak, M. (1983), "Discrete model improvement by eigenvector updating," *ASCE, J. of Eng., Mech.*, 109(6), 1437–1444.

Zimmerman, D.C. and M. Kaouk (1992), "Eigenstructure assignment approach for structural damage detection," *AIAA J.*, 30(7), July, 1848–1855.